



Title	STUDY OF SPECTRO-POLARIMETRIC BIDIRECTIONAL REFLECTANCE PROPERTIES OF LEAVES
Author(s)	Tumendemberel, Begzsuren
Citation	北海道大学. 博士(理学) 甲第13566号
Issue Date	2019-03-25
DOI	10.14943/doctoral.k13566
Doc URL	<a href="http://hdl.handle.net/2115/74299">http://hdl.handle.net/2115/74299</a>
Type	theses (doctoral)
File Information	Begzsuren_Tumendemberel.pdf



[Instructions for use](#)

学位論文

STUDY OF SPECTRO-POLARIMETRIC BIDIRECTIONAL REFLECTANCE PROPERTIES OF  
LEAVES

(スペクトル及び偏光を考慮した葉の双方向反射率特性の研究)

by

BEGZSUREN TUMENDEMBEREL

トゥメンテンプレル ベグズスレン

北海道大学

Supervisor: Prof. Yukihiro Takahashi

A dissertation submitted in partial fulfillment of  
the requirements for the degree of Doctor of Philosophy  
in the Graduate School of Science at the Hokkaido University  
Sapporo, Hokkaido, Japan

March 2019

© 2019 Begzsuren Tumendemberel

## ABSTRACT

The reflectance of the leaf consists not only of its intensity but also of polarization, and the polarization techniques are generally used for separating specular reflectance from diffuse reflectance. The internal diffuse component of the spectral reflectance contains the details of the biochemical properties of the plant, an activity of photosynthesis, an expected amount of harvest, and water condition. Specular reflectance of the leaf strongly depends on a combination of the angle of incidence of the light source and the angle of observation view. The leaves look shiny at the shallow angle, where most of this reflection is polarized from the surface of leaves. Although the leaf spectral reflectance which is a point of convergence for many types of research, the study of spectral measurement with polarization in a single leaf is largely unexplored.

This dissertation aims to connect the polarization techniques and directional relations of the leaf Bidirectional Reflectance Distribution Function (BRDF) by separating specular and diffuse reflectance. To do this, the estimation of single leaf BRDF of *Coffea canephora* Pierre (Coffee), *Epipremnum aureum* (Pothos), and *Fragaria × ananassa* (Strawberry) was carried out based on the measurements by Liquid Crystal Tunable Filter (LCTF) camera in the wavelength range of 460-780 nm with a linear polarizer. The imaging with the multispectral LCTF camera has a great advantage in measuring a selected leaf area with an arbitrary size of the field of view. There are hundreds of combinations of incident light and observation direction in single leaf Bidirectional Reflectance Factor (BRF) measurement. In order to conduct the measurements for all those conditions, we built the automatic goniometer with LCTF camera in a laboratory.

The analysis of the measured data shows unpolarized reflectance has a strong correlation with the PROSPECT model and that it can be possible to separate these light reflections with any spectral measurement device using a rotating polarizer. Polarized reflectance strongly depends on relative azimuth  $\phi$  and zenith view  $\theta_r$  angles and the unpolarized part is almost independent at that illumination angle relatively. The leaf DHRF in a field measurement has been difficult to determine in real life since the integrating sphere is needed or the hundreds of leaf BRF measurement is required at the outside. If a method of stabilizing is existed, it is possible to quickly determine the biochemical contents of the leaves using the PROSPECT model in a field.

The results of this study show that spectro-polarimetric measurement is able to do that. Mirror reflections of all leaves were measured from  $3.6^\circ$  to  $68.4^\circ$  with an accuracy of  $1.8^\circ$  for

estimating surface roughness. It was found that an optimal surface roughness of about 46.1 nm is obtained for pothos leaves, which is almost twice compared to strawberry leaves. The maximum rms of surface roughness is 71.67 nm for pothos leaves, 92.41 nm for strawberry leaves. The smoothest surfaces of leaves are pothos, and the roughest are strawberry leaves in the plants we measured. Although the surface roughness of strawberry is considerably higher than for pothos, the light penetration into the leaves is equal for all plants at same wavelengths.

In previous studies, the leaf BRF prediction is usually based on the Cook-Torrance (Cook and Torrance, 1981) prevalent model in computer graphics assuming that the surface micro-geometry acts as a set of specular mirrors. Another type of models are widely used in the optics community, computing diffraction effects caused by differences in height in the surface micro-geometry and predicts visual appearance from the frequency content of the height distribution. The Cook-Torrance model may not be suitable for the leaf reflectance in our observation because the actual measurement cannot determine the surface roughness. The Generalized Harvey-Shack (GHS) scattering theory is well studied from rebound models determined by height distribution (Krywonos, 2006) and the GHS theory is not limited to any special wavelength range and RMS roughness value. Spectro-polarimetric measurement results and physical scattering theory have led us to create a new reflectance model. We successfully created a new leaf bidirectional reflectance model which considers that the diffuse component is Lambertian inside of the leaves and an internal scattering coefficient is calculated to an output value of PROSPECT model; the specular component is explained by GHS scattering theory. The polarization property of reflected light on a single leaf is also identified and rebuild bidirectional reflectance factors including polarized, unpolarized, and the total reflectance factors according to our model in this dissertation. Finally, a new spectro-polarimetric bidirectional method is more controllable for the BRF pattern of a single leaf.

## ACKNOWLEDGMENT

I would like to express my heartfelt gratitude to those who have contributed to this dissertation and helped me in one way or the other during this fantastic journey for, without any of them, this thesis would not have been possible.

Firstly, I wish to place on records my heartfelt and sincere gratitude to my supervisor Prof. Yukihiko Takahashi for the continuous support of this Ph.D. study and related research, for his patience, for providing me an opportunity to complete this dissertation, motivation, and immense knowledge. In my memories, he visited at my previous university in Mongolia, July 2015 when he gave me the opportunity to study at Hokkaido University and bring me to Japan. In that time, he had a linear polarizing filter in his blue shirt's pocket and showed that reflected intensity of light on the tree is changed by rotation of linear polarizer filter. The color change of that moment is the clearest in my memory. His guidance helped me in all the time of research and writing of this dissertation. I am also indebted towards his for his generosity, selfless support and especially for the excellent example and patience that he has provided to me for the last three years. Big thanks once again go to him for without his this work would have never seen the light as it is today.

Besides my advisor, I would like to give special thanks to my dissertation committee: Prof. Ryouichi Tanaka for his time and careful reading to details, Prof. Kiyoshi Kuramoto, and Prof. Junichi Kurihara for their insightful comments and guidances throughout my journey, but also for challenging my thinking by helping me assumptions and view issues from multiple perspectives.

I have to thank all of the physics education and Hokkaido University professors whom I have worked with over the last three years for showing me what it means to be a dedicated, each in their own unique way. My sincere thank goes to Dr. Tetsuro Ishida, again Prof. Junichi Kurihara, Prof. Mitsuteru Sato, and Dr. Nobuyasu Naruse, who provided me information and fundamental pieces of knowledge of this study, and who have access to the laboratory and research facilities. I am incredibly grateful to our project coordinator, Ms. Eriko Momota for purchasing equipment and items needed for my laboratory experiment and supporting the daily laboratory operations. Without their precious support it would not be possible to conduct this research.

My sincere gratitude is reserved for Dr. Ito-sensei for his invaluable insights and helping me on transmission electron microscope measurements. I appreciate his willingness to help and

meet me whenever I need some clarification. The useful discussion and comments that he suggests me widen my knowledge on chemical methods of the subject throughout the course of my study. I would like to thank Prof. Hiroshi Tani for borrowing SPAD-502 chlorophyll meter, which tool is handy for our experiment.

To my friends and labmates, thank you for spending time with me, offering me advice, the stimulating discussions on studies, for the nights we were working together in the laboratory, and supporting me through this entire Ph.D. process. Special thanks to my laboratory group friends: Junji Miyazawa (supporter), Ade Purwanto (We was working together same subject), Ono Tatsuharu, Matsuoka Ryo, Masataka Imai, Kittanapat Bandholnopparat, Kaye Kristine Vergel, Benjamin Magallon, Ellison Castro, Quach Trung Dong, Nguyen Thi Thu Han, Doreena Karmina Pulutan, LJ Estrebillo, and Ahmad Shaqeer. The debates, dinners, parties, and general help and friendship were all greatly appreciated. I would like to also thanks to my friends: Enkhbat Erdenebat, Erdenebaatar Dashdondog, Uuganjargal Ariunbold, Solongo Enkhbayar, Tulga Tulga, Zaya Nergui, Javzandolgor Bud, Galtchandmani Purevdelger, Dolgormaa, Dagva ah, Badmaa egch, Javkhlantamir, Erdemsurakh Ochbayar, Enkhmaa Enkhbat, Munkh-Erdene, Baasandorj. If you had not been there at that time, Hokkaido winter snowy days would have been long dull. I am looking forward to continuing our relations and thank you for sharing your life stories with me and for your friendship.

I would like to say thank you to my family: my parents and to my brothers and sister for supporting my study of science spiritually throughout writing this thesis and my life in general. Thank you very much for being my biggest supporters. Thank you for continually putting my happiness before your own. Thank you so much for all the opportunities you have given me in order to reach the unqualified success.

Last but not least, I am thankful to the Higher Engineering Education Development Project (M-JEED program) which has enabled me to do this research and given me an opportunity to study in Japan.

T.Begzsuren

## TABLE OF CONTENTS

ABSTRACT .....	1
ACKNOWLEDGMENT .....	3
TABLE OF ACRONYMS/ABBREVIATIONS .....	8
NOTATIONS .....	10
SUBSCRIPTS AND SUPERSCRIPTS.....	11
CHAPTER 1: INTRODUCTION .....	12
1.1    Optical observations of vegetation .....	12
1.1.1    Background and why we need this study .....	17
1.1.2    Reason to start this study.....	19
1.2    Effects of biochemical contents .....	20
1.3    Effects of the leaf biophysical structure.....	25
1.4    Reflectance definitions and observation geometry .....	29
1.5    Stock’s parameters and polarization .....	32
1.6    Cook-Torrance computer graphics model .....	34
1.7    The Generalized Harvey-Shack scattering theory .....	35
1.8    The purpose of the investigation.....	39
1.8.1    Motivation and goals for writing this thesis .....	40
1.8.2    The structure of a dissertation .....	42
CHAPTER 2: EXPERIMENTAL SETUP.....	44
2.1    Data acquisition .....	45
2.1.1    Liquid Crystal Tunable Filter camera.....	45
2.1.2    Handy spectrophotometer.....	48
2.1.3    Calibrations with integrating sphere.....	49
2.1.4    SPAD chlorophyll meter and other measurement setups .....	53
2.2    The automatic goniometer .....	55
2.2.1    Light source and stabilization.....	56
2.2.2    Materials and apparatus.....	57
2.2.3    Electronics control system.....	61



2.2.4	Controlling algorithms and software .....	62
2.3	Measurement configuration .....	66
2.4	Transmission electron microscope measurement preparation .....	67
2.5	Sample leaves of plant species.....	69
CHAPTER 3: SPECTRO-POLARIMETRIC BRF MEASUREMENT RESULTS .....		70
3.1	The total BRF patterns of leaves.....	70
3.2	Polarized and unpolarized reflectance factors .....	73
3.3	Optical estimation of surface RMS roughness .....	78
3.4	Estimations of the thickness of waxy cuticle.....	86
3.4.1	Optical estimation.....	86
3.4.2	Electron microscope measurement.....	90
CHAPTER 4: LEAF SPECTRO-POLARIMETRIC BRF PREDICTION .....		93
4	.....	93
4.1	Spectro-polarimetric model expectation .....	93
4.2	Model performance.....	96
CHAPTER 5: DISCUSSIONS.....		100
5.1	About spectro-polarimetric measurement results .....	100
5.2	About optical estimations for leaf surface .....	103
5.3	About experimental setup .....	105
5.4	About new Spectro-Polarimetric BRF model of leaves.....	106
CHAPTER 6: SUMMARY AND CONCLUSIONS .....		108
6.1	Thesis conclusions .....	108
6.2	Future work.....	111
REFERENCES.....		112



## TABLE OF ACRONYMS/ABBREVIATIONS

ACV	Autocovariance (function)
ADCS	Attitude Determination Control System
ASF	Angle Spread Function
BRF	Bidirectional Reflectance Factor
BRDF	Bidirectional Reflectance Distribution Function
BSDF	Bidirectional Scattering Distribution Function
BTDF	Bidirectional Transmittance Distribution Function
DHRF	Directional Hemispherical Reflectance Factor
DoLP	Degree of Linear Polarization
EWT	Equivalent Water Thickness
FFT	Fast Fourier Transform
GHS	Generalized Harvey-Shack
LAI	Leaf Area Index
LMA	Leaf Mass per Area
LCTF	Liquid Crystal Tunable Filter
NDVI	Normalized Difference Vegetation Index
NIR	Near infra-red
OPD	Optical Path Difference
PSD	Power Spectral Density
PSF	Point Spread Function
RGB	Red, Green, Blue (Color image)
RMS	Root Mean Square
RR	Rayleigh-Rice
SAC	Specific Absorption Coefficient

SPM	Small Perturbation Method
TIS	Total Integrated Scatter
VI	Vegetation index
VIS	Visible light

## NOTATIONS

Symbols	Quantity and unit
$L$	Radiance, [ $\text{W m}^{-2} \text{sr}^{-1} \text{nm}^{-1}$ ]
$E$	Irradiance or incident flux density; $\equiv d\Phi/dA$ [ $\text{W m}^{-2}$ ]
$A$	Surface area [ $\text{m}^{-2}$ ]
$\Phi$	Radiant flux [W]
$\lambda$	The wavelength of radiation [nm]
$\rho$	Reflectance; $\equiv d\Phi_r/d\Phi_i$
$R$	Reflectance factor; $\equiv d\Phi_r / d\Phi_r^{id}$
$\theta$	Zenith angle, [rad]
$\phi$	Azimuth angle, [rad]
$\alpha$	Linear polarizer rotation angle which relative to vertical zenith axis, [rad]
$\omega$	Solid angle; $\equiv \int d\omega \equiv \int \int \sin\theta \cdot d\theta \cdot d\phi$ [sr]
$\Omega$	Projected solid angle; $\equiv \int \cos\theta \cdot d\omega \equiv \int \int \cos\theta \cdot \sin\theta \cdot d\theta \cdot d\phi$ [sr]
$\sigma$	Surface roughness
$n$	Refractive index
$\beta$	The angle between leaf plane normal and surface face normal of Cook-Torrance
$\theta_\alpha$	A half plane of the phase angle between illumination and view directions

## SUBSCRIPTS AND SUPERSSCRIPTS

i Incident or illumination

r Reflected

id Ideal (lossless)

p Polarized

w Waxy cuticle

up Unpolarized

diff Diffuse

spec Specular

Ba Barium sulfate ( $\text{BaSO}_4$ )

rel Relevant

meas Measurement

b Brewster's

NIR Near infra-red

## CHAPTER 1: INTRODUCTION

Leaves are a provider of the most fundamental needs of life on earth. Techniques of vegetation canopy identification are now well developed based on the multispectral imaging which gives an opportunity to determine various things from space such as their positioning, density of plant biomass, invasive vegetation, mapping of deforestation, and the health of the plant. These applications based on a property of the leaf spectral reflectance which is a point of convergence for many types of research. The smallest part of this study is the single leaves, and it needs to know optical properties.

### 1.1 OPTICAL OBSERVATIONS OF VEGETATION

Optical observations of vegetation are remotely sensed by obtaining the electromagnetic wave reflectance data from a cover of the plants using passive sensors. Remote sensed data of growth, yield, and their field from terrestrial vegetation can give to a high degree significant bits of knowledge to applications in natural observing, biodiversity conservation, agriculture, forestry, urban green infrastructures, and other related fields. In particular, these sorts of data connected to agriculture provide not only an objective basis for the large-scale and

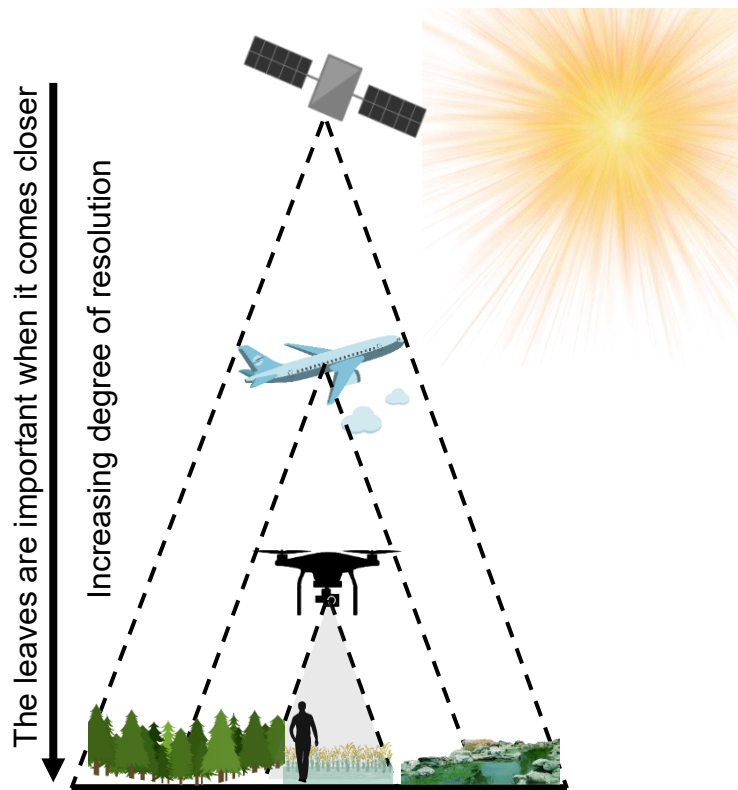


Fig. 1. Remote sensed optical observations by flying different device

micromanagement of agriculture generation yet additionally in numerous events the fundamental data for yield estimation of harvests. These optical observations can be categorized according to the apparatus used in general and Fig. 1 shows plant observation options by different flying device and ground field measurement (or human eyes). The first thing to think about optical observations of vegetation is earth observation satellites, and in this case, the leaves are very tiny and small from space with several meters squares in one pixel of a camera. Knowledge of how to reflect the light on one leaf becomes more important, and better study is needed when observation distance come closer.

The exploration of earth observation by multispectral scanning started in earnest with the launch of the first ERTS satellite (after renamed Landsat 1) by the NASA on July 23, 1972. This was the first multispectral sensor equipped satellite orbiting the Earth, and that funded a number of investigations to determine its capabilities for remote sensing. One of those early investigations was coordinated toward analyzing the spring vegetation green-up and resulting summer and fall dry-down all through the north to south territory of the Great Plains district of the U.S. This area secured a broad scope of scopes from the southern tip of Texas to the U.S. - Canada outskirts, which brought about a wide scope of sun based apex points at the season of the satellite perceptions.

Former PhD student Donald Deering and his supervisor Dr. Robert Hass (scientists of Great Plains study) found that their capacity to associate or quantify, the biophysical characteristics of the rangeland vegetation of this locale from the satellite spectral signals was perplexed by these distinctions in solar zenith angle across this strong latitudinal gradient with the help of an occupant mathematician Dr. John Schell. A team from these guys examined answers for this quandary and consequently developed the proportion of the difference of the red and infrared reflectances over their sum as a means to adjust for or "standardize" the impacts of the solar zenith angle. Initially, they considered this proportion the "Vegetation Index"; but as several other remote sensing analysts were identifying distinguishing the straightforward red/infrared proportion and other spectral ratios as the "vegetation index," they eventually started to recognize the difference/sum ratio formulation as the normalized difference vegetation index (NDVI).

The soonest announced the utilization of NDVI in the Great Plains study was in (Rouse et al., 1972) at the Remote Sensing Center of Texas A&M University. For the most part, the healthy plant absorbs the vast majority of the noticeable light that falls on it and reflects an



expansive segment of the NIR light. Unhealthy or sparse plants reflect more visible light and less NIR light. Soon after the launch of ERTS-1 (Landsat-1), NASA created a progression of early scientific journal articles describing uses of the NDVI at Goddard Space Flight Center, that index has discovered a wide application in vegetative investigations as it has been utilized to evaluate crop yields, field execution, and rangeland conveying limits among others. It is often directly connected to other ground parameters such as percent of ground cover, photosynthetic movement of the plant, surface water, leaf area index and the measure of biomass. Accordingly, NDVI is a standout amongst the best of numerous attempts to simply and rapidly distinguish vegetated section of regions and their condition, and it remains the most important and utilized index to identify live green plant sections from others based on multispectral images. When the achievability to recognize vegetation had been demonstrated, clients also tended to use the NDVI to measure the photosynthetic capacity of a plant canopy.

NDVI has usually calculated contrasts of images by the following equation

$$NDVI = \frac{R_{nir} - R_{red}}{R_{nir} + R_{red}}, \quad (1)$$

where  $R_{nir}$  is a reflectance factor (or contrast) of imagan e taken in near-infrared (NIR), and  $R_{red}$  is a reflectance factor of red in visible (VI). Fig. 2 shows an example NDVI plot which measured using multispectral Liquid Crystal Tunable Filter (LCTF) camera at Furano flower garden in Hokkaido, Japan. A camera was fixed on the ground and then taken an image. The standard form of a vegetation index is a proportion of reflectance estimated in two bands or their arithmetical mix. Spectral images (bands) to be utilized in any index calculation are chosen depending on the spectral characteristics of plants.

Color digital pictures consist of pixels, and those are made of combinations of essential colors represented by a progression of code. A band in this setting is the gray color image (or two-dimensional numerical matrix) of the same size as a digital color picture, made of only one of these primary colors. For example, an image from a standard digital camera will have a red, green and blue band. A grayscale image has just one band image. In our case, it is possible to capture hundreds of different colors using the multispectral camera. So we picked up images red 670 nm, Green 550 nm and blue 460 nm from camera output for a composition of the actual color picture. The RGB gives us precise information about shadow and their colors of plants; the vegetation indices are more comfortable to determine that the green plants grow well on the

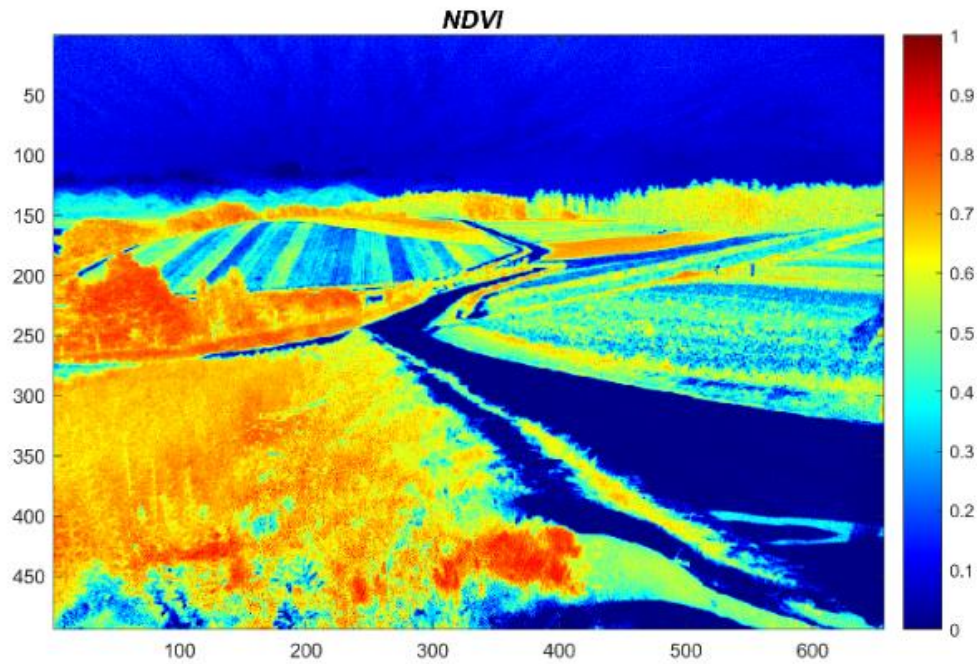


Fig. 2. Example NDVI measurement was taken by multispectral camera at the Furano flower garden in Hokkaido Prefecture. Vertical and horizontal axes are both pixel numbers of image.

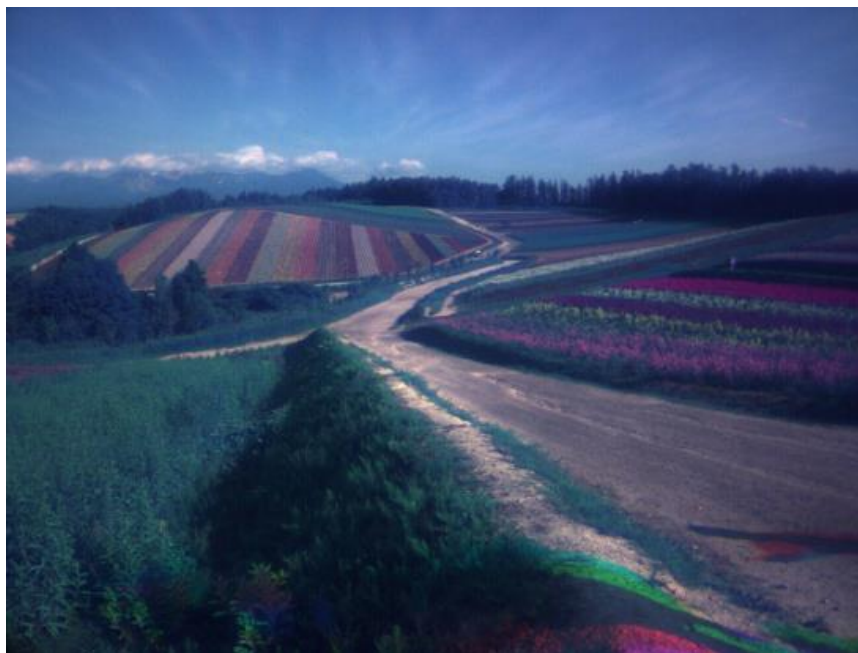


Fig. 3. Reconstruction of normal RGB image was also taken by a multispectral camera at the same place at the same time. Red, Green, Blue (RGB) were chosen for 670 nm, 550 nm, 460 nm respectively.

ground from different perspectives. Please see Fig. 2 and 3 for comparison between RGB image and remote sensing vegetation index. The advantage of spectral imaging is indicated more details information about growth and yield.

The capacity of an optical sensor to determine includes inside specific wavelengths of the optical range and narrow selection of wavelength bands into smaller additions is referred to as a sensor's spectral resolution. The spectral resolution of a sensor is continuously ranged that we called hyperspectral imaging. Pictures caught by hyperspectral imaging contains hundreds of individual bands, giving a close ceaseless perusing of the optical spectrum. Maybe the most widely recognized and promptly accessible kind of remotely sensed image is multispectral, which regularly contains somewhere in the range of two to more than ten bands that have been picked carefully along the optical range. Numerous years of distributed scientific papers concentrated on the spectral band changes experienced when vegetation practices changes in the content of water, pigments, supplements, and different properties have prompted the consideration of bands on various Earth observation satellites and airborne multispectral sensors that emphasis on the ranges of the electromagnetic spectrum that are sensitive to vacillations in optical vegetation characteristics. Our understanding of the spectral resolution of the information is vital to working effectively with vegetation indices, which frequently require information from quite specific regions of the optical spectrum connecting optical property of leaves.

Published numerous scientific researches and remote sensing specialists have concluded to understand that combinations of the measured reflectance data at least two wavelengths produce specific vegetation characteristics, otherwise called vegetation indices (VIs). More than 100 VIs exist today (Xue and Su, 2017) with additional lists developing as sensors advance and give new information. These hundreds of indices are divided into seven categories depending on their benefits, scientific importance, and relevance and those described such as broadband greenness, narrowband greenness, light use efficiency, canopy nitrogen, dry or senescent carbon, pigments in leaf, and surface water content. Every one of the above-recorded categories has at least one list that is utilized to evaluate the nearness of a specific property.

### 1.1.1 Background and why we need this study

Willstatter and Stoll (1913) considered the phenomena of light entering plant cells, and they were first researchers inspired by the spectral properties of vegetation. After this studies, concerning interactions between the light of a different wavelength with vegetation, permitted to decide bands used in VIs. Almost all usually utilized VIs are depended on near-infrared (NIR) and red (R) bands. In general, the reflectance in Red band depends on chlorophyll content and reflectance in Near Infrared on an internal structure of the plant cell. Reflectances in these spectra are uncorrelated with each other, and they indicate high spectral contrast for vegetation. The light spectral reflectance of a leaf will cover in the next subsections. The light reflection of the leaf is mostly dependent on the biochemical composition, but in the case of an extreme height such as from a satellite, hundreds of leaves are one pixel, so it is necessary to consider other parameters. The fundamental cause of such sort of this parameter is the Leaf Area Index (LAI) is characterized as one half the total green leaf area per unit of horizontal ground surface area and is called true LAI. The true LAI duplicated by the clumping index is called effective LAI. LAI measures the number of leaf components in a biological system, which imposes important controls on processes such as photosynthesis, respiration, and rain interception that link vegetation to climate (Liang et al., 2014). Subsequently, LAI shows up as a key parameter in numerous models that describe vegetation-atmosphere interactions, especially concerning the carbon and water cycles.

From a technical side point of view, there is no correlation between optical observations of vegetation and distance if no change of view angle and illumination angle. If these two angles do not change, perhaps the numerical value of vegetation indices will be stable on observation distance. However, as observation distance from the target to sensor device are approaching, the angle of view and the angle of illumination are always different for each measurement (or observations) in reality. For instance, the man who measures manually on the vegetation field will always keep changing the observation angle; because of the slow measurements, time passes then the angle of the solar illumination will change and clouds between the sun and the measurement area. Although there are too many factors depending on the situation, critical parameters are observation view and illumination angle. Spectral reflectance of the leaf strongly depends on a combination of the angle of incidence of the light source and the angle of observation view both. Fig. 4 shows a comparison between different views with different observing angles (light illumination was fixed). The

details of the spectral signature property of vegetation (or leaves) will be discussed in the next sections.

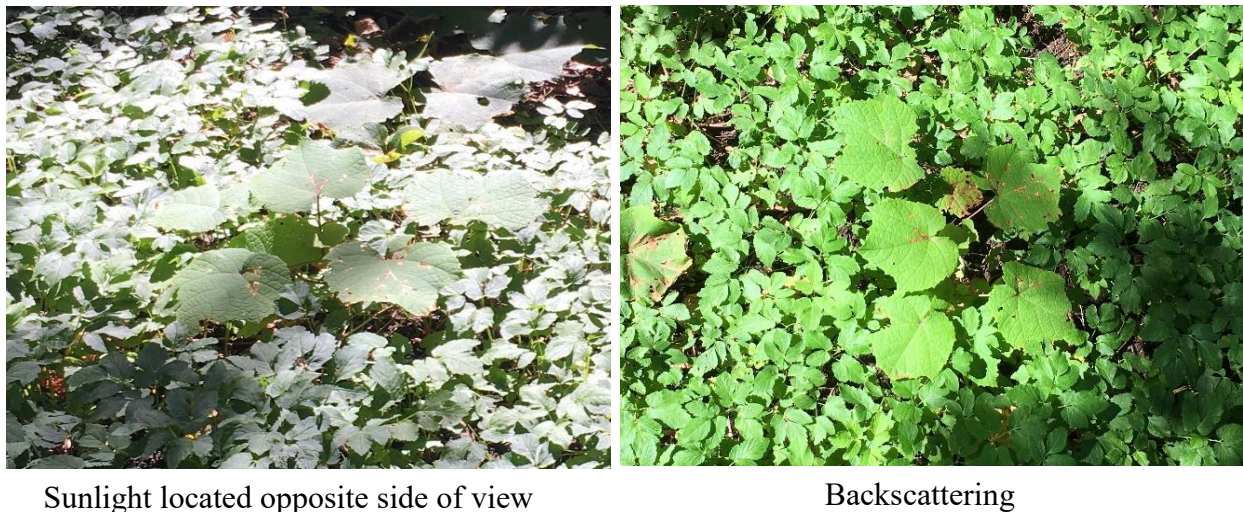


Fig. 5. Green vegetation RGB images from different observation directions

Study of the optical properties of single leaves depending on the angle of light incidence was started to investigate from 1960 by (Tageyeva S.V., 1961, 1960) and also considered as related to leaf structure (Shul'gin et al., 1960) at the almost same time. Single leaves spatial reflectance distribution was first accurately recorded for wavelengths from 450 nm to 2700 nm on philodendron, maize, and soybean leaves at different angles of illumination by (Woolley, 1971). Such measurement results discriminated white portion of reflectance which is the same understanding that reflectance is the sum of diffuse and specular reflectance components. At the same year, (Breece III and Holmes, 1971) developed setup of leaf bidirectional reflectance measurement in 19 narrow wavelength bands from 375 nm to 1000 nm and distinguished that high absorption bands have strong specular reflectance and also transmission is more like a Lambertian pattern. Although it has been quite a long time since last work, (Brakke et al., 1989) presented the first reasonable bidirectional scattering model with the physiology of the leaf and expressed a simple equation. However, measurement was made at only a single wavelength band (632.8 nm) by a laboratory goniometer. One year after similar models were investigated for single leaf scattering (Ma et al., 1990; Vanderbilt et al., 2014, 1991) that works were more related to light polarization by a surface. First complete leaf Bidirectional Reflectance Distribution Function (BRF) measurements were made by (Walter-Shea et al., 1991) and incident radiation of the painted barium sulfate plate ( $\text{BaSO}_4$ ) used for calculating relative reflectance.

The reflectance of the leaf consists not only of its intensity but also of polarization, and the polarization techniques are generally used for separating specular reflectance from diffuse reflectance. The leaves look shiny at the shallow angle, where most of this reflection is polarized from the surface of leaves. Although the leaf spectral reflectance which is a point of convergence for many types of research, the study of spectral measurement with polarization in a single leaf is largely unexplored.

### 1.1.2 Reason to start this study

Hokkaido University gives total support to space missions, from the arranging of missions and developing a mission payloads to an operation of satellites in a framework of the Asian Microsatellites Constellation program. A program goes for formation of space missions utilizing the network of specialists all over the world; proposal was put forward during the development process of microsatellites; and has been discussed by all interested Asian countries, including Japan, Philippines, Vietnam, Myanmar, Thailand, Mongolia, Malaysia, Indonesia, and Bangladesh to define it as a primary activity. Hokkaido University also proposes at organizing practical hands-on training for students who came to this university from Asian countries for remote sensing applications and space technology through lecture training until students are becoming a leader of the subproject, and thus to contribute significantly for developing space education system in participating countries of the program. While before the program implementation, the feasibility study and investigation of critical elements were also required by the next step. The main reason for writing this dissertation is that it is continuously associated with this program.

The objectives of this program are precisely in line with the Hokkaido University initiative that is to promote the awareness related to space science and technology among the faculty members and students from participating countries and universities. One of the member country Mongolia is planning to launch their first microsatellite in the near future according to National Space long term program which is approved by the Mongolian Government in 2012. National University of Mongolia (NUM) is preparing a human source of space engineering and collaborating with Japanese Universities. On the other hand, the Japan International Cooperation Agency (JICA) signed a Japanese ODA loan agreement with the Government of Mongolia in Ulaanbaatar on March 11, 2014, for the Higher Engineering Education Development Project which has enabled us to do this research and given me an opportunity to study in Japan.

## 1.2 EFFECTS OF BIOCHEMICAL CONTENTS

Every year each autumn over the northern hemisphere, the extending evenings (nights) and decreasing temperatures induce prompt to prepare for winter, and they shed billions of vast amounts of leaves in these preparations. In specific areas such as our own, the shedding of leaves is gone before by a spectacular color show. Formerly green leaves, contingent upon the species, may swing to beautiful shades of yellow, orange, and red, and in addition, brown colored. This shading changes the consequence of transformations in leaf pigments.

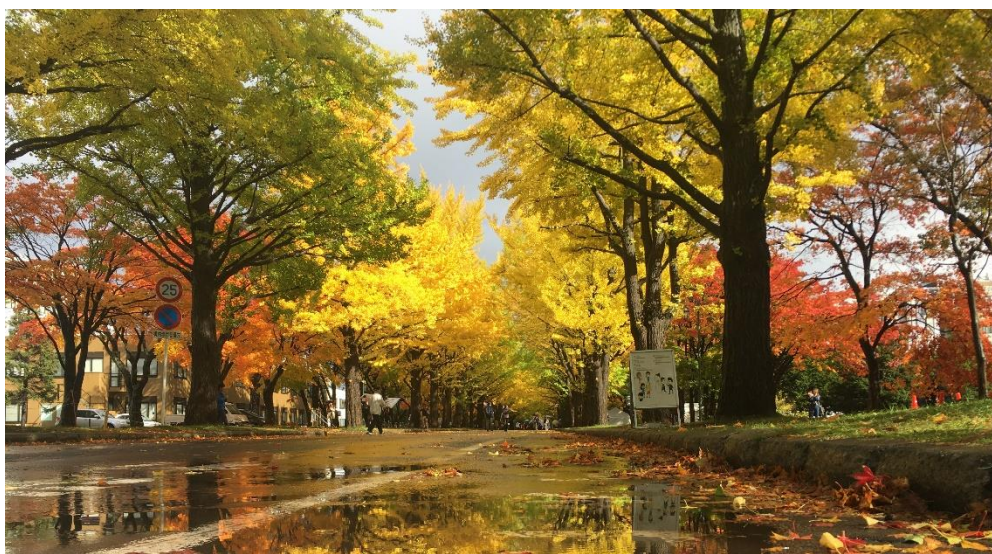
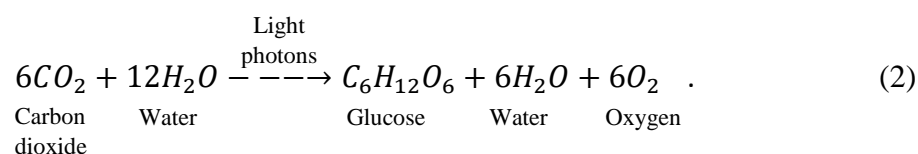


Fig. 6. Golden leaf street North 13 Gate Avenue (Gingko Avenue) at Hokkaido University on Oct, 27 2018.

Leaves contain an astounding assortment of pigment molecules, definitely more than other species. Vegetation leaves are creatures of light color in nature. Leaves utilize light to control their growth and quick reactions to the environment, and they convert light as their source of energy. Vegetation creates pigments to advertise for creatures which fertilize flowers and scatter seeds. In this manner, pigments may have physiological or potentially organic capacities. There are four types of pigments present in the leaves of vegetation, and their maintenance or creation decides the colors of leaves before they tumble from, molecules, past the straightforward chemical formulas that depict the quantities of atoms of various components making up the molecule. Glucose can be obtained as a lump of sugar, and most generally are one portion of the usual table sugar which is a disaccharide. Increasingly confused outlines will be shown to represent the structures of the four types of pigments, these are present during the aging of leaves. Names of pigments are chlorophylls, carotenoids, lutein, and anthocyanins; perhaps lutein is similar to carotenoids chemically.

The primary reason why the healthy leaves are green is the chlorophyll (green pigment) which absorbs red and blue colors from the daylight that decreases on leaves. Accordingly, the light reflected by the leaves is reduced in red and blue and seems green. So chlorophyll is a green photosynthetic pigment contained in plants, algae, and cyanobacteria. This pigment separates similar two pigments, chlorophyll a and chlorophyll b (the sum of these two is the total chlorophyll). The molecules of these compounds are  $C_{55}H_{72}MgN_4O_5$  for chlorophyll a, and  $C_{55}H_{70}MgN_4O_6$  for chlorophyll b respectively. The molecules of these two chlorophylls are joined to the membranes of plate-like structures, called chloroplasts, inside the cells. Chloroplasts are the site of photosynthesis, the procedure in which light energy is changed to chemical energy. In chloroplasts, the light absorbed by chlorophyll pigments the energy utilized by vegetation to change  $CO_2$  and water into oxygen and sugars, which can be written by chemical formula as



Various type of carotenoids exists in leaves such as beta-carotene, lutein, and zeaxanthin. Carotenoids are plant pigments in charge of bright red, yellow and orange tints in numerous foods grown from the ground. These pigments assume an essential job in plant health. Individuals who eat foods containing carotenoids get defensive health advantages also. These leaves pigments absorb blue-green and blue light and the light reflected from them in this way seems yellow. Like the chlorophylls, carotenoids are also big molecules and are additionally contained in the chloroplasts. Some are hydrocarbons, compounds that contain just carbon and hydrogen, for instance, beta-carotene  $C_{40}H_{36}$ . Others, called xanthophyll, contain atoms in addition to carbon and hydrogen, an example being lutein  $C_{40}H_{56}O_2$ , which likewise contains oxygen. The carotenoids capacity to shield chlorophylls from oxidation and as accessory absorbers (Ougham et al., 2005). These pigments absorb energy from the light of different colors than that absorbed by chlorophyll, and the energy they absorb is exchanged to chlorophyll. Since leaves contain considerably more chlorophyll than carotenoids, the carotenoids have little impact on the color of the leaves.

The last group of pigments that happens in leaves is the anthocyanins which absorb blue, blue-green, and green light. Anthocyanin is one of the flavonoids, but there are examples of people who call flavonoids generally called Anthocyanin. Plants accumulate anthocyanin in



leaves when they have some abiotic stresses such as intense light or low temperatures. Anthocyanin functions as an antioxidant, and it also has some light shielding effects when the environmental light is too strong compared with the metabolism. When the temperature is low, plants feel usual light intensity too high because they cannot metabolize the products of photosynthesis. In fruits and flowers, anthocyanins may be a color signal for insects and animals. In this manner, light reflected by leaves containing anthocyanins seems red.

In contrast to the chlorophylls, and the carotenoids, anthocyanins not appended to cell membranes. They are produced in the cell by an energy-consuming procedure that is initiated by light. As they are made, anthocyanins are released into the cell sap. Anthocyanin pigments are in charge of the red skin of ripe apples and the purple of ripe grapes. Since exposure to light is required to create the red pigment, apples regularly seem red on the single side and green color on the other, the red color side was in the sun, and the green color side was in the shade. Similarly, leaves on trees are reddest on the bright side.

This thesis is mainly about the optical properties of the leaf and light polarization on leaves, due to these pigments how to influence the color of the leaves is essential. These pigments need to be considered into account when they are in the leaves optically. The Specific Absorption Coefficient (SAC) is used in utilized estimations for modeling the optical property of leaves. One of its applications in science is for evaluating the concentration, such as of the chlorophyll pigments when absorbances of the pigment sample are resolved through a spectrophotometer. To get the specific absorption coefficient, the pigment is first filtered from contaminants and

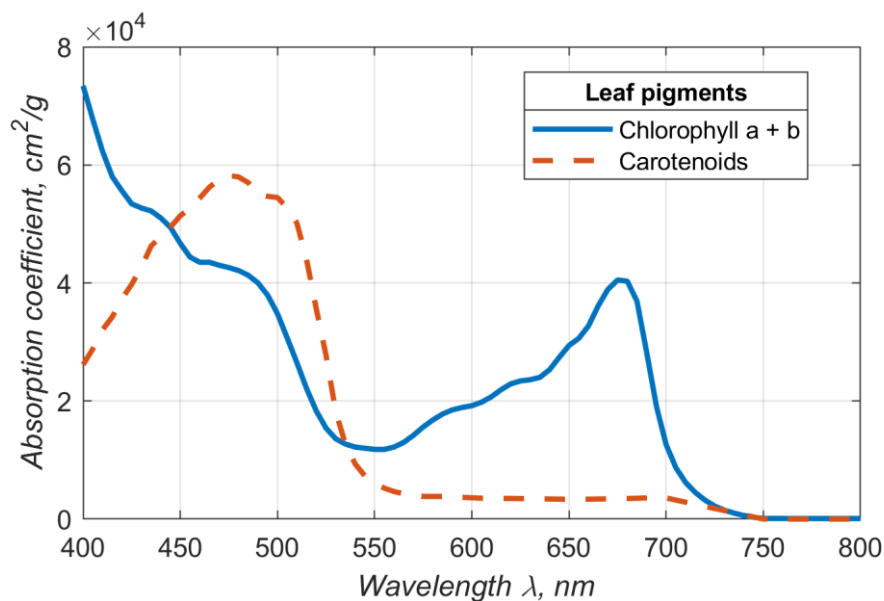


Fig. 7. Specific absorption coefficient (SAC) of chlorophylls a,b and carotenoids (Jacquemoud et al., 1996).

then dissolved in a specific solvent. After the pigment is sanitized, its absorbance is estimated utilizing a spectrophotometer. This value would then fill in as the all-inclusive standard while evaluating pigment concentrations from absorbance measurements. Fig. 7 shows SAC of chlorophylls a, b and carotenoids (Jacquemoud et al., 1996) in the wavelength region from 400 nm to 800 nm and after near infra-red light of the electromagnetic waves, the absorption of these pigments are non-calculable low that almost equal to zero relatively.

By observing the amount of pigment within the leaves, the modeling of the optical properties using mathematical methods plays a major role in remote sensing. Such kind of work was first established by (Allen et al., 1969) when he estimated the effective index of refraction and an absorption coefficient of a corn leaf by inverting the plate model on the geometric optic. Most of the papers have focused on spectral reflectance and transmittance of the leaf in connection with their chlorophyll content, water, dry matter, cellulose, nitrogen content and their structure of layers. Based on these research works, a radiative transfer model PROSPECT has been designed by (Jacquemoud and Baret, 1990), which has widespread usage in the remote sensing community and based on Allen's generalized "plate model" consider in the optical visible and infra-red band from 400 nm to 2500 nm. This optical region is divided into three parts by the absorption property of contents (Jacquemoud and Ustin, 2001). 400-800 nm visible light (VIS) and near infra-red (NIR) has a strong absorption by photosynthetic chlorophyll and other pigments in the leaf. 800-1100 nm near infra-red where absorption is limited to dry matter but where be multiple scattering within the leaf. 1100-2500 nm middle infrared also has strong absorption by water in a fresh leaf and dry matter. From such separation, pigment contents

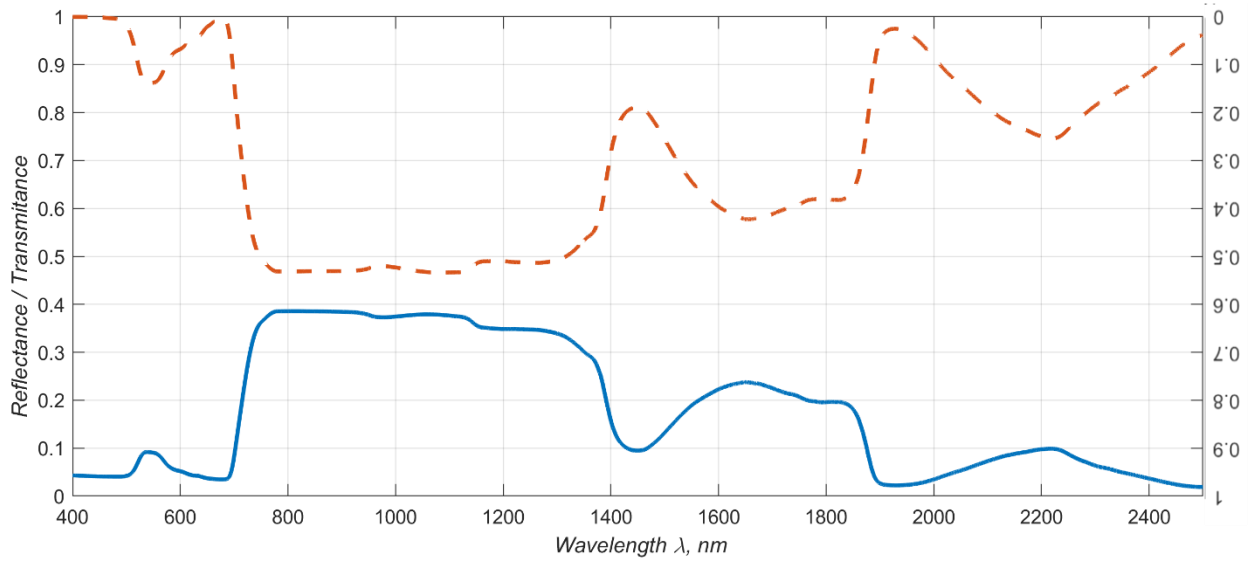


Fig. 8. Prospect D model's simulation results; Input parameters of model simulation were about the structure coefficient 1.2, chlorophyll content  $50 \mu\text{g}/\text{cm}^2$ ,  $C_{ab} = 50$ , carotenoid content  $10 \mu\text{g}/\text{cm}^2$ , Anthocyanin content  $1.0 \mu\text{g}/\text{cm}^2$ , brown pigment content 0.0 (unitless), Equivalent Water Thickness (EWT) 0.015 cm, Leaf Mass per Area (LMA)  $0.009 \text{ g}/\text{cm}^2$  respectively.

occupy the most important role on the leaf spectral reflectance that has a weak correlation with water and dry matter content in the VIS and NIR.

Biochemical and optical properties of leaves (fresh or dry) estimated to explore the capability of remote sensing to estimate the leaf biochemistry from space. The hemispherical reflectance and transmittance measurements with the integrating sphere are generally required from 400 nm to 2500 nm utilizing a research laboratory spectrophotometer. The measure of chlorophyll, water, protein, cellulose, hemicellulose, lignin, and starch is determined on leaves using standard wet chemistry techniques for approving optical estimation and demonstrating.

### 1.3 EFFECTS OF THE LEAF BIOPHYSICAL STRUCTURE

Radiation scattered by leaves and exiting the plant's canopy toward the sensor is influenced by canopy biophysical structure. The majority of the current methods and models to relate canopy reflectance and leaf biochemical constituents utilize statistical methodologies. The most considerable weakness of biochemical based methods is the absence of causal mechanisms that relate satellite data and leaf biochemistry. Although statistical relationships are significant, that can be counterfeit (Knyazikhin et al., n.d.; Lloyd et al., 2013) and that can lead to misinterpretation of satellite information. Radiative transfer theory-based methodologies give physically strong linkage between biophysical parameters and canopy reflectance and can usually recognize causality from a connection. Their improvement is required to take a full favorable position of accessible and future satellite information.

The surface of the leaves, are crinkly, veined, convex, or hairy, and is also vary greatly depending on their type on and morphological structures in nature. If we consider cutting a small part of the leaf area, a surface can be smooth to touch no apparent surface rough, perceptible rough, or hairy (trichomes). The rough surface of the leaf mainly connects with a mechanism of water drops and adhesion (Wang et al., 2014); however another essential responsibility of leaf rough is to increase solar harvesting efficiency into internal leaf photosynthesis (Huang et al., 2015).

Every leaf is covered oil-like (polymer) transparent compounds which are the outermost layer and secretes a waxy substance called the cuticle (See Fig. 10). This is the most critical layer since our study looks at the optical side of the leaf. Cutin and suberin are cell wall-associated glycerolipid polymers that are explicit to plants. Cutin forms the system of the cuticle fixing the aerial epidermis, while suberin is available in the periderm of barks and underground organs. Suberised dividers are likewise found in the root endodermis. Barriers dependent on cutin and suberin confine the transport of water and solutes across cell walls and limit pathogen occupations. Chemical investigation demonstrates that both polymers are polyesters composed the most part out of fatty hydroxyacids, diacids and epoxyacids esterified to each other and to glycerol (Li-Beisson et al., 2016).

The light from the sun firstly encounters an outer layer of the leaf, which is a transparent layer, it means optical property of the waxy cuticle is similar to glass. Although we can see the upper epidermis and mesophyll layers, the reflectance on the leaf increases

dramatically at a sharp illumination angle. In this case, we must consider the polarization of reflected light on the leaves. Polarized reflectance from a leaf is a surface phenomenon emanating from light scattered at the air-cuticle interface, the first refractive discontinuity encountered by incident radiation. So the polarized light component is reflected by the leaf surface (wax cuticle), not by its internal scattering (Grant et al., 1993, 1987; Vanderbilt and Grant, 1985). Most previous investigations of leaf reflectance have measured total reflectance, which includes both the reflectance from the surface and the reflectance from the inner structure of the leaf. Estimating the polarized leaf reflectance permits separation of the surface component of reflectance from light reflected from the heft of the leaf tissue. Two light scattering mechanisms can contribute to this polarized reflectance. These are specular reflectance and molecule scattering. The cuticle helps leaves retain water inside the leaf cells.

The amount of reflected light on the flat and smooth surface can be calculated by Fresnel's equations, which describe reflections and transmissions of electromagnetic waves at an interface and also describe polarized reflectance along to parallel and perpendicular directions. The primary parameter of these equations is a refractive index. (Kuusk, 1994; Vanderbilt and Grant, 1985) calculated refractive index (real part) of the waxy cuticle layer. Refractive index of wet mesophyll cell wall computed utilizing the Dale and Gladstone law (Baranoski, 2006), and considering refractive indices of water provided by (Palmer and Williams, 1974) as well as the refractive index of a dry mesophyll cell wall, which was

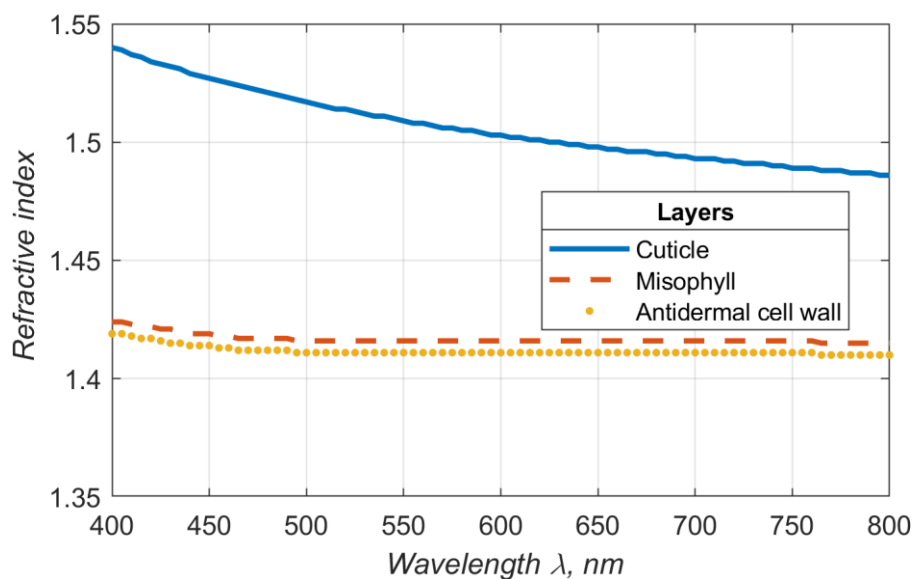


Fig. 9. Real part of refractive indices of the epicuticular wax, wet mesophyll cell wall, and the wet antidermal cell wall (Kuusk, 1994; Vanderbilt and Grant, 1985; Palmer and Williams, 1974; Woolley, 1975).

estimated to be 1.5479. This value was likewise gotten utilizing the Dale and Gladstone's law and considering the refractive index of wet mesophyll cell walls measured by (Woolley, 1975) at 800nm equal to 1.415 (Woolley, 1975). Refractive index of the wet antidermal cell wall, computed using expressions showed in work by Baranoski (2006), and the refractive index of water provided by Palmer and Williams. Fig. 9 shows mentioned real part of refractive indices in the wave region from 400 nm to 800 nm. Previous all computational the refractive index values are started from 400nm to 2500 nm, with a step of 5 nm.

Upper epidermis is a solitary layer of cells containing few or no chloroplasts. The cells are very transparent and allow the most of the light that strikes them to go through to the underlying cells. The epidermis houses the monitor cells which manage the movement of water into and outside cells. Guard cells do so by controlling sizes of the pores likewise called stomata. Epidermis layer covers the upper and lower surfaces of the leaf. Ordinarily, a solitary of tightly-packed cells, the epidermis mediates exchanges between the plant and its condition, constraining water loss, controlling gas exchange, transmitting daylight for

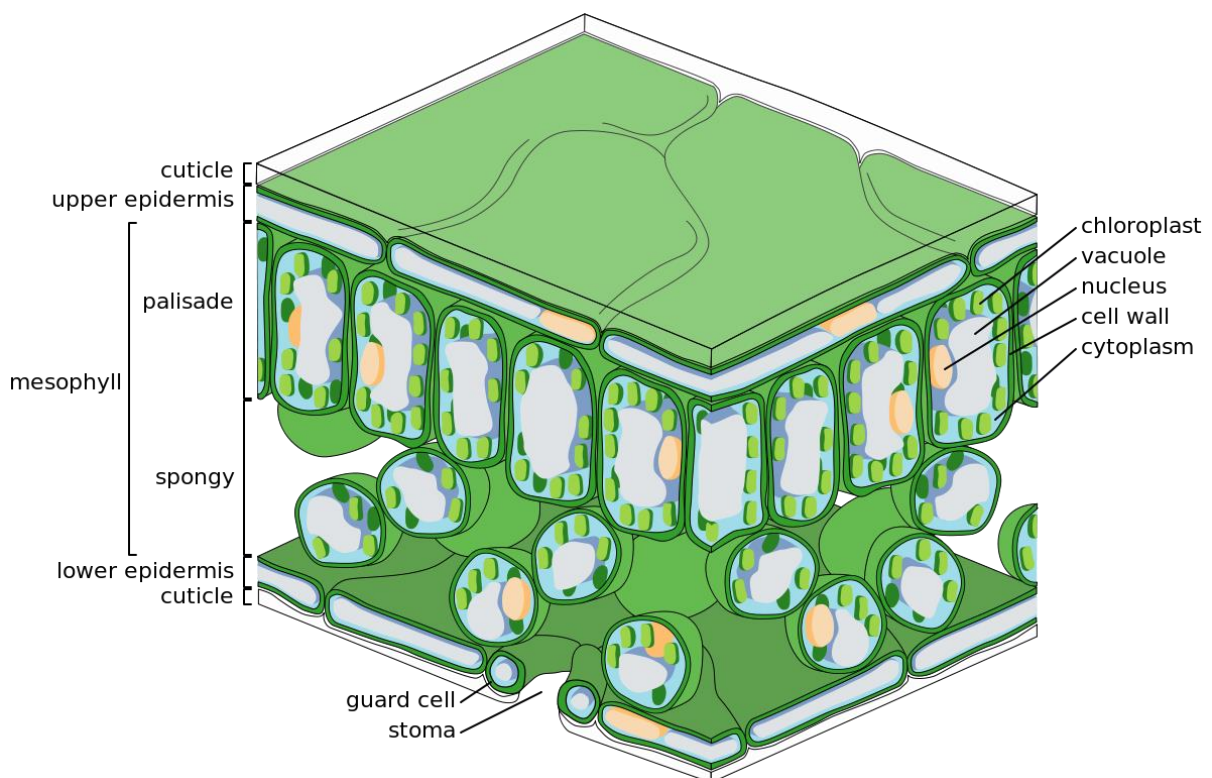


Fig. 10. Representation of tissue structure of tree leaf. The fine-scale structure of a leaf including the significant tissues; the upper and lower epithelia (and related cuticles), the palisade and spongy mesophyll and the guard cells of the stoma. Vascular tissue (veins) doesn't appear. Key plant cell organelles (the cell wall, nucleus, chloroplasts, vacuole, and cytoplasm) additionally appear. Photo credit goes to Zephyris - commons.wikimedia.org.

photosynthesis, and demoralizing herbivores. The epidermis has a tiny waxy cuticle of cutin, which confines vanishing of water from the leaf tissue. This layer might be thicker in the upper epidermis contrasted with the lower, and in dry air compared to wet ones. As noted in the section on adaptation, epidermal hairs can debilitate herbivores, limit the effects of wind, limit the impacts of wind, and trap a layer of moisture to reduce water loss.

Mesophyll forms the center layer of the leaf and is separated into two layers depending on the sort of cells found. These are palisade and spongy mesophyll layers. The palisade contains the chloroplast, which are cell organelles that contain chlorophylls which are required for photosynthesis. The vascular tissues of the leaves are contained in the sporadically orchestrated springy mesophyll cells. Vascular Tissue is indeed found in the veins of the leaf. The vascular tissues are made out of xylem and phloem which are in charge of transport of water and nourishment.

#### 1.4 REFLECTANCE DEFINITIONS AND OBSERVATION GEOMETRY

The essential for physically based, quantitative examination of airborne and satellite sensor estimations in the optical domain is their calibrations to spectral radiances. The spectral radiance is the radiant flux in beams per unit wavelength, and per unit area and solid angle of that beam and is expressed in the SI units [ $\text{W m}^{-2} \text{sr}^{-1} \text{nm}^{-1}$ ]. The proportion of the radiant exitance ( $M$  [ $\text{W m}^{-2}$ ]) with the irradiance ( $E$  [ $\text{W m}^{-2}$ ]) results in the so-called reflectance. Following the law of energy conservation, the estimation of the reflectance is in the comprehensive interval 0 to 1. The reflectance factor is the proportion of the radiant flux reflected by a surface to that reflected all way direction same reflected-beam geometry and wavelength range by an ideal (lossless) and diffuse (Lambertian) standard surface, lighted under similar conditions. For estimation purposes, a spectral board usually approximates the perfect diffuse standard surface. Reflectance factors can achieve values beyond 1, especially for strongly forward reflecting surfaces such as snow (Painter and Dozier, 2004). BRF is defined as the ratio between radiant flux,  $d\Phi_r$  of the leaf and an ideal radiant flux,  $d\Phi_r^{id}$  which would be reflected by an ideal (lossless) lambertian surface (Nicodemus et al., 1977; Schaepman-Strub et al., 2006; Walter-Shea et al., 1989).

$$BRF(\theta_i, \phi_i, \theta_r, \phi_r, \lambda) = \frac{d\Phi_r}{d\Phi_r^{id}} = \frac{dA \int_{\omega_r} \int_{\omega_i} f_r(\theta_i, \phi_i, \theta_r, \phi_r, \lambda) L_i(\theta_i, \phi_i, \lambda) d\Omega_r d\Omega_i}{\frac{dA}{\pi} \int_{\omega_r} \int_{\omega_i} E(\theta_i, \phi_i, \lambda) d\Omega_r d\Omega_i} \quad (3)$$

Eq. (3) where  $E(\theta_i, \phi_i, \lambda)$  is incident radiance coming from the light source, and an ideal Lambertian surface reflects the same radiance all way direction.

When those radiant fluxes are measured with the same device, the surface area  $dA$  of reflected flux must be same as ideal Lambertian surface area  $dA$ . The corresponding Eq. (3) BRF is  $\pi$  times higher than the Bidirectional Reflectance Distribution Function (BRDF). Reflectance factor becomes a ratio of the reflected radiance of the target leaf to the reflected radiance of an ideal Lambertian surface at the identical view and illumination geometry.

Azimuth view  $\phi_r$  and azimuth incident  $\phi_i$  angles are relative to the coordinate system, however, these two angles can be replaced by relative azimuth  $\phi = \phi_i - \phi_r$  in a laboratory measurement. We added new parameter polarizer rotation angle  $\alpha$  on the BRF measurement for relationship bewtween bidirectional reflectance and polarization. This additional variable doesn't change definition the of relevant quantities, and the number of measurements will



increase at the one point. We accept further that an isotropic behavior infers a spherical source that radiates the same in all directions, i.e., the intensity [ $\text{W sr}^{-1}$ ] is the same in all directions, whereas the diffuse (Lambertian) behavior refers to a flat reflective surface. Consequently, the intensity falls off as the cosine of the observation angle with respect to the surface normal (Lambert's law) and the radiance  $L$  [ $\text{W m}^{-2} \text{sr}^{-1}$ ] is independent of direction. Be that as it may, the proportion of the radiant exitance  $M$  [ $\text{W m}^{-2}$ ] to the radiance  $L$  [ $\text{W m}^{-2} \text{sr}^{-1}$ ] of an ideal Lambertian surface is a factor of  $\pi$ .

$$BRF(\theta_i, \phi, \theta_r, \lambda, \alpha) = \pi \cdot BRDF(\theta_i, \phi, \theta_r, \lambda, \alpha) = \frac{L_r(\theta_i, \phi, \theta_r, \lambda, \alpha)}{L_r^{id}(\theta_i, \lambda)} \quad (4)$$

where  $L_r^{id}$  is reflected the radiance of ideal Lambertian (diffuse) surface and doesn't not depend on relative azimuth, zenith view, and polarizer rotation angle. For an ideal Lambertian surface, the high electron density of barium sulfate is selected, it is white crystalline powder which has a long tradition as a standard material for diffuse reflectance measurements. Reflected radiance  $L_r^{id}$  can be written from the incident angle  $\theta_i$  as (Walter-Shea et al., 1989):

$$L_r^{id}(\theta_i, \lambda) = \frac{L_r^{Ba}(0, \lambda) \cdot \cos \theta_i}{\rho^{Ba}} \quad (5)$$

where  $L_r^{Ba}(0, \lambda)$  is a spectral radiance of BaSO<sub>4</sub> plate at illumination from the highest position ( $\theta_i = 0$ ) and  $\rho^{Ba}$  is the reflectance of the barium sulfate plate which was determined by laboratory measurement in lots of papers. For instance, the reflectance comparison between the pressed powder plate and coating paint plate was investigated by (Grum and Luckey, 1968) and Fig. 12 shows reflectances. There was no huge difference between two plates and reflectance

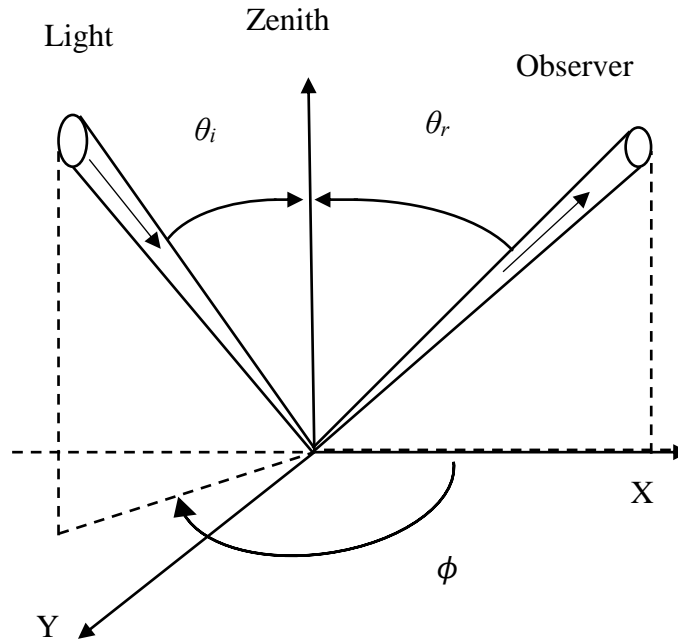


Fig. 11. Representation definitions of illumination and observation geometry. Where  $\theta_i$ ,  $\phi$  are source zenith and relative azimuth angles, respectively, and  $\theta_r$  is view zenith. LCTF camera is positioned at view zenith  $\theta_r$  and fixed at azimuth  $0^\circ$  in a spherical coordinate system.

value is higher than 99.2% for both plate in our measurement band. Spectral shape of the reflected radiance of BaSO<sub>4</sub> should be same as spectral irradiance of the light source for the reason that the reflectance of barium sulfate is very nearly 100%.

Spectral radiance is based on the digital number of one pixel by next chapter of this dissertation, and one pixel's ground FOV is 0.15x0.15 mm for nadir view. If observation view zenith angle  $\theta_r$  is going to increase (slope view), vertical side of ground FOV will be divided by  $\cos\theta_r$ . When the viewable (visible) area decreases at the shallow angle, on the other hand, the area corresponding to a pixel increases so that radiance will be constant in this case. Radiances of at least 45 pixels are averaged from a visible area of the leaf for reducing the error of measurement and number of pixels depends on view zenith angle  $\theta_r$ .

The Directional Hemispheric Reflectance factor (DHRF) has an important role for measuring the optical property of the leaf; it is often measured by spectrophotometer equipped with integrating spheres (Pickering et al., 1992). In this analysis, DHRF is defined as:

$$DHRF(\theta_i, \lambda) = \int_0^{2\pi} \int_0^{\pi/2} BRDF(\theta_i, \phi, \theta_r, \lambda) \times \cos\theta_r \sin\theta_r d\theta_r d\phi \quad (6)$$

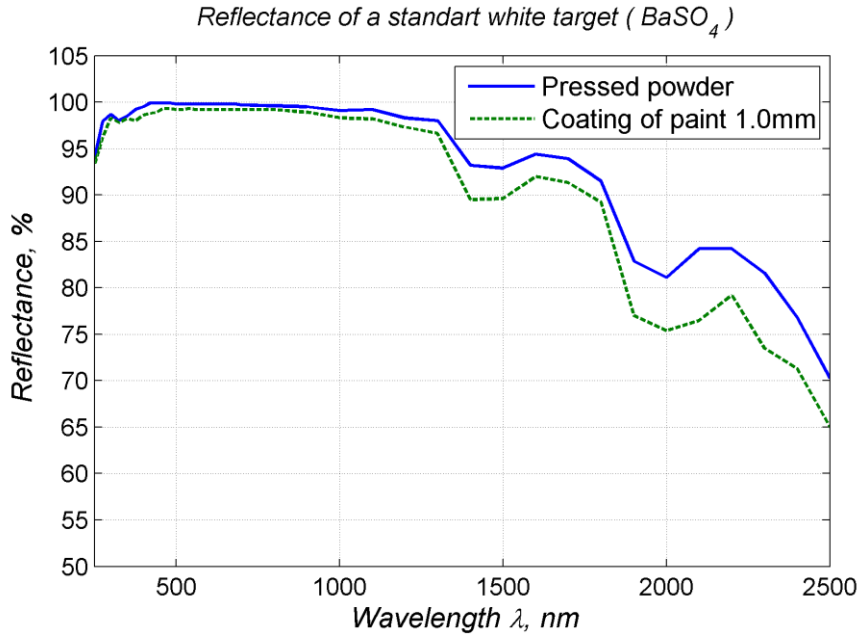


Fig. 12. Reflectance of barium sulfate plate ( $\rho^{Ba}$ ) (Grum and Luckey, 1968)

### 1.5 STOCK'S PARAMETERS AND POLARIZATION

The reflectance of the leaf can describe not only regarding its intensity but also in terms of its polarization and polarization techniques are generally used for separating specular reflectance from diffuse reflectance. (Grant et al., 1987) measured that polarized reflectance is no constant value on leaves of *Sorghum bicolor* and the difference probably associated with variations in details of the property of the leaf surface. Although the polarized reflectance is not equal to specular reflectance, it gives information about the canopy of the leaf and a chance to estimate specular reflectance. Using this method, (Brakke, 1994) summarized as there is no relationship between specular reflectance and pigment content inside a leaf, specular compounds have no difference in the VIS and NIR, and the diffuse compound is small in VIS band. The main dependence of BRDF measurement shape caused on the specular reflectance by waxy cuticle which is the outer surface layer of leaves. (Bousquet et al., 2005) found specular component's BRDF shape is mainly driven by a surface roughness of the leaf in the wavelength

range from 480 to 880 nm. Specular compound not correlated with the wavelength which means the surface of the leaf is optically non-dispersive in that band.

Radiances of polarized and unpolarized portions are originally defined on boundary radiance values of the reflected light, and ratio of those portions is a degree of linear polarization (DoLP) which is given by:

$$DoLP = \frac{L_{max} - L_{min}}{L_{max} + L_{min}} = \frac{R_{max} - R_{min}}{R_{max} + R_{min}}, \quad (7)$$

where reflectance factors can replace radiance values using Eq. (3), the unpolarized factor is equal to the minimum of reflectance factor ( $R_{up} = R_{min}$ ), and the polarized reflectance factor is the difference between maximum and minimum of reflectance factor ( $R_p = R_{max} - R_{min}$ ). Although the original definition of DoP is precise, it requires a lot of polarizer directions. Another way is that the polarization property of reflectance can be described by Stokes parameters ( $I$ ,  $Q$ ,  $U$ , and  $V$ ).  $V$  describes the circularly polarized reflectance, therefore, this parameter usually can be neglected for light reflection on the leaf (Talmage and Curran, 1986; (Sun et al., 2017a).

$$I = (L_{0^\circ} + L_{45^\circ} + L_{90^\circ} + L_{135^\circ})/2, \quad (8.a)$$

$$Q = L_{0^\circ} - L_{90^\circ}, \quad (8.b)$$

$$U = L_{45^\circ} - L_{135^\circ}, \quad (8.c)$$

$$DoLP = \sqrt{Q^2 + U^2}/I = -Q/I, \quad (8.d)$$

where  $L_{0^\circ}$ ,  $L_{45^\circ}$ ,  $L_{90^\circ}$  and  $L_{135^\circ}$  are obtained for  $0^\circ$ ,  $45^\circ$ ,  $90^\circ$ , and  $135^\circ$  linear polarizer directions those angles are relative to the vertical axis of camera lens plane (see Fig. 21), and the meaning of  $I$  is the total reflected radiance ( $I = L_r^{total}$ ). The sum of polarized and unpolarized radiances are the total radiance ( $L_{total} = L_p + L_{up}$ ) those two parts can be found below:

$$L_p = \sqrt{Q^2 + U^2}, \quad (9.a)$$

$$L_{up} = I - \sqrt{Q^2 + U^2}. \quad (9.b)$$

The polarized reflectance factor is able to express by the polarized reflected radiance with a barium sulfate reference:

$$R_p(\theta_i, \phi, \theta_r, \lambda) = \frac{L_p(\theta_i, \phi, \theta_r, \lambda)}{L_r^{Ba}(\lambda) \cdot \cos\theta_i}, \quad (10.a)$$

$$R_{up}(\theta_i, \phi, \theta_r, \lambda) = \frac{L_{up}(\theta_i, \phi, \theta_r, \lambda)}{L_r^{Ba}(\lambda) \cdot \cos\theta_i}. \quad (10.b)$$

## 1.6 COOK-TORRANCE COMPUTER GRAPHICS MODEL

The research of scattering from the rough surface is a continuously active area in optics (Simonsen, 2010). There is two type of surface roughness theory: The prevalent model in computer graphics is the Cook-Torrance (Cook and Torrance, 1981) that based on the assumption that surface micro-geometry acts as a set of specular mirrors; Another type of models are widely used in the optics community, compute diffraction effects caused by differences in height in the surface micro-geometry and predicts visual appearance from the frequency content of the height distribution (Holzschuch and Pacanowski, 2016).

Reflection of smooth surfaces, for example, mirrors or a calm body of water makes to a type of reflection known as specular reflection. Reflection of rough surfaces such as clothing, paper, and the asphalt roadway makes to a kind of reflection known as diffuse reflection. Regardless of whether the surface is microscopically rough or smooth has a colossal effect upon the consequent reflection of light emission. However, in terms of optical properties of the leaves, specular component directly connects to light reflection on the surface of the leaf, especially on the most exterior surface in most previous studies (Bousquet et al., 2005; Brakke, 1994; Combes et al., 2007; Grant et al., 1987). Because the diffuse component connects the scattering of the pigments in the leaves, it is thought that this reflection will be equal to all way directions (Lambertian). Since these two components contain both a spectral and a bidirectional property, we need to identify specular and diffuse reflection components and to look at surface roughness effects. It will allow to survey the spectral invariance of the specular component and to assess the amount of light reflected.

The total BRDF is equal to the sum of specular and diffuse reflectance factors, which is written as

$$BRF_{total} = BRF_{spec} + BRF_{diff}. \quad (11)$$

Prior to studies of bidirectional property, the diffuse component is no correlation with observation angles and it is a diffuse component. Researchers of this type of study planned to infer a primary and general expression of bidirectional reflectance of leaves that can be utilized for model inversion or for plant canopy reflectance simulations. The diffuse reflectance shows the division of reflected light which is definitely not a solitary specular reflection at the leaf surface. The Cook-Torrance model predicts the spread of specular light rebounds at the angle of the observation plane.

Specular bidirectional reflectance factor ( $BRF_{spec}$ ) is defined in previous studies of an optical property of leaves (Bousquet et al., 2007, 2005; Comar et al., 2014; Combes et al., 2007) as

$$BRF_{spec}(n, \sigma, \theta_i, \theta_r, \phi) = \frac{F(n, \theta_a)G(\theta_i, \theta_r, \phi)}{2\pi \cos \theta_i \cos \theta_r} \times \frac{e^{-\tan^2 \beta / \sigma^2}}{\sigma^2 \cos^4 \beta} \quad (12)$$

where  $\sigma$  is roughness parameter, which is different from physical RMS surface roughness, and  $F(n, \theta_a)$  is the Fresnel factor that describes the amount of light reflected at the boundary between air and leaf surface. The Fresnel factor only represents the unpolarized light between two intervals medium:  $F(n, \theta_a)$  is defined as

$$F(n, \theta_a) = \frac{1}{2} \left( \frac{g - \cos \theta_a}{g + \cos \theta_a} \right) \left[ 1 + \frac{\cos \theta_a (g + \cos \theta_a) - 1}{\cos \theta_a (g - \cos \theta_a) + 1} \right] \quad (13)$$

where  $g = n^2 + \cos \theta_a - 1$ . In Eq. 12,  $G(\theta_i, \theta_r, \phi) = \min(1, E_1, E_2)$  with  $E_1 = \frac{2 \cos \beta \cos \theta_r}{\cos \theta_a}$  and  $E_2 = \frac{2 \cos \beta \cos \theta_i}{\cos \theta_a}$ . The angle  $\theta_a$  is a half of the phase angle between illumination and view directions, and  $\beta$  is the angle between leaf plane normal and rough surface face normal. So  $\theta_a$  is calculable by  $\beta$  using basin geometry as  $\theta_a = (\cos \theta_i \cos \theta_r + \sin \theta_i \sin \theta_r \cos \phi) / 2$ .

## 1.7 THE GENERALIZED HARVEY-SHACK SCATTERING THEORY

The single leaves reflectance models usually use the Cook-Torrance model (Bousquet et al., 2005) that is may not suitable for leaf reflectance in our observations because the surface roughness cannot be determined by the actual measurement. The Generalized Harvey-Shack (GHS) scattering theory is well studied from rebound models determined by height distribution (Krywonos, 2006) and the GHS theory is not limited to any particular wavelength range and RMS roughness value.

For the leaves, the BRF of the surface due to specular reflection by the GHS is related to the angle spread function (ASF). At a given wavelength, the leaf  $BRF_{spec}$  is can be described by (Krywonos, 2006; Krywonos et al., 2011)

$$BRF_{spec}(\theta_i, \phi, \theta_r) = \pi \cdot R(\theta_i) \cdot ASF(\theta_i, \phi, \theta_r), \quad (14)$$

where  $R$  is Fresnel reflection (or the scalar reflectance of the scattering surface) determined on a given illumination angle, and  $R$  is equal to the directional hemispheric reflectance, if the rough surface of the leaf is solitary. In ASF, the angular variables  $\theta$  and  $\phi$  can be changed by direction cosines  $\alpha$ ,  $\beta$ , and  $\gamma$  in conventional spherical coordinates by the following definitions.

$$\alpha = \sin\theta \cos\phi, \quad \beta = \sin\theta \sin\phi, \quad \gamma = \sin\theta, \quad (15)$$

where  $\phi \in [0, 2\pi]$ , and  $\theta \in [0, \pi]$ . Note that  $\alpha$  and  $\beta$  are different angles from previous sections. The above definitions can be reduced three variables to two variables by:

$$\gamma = \text{sign}\left(\frac{\pi}{2} - \theta\right) \sqrt{1 - \alpha^2 - \beta^2}, \quad (16)$$

where  $\text{sign}(x)$  is 1 for  $x \geq 0$  and -1 otherwise.

The relevant surface roughness  $\sigma_{rel}$  is not an intrinsic surface characteristic and  $\sigma_{rel}$  is given by the square root of integrating surface power spectral density (PSD) function in a disc with radius of  $1/\lambda$ , and surface PSD is the Fourier transform of the ACV (these two functions are the Fourier transform each other). When spatial frequencies are greater than  $1/\lambda$ , propagation goes to evanescent waves and completely irrelevant with regard to scattered light (Church, 1979; Harvey et al., 2012; Krywonos et al., 2011). Relevant surface roughness is then written as:

$$\sigma_{rel} = \sqrt{\int_{-1/\lambda+f_0}^{1/\lambda+f_0} \int_{-\sqrt{1/\lambda^2-(f_x-f_0)^2}}^{\sqrt{1/\lambda^2-(f_x-f_0)^2}} PSD(f_x, f_y) df_y df_x}, \quad (17)$$

where

$$f_0 = \frac{\sin\theta_0}{\lambda}, \quad \theta_0 = \theta_i.$$

If you look at the 2D projection at the top of the PSD function for an arbitrary illumination angle  $\theta_i$ , the integral circle is located at  $f_x, f_y$  -plane with a  $1/\lambda$  radius centered at  $f_0$  point.

The surface PSD is Gaussian function, and the Fourier transform of this kind of round symmetric function can be simplified that

$$PSD(f_r) = \pi l_c^2 \sigma_s^2 e^{-(\pi l_c f_r)^2}, \quad (18)$$

where  $f_r = \sqrt{f_x^2 + f_y^2}$ .

If the rotation of the leaves is not affected to the measurement, the surface of the leaf is isotropic and homogenous, the ASF is then expressed as (Johansen, 2015; Krywonos et al., 2011)

$$ASF(\beta_i, \alpha_r, \beta_r) = A(\gamma_i, \gamma_0)\delta(\alpha_r, \beta_r - \beta_0) + K(\gamma_i)S(\beta_i, \alpha_r, \beta_r), \quad (19)$$

where,  $\alpha_i$  is assumed to be zero without loss of generality,  $\delta$  is a delta function, which is equal to zero except when  $\beta_r = \beta_0$ , and  $A$  indicates the amount of light reflected to a specular direction ( $\gamma_i = -\gamma_r$ ) of the total reflected energy, and it is also included in the scattering function (or the TIS). The specular reflection function  $A$  can thus be written as

$$A(\gamma_i, \gamma_r) = e^{-(2\pi(n_1\gamma_i - n_2\gamma_r)\hat{\sigma}_{rel})^2}, \quad (20)$$

where  $n_1$  and  $n_2$  are the refractive indices of the media before and after the interface, respectively. In generally, these indices are  $n_2 := -n_1$  for reflection. Note that a scaled coordinate system is utilized in which the spatial variables are normalized by the wavelength  $\lambda$  of light (i.e.,  $\hat{\sigma}_{rel} = \frac{\sigma_{rel}}{\lambda}$ ).

In Eq. 26,  $S$  is the scattering function that describes the distribution of scattered radiance and known over the entire observation hemisphere.  $S$  is then given by

$$S(\beta_i, \alpha_r, \beta_r) = B(\gamma_i, \gamma_r)\mathcal{F}\{G(\hat{x}, \hat{y}, \gamma_i, \gamma_r)e^{-i2\pi\beta_0\hat{y}}\}, \quad (21)$$

where

$$B(\gamma_i, \gamma_r) = 1 - e^{-(2\pi(n_1\gamma_i - n_2\gamma_r)\hat{\sigma}_{rel})^2}, \text{ and} \quad (22)$$

$$G(\hat{x}, \hat{y}, \gamma_i, \gamma_r) = \frac{e^{\left(\frac{2\pi(n_1\gamma_i - n_2\gamma_r)\sigma_{rel}}{\sigma_s}\right)^2 \cdot AVC(\hat{x}, \hat{y})} - 1}{e^{-(2\pi(n_1\gamma_i - n_2\gamma_r)\hat{\sigma}_{rel})^2} - 1}. \quad (23)$$

In the previous equation, the surface ACV function of rough is written for isotropic surface and type of ACV is also a Gaussian function (similar to PSD).

$$AVC(\hat{x}, \hat{y}) = \hat{\sigma}_c^2 e^{-\left(\frac{\hat{r}^2}{l_f^2}\right)} \quad (24)$$



$K$  in Eq. 27 is the renormalization constant, is used to normalize  $S$  by assuming no energy is lost in evanescent modes, and also the scattering function will need to be renormalized in accordance with the nonparaxial scalar diffraction theory. It is verifying that energy not left in the specular reflection is in the scattered term, and is the renormalization constant for the scattering function is given by

$$K(\gamma_i) = B(\gamma_i, \gamma_0) \left( \int_{-1}^1 \int_{-\sqrt{1-\alpha^2}}^{\sqrt{1-\alpha^2}} S(\beta_i, \alpha, \beta) d\alpha d\beta \right)^{-1}. \quad (25)$$

The goal of authors of this work is not to develop the GHS surface scatter theory, but this theory will be used in the future to demonstrate the suitability of the single leaf surface roughness. The surface area of our measurements was teeny compared to other similar BRDF measurements, so we were replaced the prevalent micro-geometry models by the GHS scatter method in this work. Although various commercial optical software such as the ASAP, Trace-Pro, ZEMAX, and FRED are used as a method of the Harvey–Shack BRDF model, numerical implementation was made for leaf specular BRDF in Matlab. This code is based on work of (Johansen, 2015) who demonstrates how to implement the GHS surface scattering theory for isotropic rough surfaces using the Discrete Ordinates Method in Python. A more detailed understanding and concepts were obtained from the original papers of Harvey’s group (Harvey, 2012, 1977; Harvey et al., 2010; Krywonos, 2006; Krywonos et al., 2011).

## 1.8 THE PURPOSE OF THE INVESTIGATION

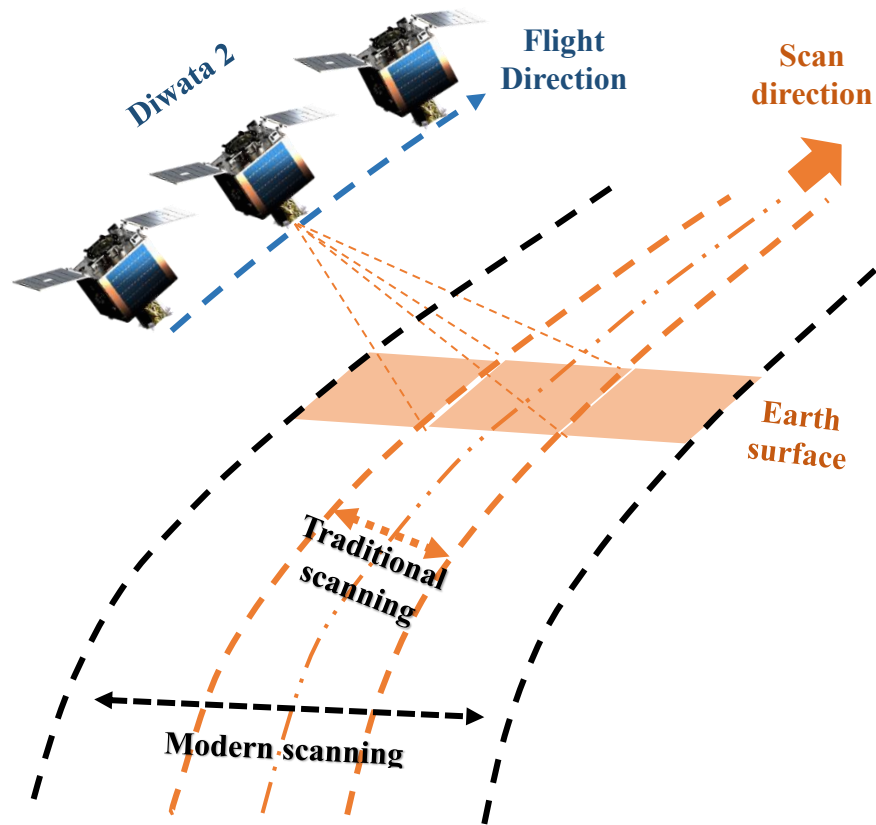


Fig. 13. Imaging operation mode of modern Earth observation satellite. For instance: Diwata-2 Philippine microsatellite (from Hokkaido University).

Earth observation satellites typically look straight down (nadir), although modern satellite became able to take an image from arbitrary direction using attitude determination control system (ADCS). For instance, the Landsat 8 satellite images the entire Earth every 16 days in an 8-day offset, and data are acquired in 185 km swaths and segmented into  $185 \text{ km} \times 180 \text{ km}$ . Modern satellites can take a larger area by taking multiple pictures of certain areas and changing view angle. Fig. 13 shows imaging operation mode of modern Earth observation satellite.

The leaf surface is tiny from space, although the sum of each leaf reflection felt like the total incoming intensity for the camera. Previous measurements on BRDF of vegetation can divide into three by field of view or distance between target and data collector (ex: camera, spectrophotometer). Long distance measurements are often collected from satellite (or plane, or drone) and needed to consider an atmospheric radiative transfer. Medium distance is measured one kind of the whole plant that characterized by a leaf area index and leaf angle distribution; Short distance or single leaf is usually measured in a laboratory. From such

measurements, many models have been published during the last two decades, but the most popular is the single leaf bidirectional reflectance model (Bousquet et al., 2005) which is combined with PROSPECT model. These two models give a chance to determine spectral and directional reflectance by ground observation sensors regarding leaf biochemical contents and canopy structure. Radiation scattered by leaves and exiting the plants canopy toward the sensor is influenced by canopy biophysical structure. The majority of the current methods and models to relate canopy reflectance and leaf biochemical constituents utilize statistical methodologies. The largest weakness of biochemical based methods is the absence of causal mechanisms that relate satellite data and leaf biochemistry. Due to single leaf BRDF modeling is still most important to study and develop it.

### 1.8.1 Motivation and goals for writing this thesis

The goal of this dissertation is to introduce a spectro-polarimetric BRF measurement of leaves using Liquid Crystal Tunable Filter camera in a laboratory and to verify directional optical properties how consistent with previous works. The contrast of this work is that the camera is being used for the first time in a single leaf BRF measurement, as well as the spectrum signature and polarization both are considered in this dissertation. However polarization method is not new for measuring vegetation, with LCTF camera measurement can be made more accurately than the traditional spectrophotometric analysis, and the combination between spectral measurement and polarimetry experiments is quite unique for modeling of an optical property of the leaf. We were committed to fulfilling the following goals:

- In any case, since it is basically difficult to record reflectance at all angles, the BRDF is rather evaluated as a function of multiple reflectance data acquired at discrete points. In the field, and also in laboratory experiments, the direct measurement of bidirectional reflectance factor is recorded with the guidance of a goniometer, which is an instrument that positions a sensor to obtain spectral measurements over a full scope of viewing angles. The subsequent BRDF of an objective yields important information about the physical structure of the object that can't be created from single-point spectral measurements (Barnsley et al., 1994; Combal et al., 2003). For this reason, our first goal is to create a new measuring goniometer system, which is suitable for Liquid Crystal Tunable Filter (LCTF) camera with polarization filters.
- Polarimetric systems are a well-established technique in a variety of systems for improving the visibility of objects such as differentiating specular and diffuse reflection,

edge identification between objects and background and discrimination between metal and dielectric surfaces. Although the leaf spectral reflectance which is a point of convergence for many types of research, the study of spectral measurement with polarization in a single leaf is largely unexplored. Our another plan is to introduce a spectro-polarimetric BRDF measurement of leaves using Liquid Crystal Tunable Filter camera in a laboratory. Such kind results will be totally new for optical property of single leaves.

- We mentioned that the reflectance of the leaf consists not only of its intensity but also of polarization. The leaf BRDF intensity was measured (Bousquet et al., 2007, 2005, Comar et al., 2014, 2012; Combes et al., 2007; Peltoniemi et al., 2005; Weiss and Baret, 1999) or the canopy polarization measured alone for whole vegetations (Dong et al., 2018; Sokolov et al., 1999; Sun et al., 2018) in many articles and the polarization of reflected light on the leaf was well studied by (Grant et al., 1993; Vanderbilt et al., 1991; Vanderbilt and Grant, 1985; Vern C. Vanderbilt and Lois Grant, 2000). However, as well as both the spectrum signature and polarization were not considered simultaneously. So we will verify our experiment directional optical properties how consistent with previous works.
- Hyperspectral LCTF camera is being used for the first time in a single leaf BRDF measurement. This imaging technique has a great advantage in measuring a selected leaf area with an arbitrary size of the field of view. One of the purposes of this work is to develop a methodology for measuring leaf BRDF using LCTF cameras.
- Polarization models exist for natural Earth surfaces such as Nadal-Breon (NB) Polarized Reflectance Model (Nadal and Breon, 1999), One-Parameter Polarized Reflectance Model (Maignan et al., 2009), and Diner Polarized Reflectance Model (Diner et al., 2002). But in case of a single leaf, the polarization model is not yet studied. After our experiment of light polarization, it is possible to formulate of bidirectional polarized reflectance pneumonia on the leaves with spectral information.
- The single leaves reflectance models usually use the Cook-Torrance model (Bousquet et al., 2005; Comar et al., 2014a; Combes et al., 2007) that is may not suitable for leaf reflectance in our observations because the surface roughness cannot be determined by the actual measurement. The Generalized Harvey-Shack (GHS) scattering theory is well studied from rebound models determined by height distribution (Krywonos, 2006) and the GHS theory is not limited to any special wavelength range, and RMS roughness

value. Our biggest goal is to replace a method of the specular component descriptions by physical surface roughness theory by GHS scattering theory.

- Final aim of this work is to create a new spectro-polarimetric model for single leaf based on actual spectro-polarimetric BRF measurement and disseminate it to the public.

### 1.8.2 The structure of a dissertation

This doctoral dissertation consists of six chapters including an introduction and conclusion. The structure of the dissertation is organized in the following chapters:

Chapter one (an introduction) explains the basic outline of what you are doing in the dissertation, why we have chosen this topic and how the dissertation is structured, and common background of leaf BRF measurement and BRF prediction theories. It is common for introduction to situate the dissertation briefly in the wider field or in relation to contemporary issues, and for it introduced what will be done in each chapter or section.

Chapter two experimental setup consists of primary quantitative or qualitative research, data acquisition (DAQ) of reflected light radiance using LCTF camera and handy spectrometer, and their calibrations with integrating sphere. In this chapter, we will also consider procedure of making the automatic goniometer device including the light source selection in a laboratory, goniometer's material and apparatus, electronic control system, and measurement configuration algorithm development with operational modes. The importance and size of this chapter varies with discipline and with the method chosen. As well as setting out methods used, this section will also explain why it has been chosen in preferences over other methods, and how it was deployed in the substantive research. Spectro-polarimetric BRF measurement of leaves required to record pigments concent measurement using chemical analysis or optical method, a leaf thickness, and leaf mass area by weight meter. In addition to the circumstances, the mirror reflected light of the leaf was needed to measure, and also to use the electron microscope for verifying method to thickness of waxy cuticle layer of the leaf. In this chapter, we usually write about the preparation and configuration of measurements.

In chapter three, three different surface type in appearance of leaves were measured on automatic for building polarimetric BRF pattern and differentiating specular and diffuse reflectance factors. This chapter shows that measured bidirectional optical properties will be verified how consistent with previous single leaf BRF measurements (Bousquet et al., 2005;

Brakke, 1994; Comar et al., 2014; Combes et al., 2007; Walter-Shea et al., 1989). The contrast of this work is that the camera is being used for the first time in a single leaf BRF measurement, as well as the spectrum signature and polarization both are considered in this chapter. This section will show only the results of the actual measurement and their analyzed results. Additionally, methods to find surface roughness of leaves and estimation of thickness of epidermal cuticle layer will be explained first time.

In chapter four, the Generalized Harvey-Shack surface scatter theory is used first time for BRF prediction of leaves. This leads to a new parameter range selection of surface characteristics, which allows to use physical based surface roughness values of height distribution behavior that agrees well with the roughness measurement of scanning electron microscope for surface of leaves.

## CHAPTER 2: EXPERIMENTAL SETUP

This chapter explains the configuration of data acquisition instrument, automatic goniometer system, and how to collect data for spectro-polarimetric BRDF measurement of leaves. Research facility measurements of the BRDF have incredibly enhanced our understanding of the bidirectional reflectance qualities of natural and artificial surfaces. Exploration research and model approval studies in remote sensing, material science, astronomy, and computer graphics have in like manner expanded the information of BRDF and its relationship to surface characteristics (Sandmeier and Itten, 1999). In this chapter, a measuring technique of leaf BRDF research works relevant to remote sensing is given along with advantages of hyperspectral LCTF camera and preparation of laboratory BRDF experiments and how to build a laboratory goniometric experimental setup. The studies displayed in this dissertation were done under laboratory experiments and field measurements. Most parts of the laboratory experiments was made at Graduate School of Science building 8, 208 in Hokkaido University Campus, Sapporo.

Bidirectional spectral signature reflectance measurements gained under controlled laboratory conditions have played an essential role in investigating impacts identified with the BRDF. Planetary observation scientists performed various BRDF laboratory calculations for examining the bidirectional impacts explored in lunar (Cole et al., 2016) and other planet light. Material scientists and most as of late computer graphics and machine vision authorities have been considered BRDF impacts of human-made and common surfaces in controlled laboratory experiments for adjustment and object visualization increasingly. In optical observation of vegetation, although most BRDF measurements have been required in the field, and not enough information is accessible to date from goniometric laboratory experiments. Results from the BRDF studies in a laboratory with connections for remote sensing applications in the VIS and NIR wavelength range are most important, so due to experimental setup of the leaf BRDF is prepared with LCTF camera in Hokkaido University.

## 2.1 DATA ACQUISITION

Nowadays spectrophotometric experimental equipment becomes smarter, smaller, and more cost-effective. Consequently, it is utilized in increasingly more new application fields close to the traditional one in an examination. Spectrophotometric reflectance measurement methods are more strongly applied in science, for instance especially creation for color material, chemical analysis, and factory quality control, pharmaceutical testing, medical tests (blood), plant growth and health observation, testing of light emitting devices, food health control, and pollution measurement. Two different survey instruments for spectrum measurement are widely used such as hyperspectral camera and single point spectrophotometer.

The traditional spectrophotometer contains an input slit hole, a rotating dispersive element such as prism or grating, an output slot, and an optical sensor, so this course of action permits the detachment of multichromatic radiation into its spectral components. The principal points of interest are the high sensitivity and low stray light. Several downsides, for example, the non-parallel measurement, the moveable components, and the space-consuming dimensions were overcome by the development of array spectrometers. This kind of spectrophotometer uses a sensor array instead of a single detector, and therefore only needs fixed components. Meanwhile, they are widely used in a computer coupled, independent as well as handheld devices and begin to find their applications even in the online process measurement.

Recently, the widely used spectral measurement device is a hyperspectral camera and, in other words, can be called a two-dimensional spectrophotometer.

### 2.1.1 Liquid Crystal Tunable Filter camera

We used the spaceborne hyperspectral camera with Liquid Crystal Tunable Filter (LCTF) to measure the bidirectional reflectance factors of a single leaf in a laboratory. Hyperspectral LCTF camera is installed on the first Earth-observation microsatellite of the Philippines (DIWATA-1, and 2) and the Rising-2 microsatellite (Skamoto et al., 2015), and manufactured by Genesia Corporation. This camera works on wavelength bands from 460 nm to 780 nm with a sampling interval of 1nm. The pixel size of the CCD element is the spatial resolution of 656 x 494 pixels. The horizontal and vertical viewing angles are 68.78°, and 50.34° degrees, respectively. LCTF camera has two output file: 8 bit of bitmap image and 10 bit of tabular data with comma-separated values (CSV). (Ishida et al., 2018) produced a high-



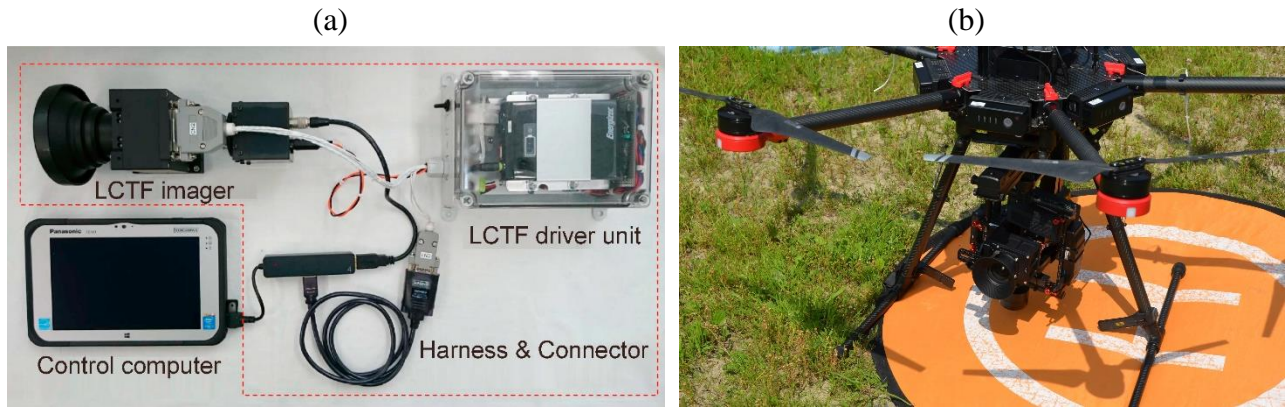


Fig. 14. (a) Liquid Crystal Tunable Filter camera system, an image is representation of (Ishida et al., 2018), and exactly same camera is used in this work. (b) An example application usage of the hyperspectral LCTF camera at Central Agricultural Experimental field of Hokkaido Research Organization in Iwamizawa, Hokkaido Summer Institute.

resolution classification map based on the spectral reflectance factors with an accuracy of 94.5% using the same type of camera and machine learning algorithm.

The LCTF imager consists of several lenses, Liquid Crystal Tunable Filter, and CCD array sensor with USB connection. A tunable filter does not have a direct connection to control computer, so thinking of portable to usage in the field, a field-programmable gate array (FPGA) controls unit ( for controlling via computer USB port) with a battery pack. Fig. 14 presents a LCTF camera with a control system and an example of application usage.

Tunable-channel spectral imaging frameworks continually excite and gather emission from the whole tissue surface and utilize an electronically tunable bandpass filter, such as a liquid-crystal tunable filter, and an acousto-optic tunable filter (AOTF), to transmit or diffract, respectively, one band of the emission range to the CCD camera at once. Along these lines, tunable filter spectral imaging frameworks utilize the channel to parse the wavelength dimension of the spectral image directly. A requirement of CCD sensor sensitivity is obtained for each band of the emission spectrum, using the entire CCD sensor array for spatial resolution. The spectral dimension of the image is built by procuring progressive CCD frames as the filter tuning wavelength is cleared over the spectral scope of interest. The latest generations of these filters possess a broad spectral range over the VIS or infrared regions of the spectrum with a great spectral resolution about  $\pm 1$  nm and can be tuned on the request of microseconds to milliseconds for LCTF.

The advantage of using LCTF implementation in a spectral imaging system is the simplicity in the optical structure. Without disturbance of the pass band beam or moving parts

to make ancient vibration rarities in the images, the system requires just a camera lens to focus the transmitted light onto the CCD focal plane. Be that as it may, the peak transmission of liquid-crystal devices for co-polarized light ranges very low across the visible spectrum, and a significant disadvantage to any filter-based imaging system is the characteristic trade-off between the optical system throughput 3-10% defined as the fraction of light gathered by the imaging system which is at last distinguished by the camera and its spectral resolution.



Fig. 15. Sample images of hyperspectral LCTF camera at Furano flower garden in Hokkaido, five different wavelength of images are chosen to present, and a color image is representation of Fig. 3.

### 2.1.2 Handy spectrophotometer

Gray box handy spectrometer is a scientific instrument for reflectance and scattering of light experiment. It was made for the Japanese High School students and developed by Hokkaido University. The Real-time Camera Spectrometer software (RCS) has been written by us in June 2016 in Planetary and Space Group, Hokkaido University. The handy spectrometer with this gray box consists of a long pass filter from 600 nm, slit hole, collector lenses, transmission diffraction grating, and MCM 4304 monochromatic CCD camera.

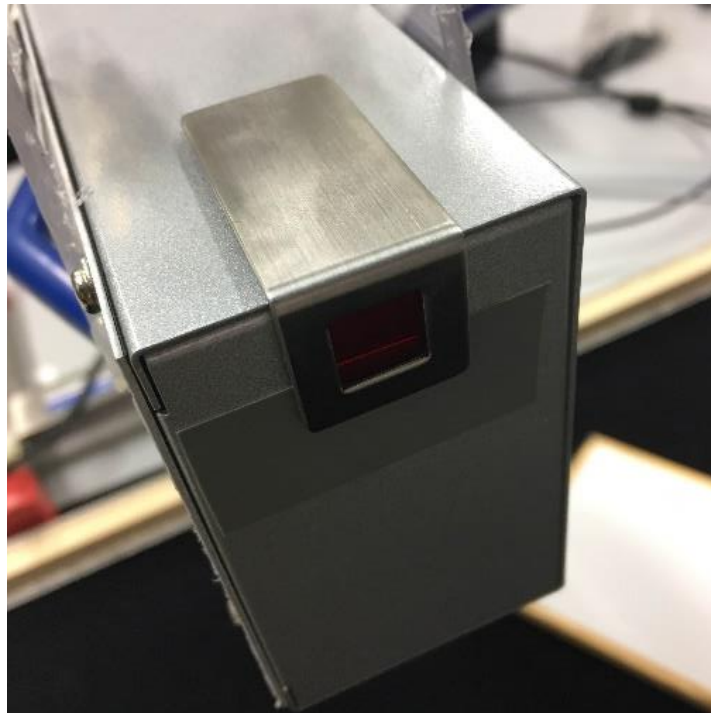


Fig. 16. The gray box handy spectrophotometer with a long pass filter (600 nm).

A camera-based spectrophotometer can be made with either reflection or transmission diffraction gratings. For some random spectrometer arrangement with mirrors/lenses, grating, and detector, it likely changes the wavelength range and resolution by changing the diffraction grating to one with a different groove density. For spectrometers dependent on reflection gratings, it is moreover conceivable to the wavelength range by rotating the grating. Transmission gratings are intended to disperse incident light at specific angles. Angular scattering is a function of an angle of illumination and groove spacing. Dispersion increments as the angle of incidence increases or as groove spacing diminish. Coarse groove spacing keeps up high effectiveness while narrow groove spacing reduces transmission at long wavelengths bringing about low proficiency.

Fig. 17 shows the internal structure of the gray box handy spectrophotometer with a transmission grating between two lenses. As can be seen, our measurement device has 1200 grooves/mm grating, which means effective observation wavelength range of the light is from 400 nm to 800 nm. If the light source has strong intensity at ultraviolet light (lower than 400 nm), long pass filter (600 nm) must be used.

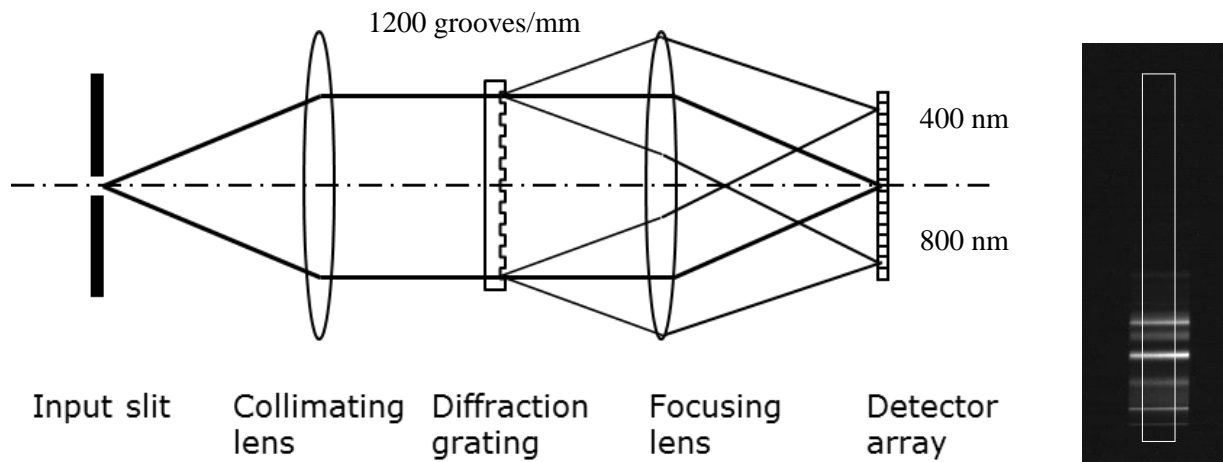


Fig. 17. The gray box handy spectrophotometer's internal structure design.

### 2.1.3 Calibrations with integrating sphere

Calibration and validation of sensors, derived products to quantify and reduce uncertainties are significant for remote sensing measurements, and (Nicodemus et al., 1977) defines the underlying concept of reflectance quantities. Both hyperspectral LCTF camera and handy spectrophotometer are calibrated and validated using the integrating sphere in Space Mission Center, Hokkaido University. In this section, a calibration coefficient is considered as an optical spectrum measurement devices in the integrating sphere for collecting data of Bidirectional Reflectance Distribution Function (BRDF) purposes. Relations between gain, exposure time and calibration coefficient are also considered in this calibration.

Digital numbers of camera pixels were calibrated with the spectral radiance  $L$  ( $W/m^2/sr/nm$ ) in such a method as to be able to hold it as an accurate spectroradiometric measurement in a simple application. The calibration used the integrating sphere (Labsphere) with a halogen HES-150 lamp, that is a simple, yet often undefined instrument for measuring optical band radiation. The function of the integrating sphere is to integrate radiant flux spatially. Integral sphere output

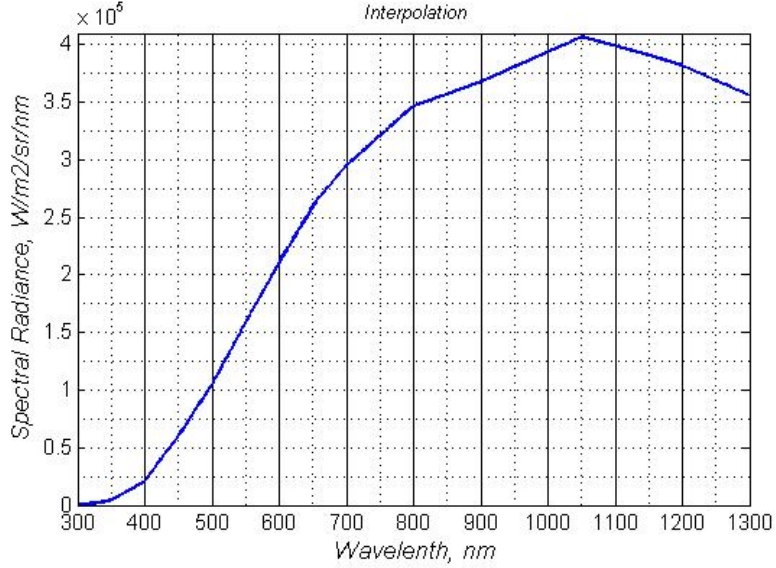


Fig. 18. Representation of spectral radiance distribution of integrating sphere in wavelength range between 300 nm and 1300 nm.

radiance is shown in Fig. 18, the total intensity of intensity of the lamp is about 12320cd/m<sup>2</sup> in the whole spectrum range.

The radiance distribution of integrating sphere output can adjust a constant, and the brightness values at each wave frequency are linearly proportional to total intensity. (López-Álvarez et al., 2009) described the detailed steps of the calibration method and our camera shows reliable results and the pixel response of CCD cameras linearly when compared with

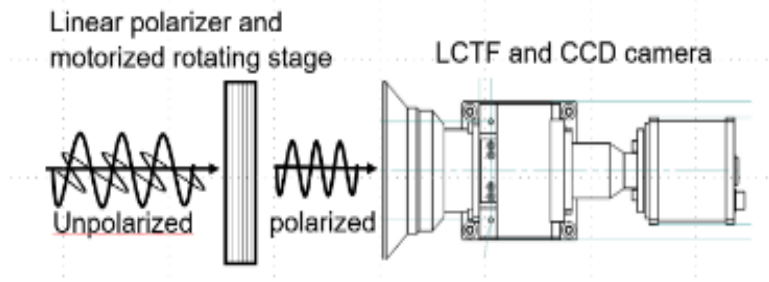


Fig. 19. LCTF camera with motorized linear polarizer

measurements taken simultaneously with other spectroradiometers. The radiance of one pixel is defined by how many light photons can be harvested by CCD element over the complete band targeted. It can be found from the experimental calibration as:

$$L(\lambda, \alpha) = \frac{c_{(G, \lambda)}}{\tau_e} \cdot (DN(\lambda, \alpha) - B) \cdot \frac{1}{2T(\lambda)} \cdot A_{adj}(\alpha) \quad (26)$$

where  $DN(\lambda)$  digital number of the pixel,  $B$  is background,  $\tau_e$  is exposure time,  $C_{(G, \lambda)}$  is the calibration coefficient,  $T(\lambda)$  is a transmission coefficient of the linear polarizing film,  $A_{adj}(\alpha)$  is the adjustment coefficient of rotating polarizer axis. The result of the calibration results are plotted in Fig. 20. Motorized linear polarizer was putted in front of LCTF camera lens, normally when making a calibration and doing the measurement at every different angles of rotation. Fig. 2 shows the operation of data acquisition instrument.

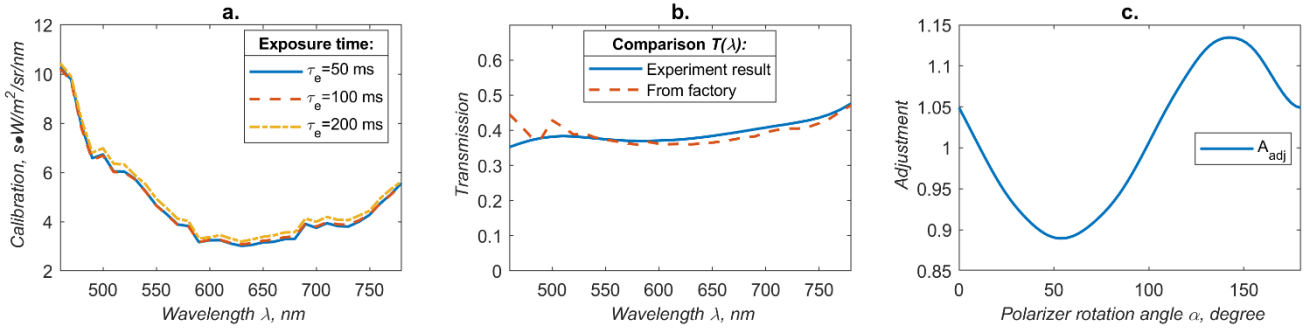


Fig. 20. a. The calibration coefficient for radiance measurement by LCTF camera at gain 256. b.  $T(\lambda)$  and comparison between factory's specification and laboratory experimental result. c. Polarization adjustment coefficient which is caused by tunable filter.

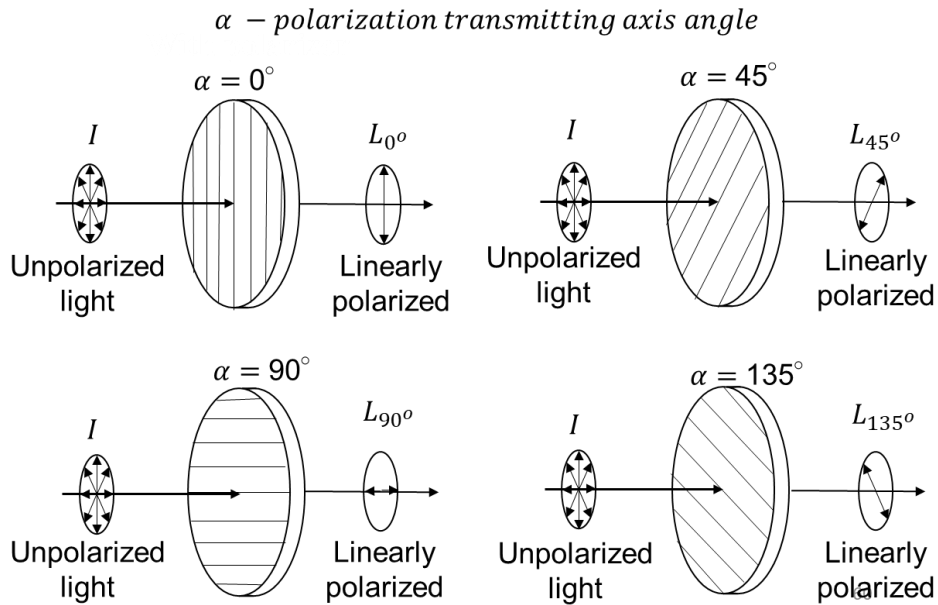


Fig. 21. Linear polarizer's rotation positions, here  $L_{0^\circ}$ ,  $L_{45^\circ}$ ,  $L_{90^\circ}$  and  $L_{135^\circ}$  are obtained for  $0^\circ$ ,  $45^\circ$ ,  $90^\circ$ , and  $135^\circ$  linear polarizer directions those angles are relative to the vertical axis of camera lens plane.

Gray box of spectrometer's shape is rectangular, and a direction of a field of view is along the right downside of the corner. Along with this direction, a spectrophotometer is put in front of the integral sphere at a distance of approximately 3cm from the output. It is the same

direction to radiation flux of light source. A digital number of a camera had no change when a distance between these two instruments is varied between 1 cm to 12 cm (Fig. 22). All other stuff was used as before. The luminance of light source was adjusted between minimum 1000 cd/m<sup>2</sup> and maximum 10000 cd/m<sup>2</sup> during the measurement by rotary ear, which is located on the upper right side of the integrating sphere.

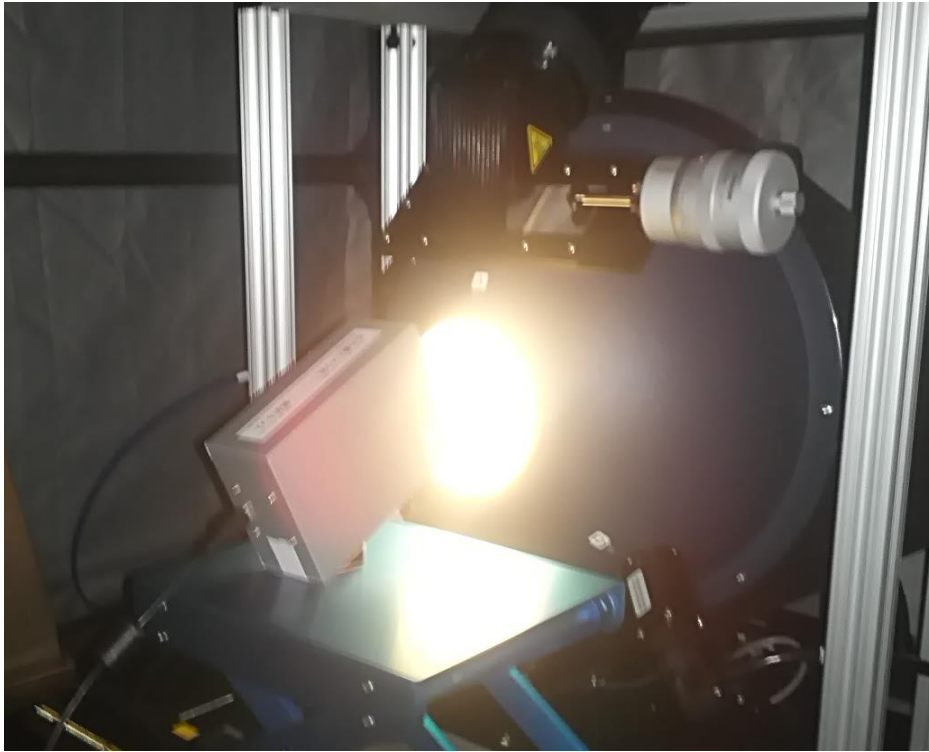


Fig. 22. The integrating sphere and the handy spectrophotometer.

Certificate of integrating sphere is Helios Spectral Radiance Calibration Certificate NO. DM-02043-001, REV. 01. This calibration work used the standard fitting function of MATLAB for finding the best model of calibration coefficient. Data is imported from a text file of a relation between digital number and wavelength number, which is implemented and exported by RCS software.

The most critical parameter of a spectrophotometer is the calibration coefficient, which is calculated in a wavelength band between 300 to 1300 for this spectrometer. It is shown that the calibration coefficient is very stable in 400nm to 900nm wavelength range. The gain is in linear relation to a digital number in the result analysis section, which also means a radiance and the gain has a linear proportional relationship. Using this result, we can define a radiance of spectrometer using the camera's parameters. Eq. 27 shows all relationships of technical configuration inputs of the handy spectrophotometer, that can be defined as:

$$R(\lambda) = \frac{c(\lambda)}{\tau_e} \cdot (DN(\lambda) - B(\lambda)) \cdot \frac{1}{G}, \quad (27)$$

where  $\tau_e$  is an exposure time,  $C(\lambda)$  is a calibration coefficient of calibration,  $B(\lambda)$  is background (normally it is 8),  $G$  is a gain, and  $DN(\lambda)$  is the digital number of MCM 4304 camera.

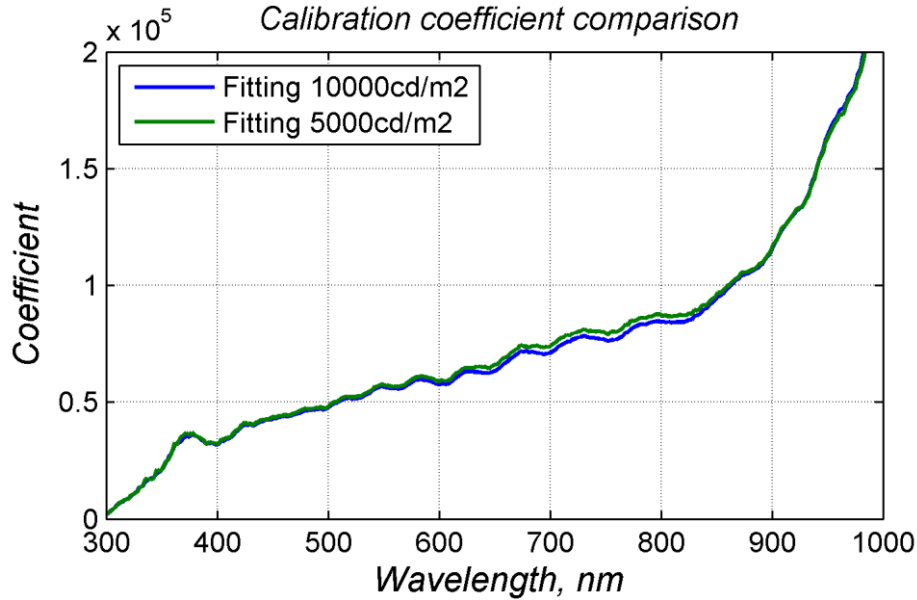


Fig. 23. Comparison result of calibration coefficient in wavelength band from 300 nm to 1000 nm.

#### 2.1.4 SPAD chlorophyll meter and other measurement setups

Spectro-polarimetric measurements were made on leaves of *Coffea canephora* Pierre (Coffee), *Epipremnum aureum* (Pothos), and *Fragaria × ananassa* (Strawberry) during spring of 2017. The spectral signature of reflectance mainly depends on pigment concentration in VIS band (Jacquemoud and Ustin, 2001) and fresh green leaves were mostly selected for measurements. Therefore water and dry matter content were not measured for all the leaves and pigment concentrations were measured by SPAD 502 plus chlorophyll meter (Konica Sensing, Inc., Japan). This well known hand-held equipment measures the ratio of transmittances between two bands (650 nm and 940 nm) and shows digital numbers on display that are related to leaf chlorophyll content, and other pigments. Researchers calibrated display numbers with chlorophyll content for almost all of the plants that have a leaf. Such as correlation coefficients of the coffee, strawberry, and pothos are higher than ninety percent with chemical analysis. Table 1 shows the relationship between display numbers and chlorophyll contents. Although



we focused on canopies of the leaf and waxy cuticle in this paper, the importance of chlorophyll content is high for accurate separation of diffuse reflectance.

Table 1

Conversion of SPAD chlorophyll meter readings Note for unit conversion: The molecular weight of chlorophyll a: 893.51 g/mol, C<sub>55</sub>H<sub>72</sub>MgN<sub>4</sub>O<sub>5</sub>. The molecular weight of chlorophyll b: 907.492 g/mol, C<sub>55</sub>H<sub>70</sub>MgN<sub>4</sub>O<sub>6</sub>. Wild strawberry (*Fragaria virginiana*) average mass density: 48±4.1 g/m<sup>2</sup>, (Jurik et al., 1982).

Plants	Chl	R <sup>2</sup>	Equations	Unit	Reference
Coffee plant ( <i>Coffea canephora</i> Pierre)	chl a	0.97	$y=15.5866+1.0338x+0.0679x^2$	μmol/m <sup>2</sup>	(Netto et al., 2005)
	chl b	0.94	$y=30.1471-0.4592x+0.02270x^2$		
	total chl	0.96	$y=44.5885+0.7188x+0.0933x^2$		
Strawberry ( <i>Fragaria</i> × <i>ananassa</i> )	chl a	0.93	$y=-0.27+0.050x$	mg/g	(Himelrick et al., 1992)
	chl b	0.89	$y=0.04+0.013x$		
	totalchl	0.92	$y=-0.24+0.052x$		
Pothos ( <i>Epipremnum aureum</i> )	chl a	0.92	$y = -0.01779 + 0.00070x$	mg/cm <sup>2</sup>	(Wang et al., 2005)
	chl b	0.92	$y = -0.00321 + 0.00020x$		
	total chl	0.94	$y = -0.02099 + 0.00090x$		

## 2.2 THE AUTOMATIC GONIOMETER

There are thousands of combinations of incident light and observation direction, due to this reason we built the automatic goniometer with LCTF camera starting from summer of 2016 in Hokkaido University. The laboratory goniometer is made at next room of 208, Graduate school of Science, HU and that room's window is closed by dark carton paper, which means the room is almost completely dark. The laboratory and its equipment, including goniometer, control units, and sensor instruments covered with black absorbing materials to minimize diffuse irradiance scattering. The control system programmed the geometrical precision and the angular positioning accuracy of the goniometer and taken into account in the experimental design. Room temperature and humidity are monitored during BRDF data acquisition. Data acquisitions are software-based and automated to reduce operator-related errors.

Many types of research facility goniometers of radiometric measurement have been constructed for studying the BRDF of materials, earth surface even other planet or moon. Cosmologists have utilized goniometers for reflectance estimations of terrestrial surfaces, for example: rock samples, soils, powders, and snow so as to clarify the reflectance properties of lunar surface (Coulson et al., 1965; Di Girolamo, 2003; Hapke and van Hoen, 1963; Kamei et al., 1997; Yin et al., 2018). Remote sensing researchers previously investigated the scattering and polarization properties of vegetation leaves with small-target goniometers (Bousquet et al., 2005; Brakke, 1994; Brakke et al., 1989; Breece III and Holmes, 1971; Vanderbilt and Grant, 1985), and since the beginning of the 1990s to until now, substantial goniometers have been deployed to explore the BRDF properties of vegetation canopies for instance (Sun et al., 2017b).

Both experiments in the laboratory and the field observation have significant advantages and disadvantages. Laboratory measurements are less influenced commonly by ecological impacts, for example, weather conditions and wind than field measurements, and enable to control the position of the light source completely. Conversely, during field campaigns, plant targets are estimated in their characteristic natural habitat and under customary incident conditions. Every research facility goniometer system has its particular weaknesses and benefits. Subsequently, the careful arranging of a laboratory measurement is necessary to address the typical commonplace deficiencies of lab estimations.

The optical property of the leaf is usually studied using short distance or small target goniometers for instance: (Brakke, 1994; Breece III and Holmes, 1971; Vanderbilt et al., 1985)

and measured in a laboratory. Darkroom measurements supply much better control of the light source incidence angle than outside field measurements, and also it can be more precisely defined the diffuse compounds (Dangel et al., 2003).

2.2.1 Light source and stabilization

Two different intensity of cold type halogen bulb lamp (50W and 120W) is selected for illuminating targets, and depending on the color of a target; we choose a power of light source if bright materials are selected to measure, low power of the light source is chosen. The illumination spot size is relatively more extensive than the sensor sampling size to reduce light intensity edge effects. The light intensity was selected sufficiently concerning the sensor sensitivity to obtain an adequate signal-to-noise ratio over the whole spectral range. The power supply of the light source is stabilized to wait 20 minutes, then we usually start a measurement and remaining irradiance fluctuations and drifts was monitoring during data acquisition. The



Spectrum of reflected light

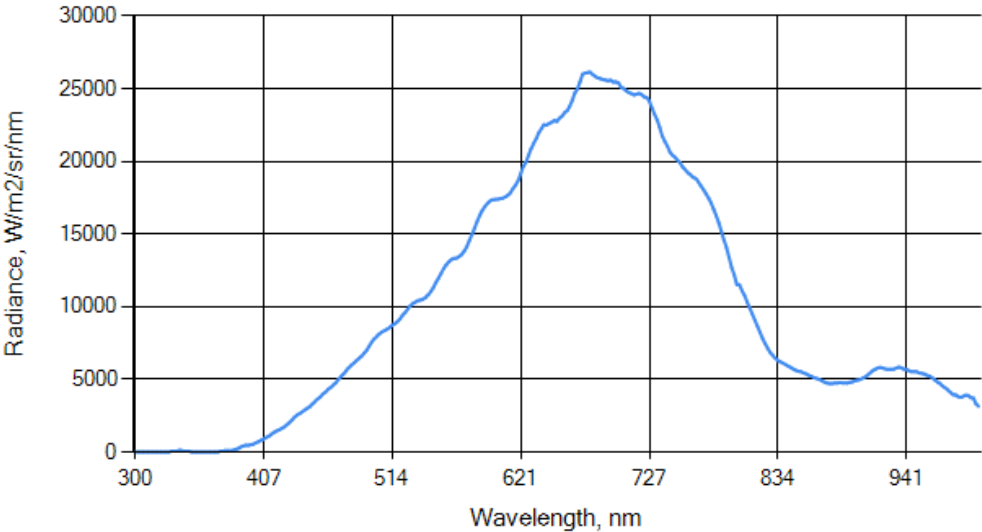


Fig. 24. Halogen lamp and spectral signature of reflected radiance on white reference material (BaSO<sub>4</sub>).

spectral characteristics of the light source were known from a calibration protocol or assessed in conjunction with a well-calibrated reflectance-reference panel. Light source irradiance was homogeneous and parallel using only one light source with the collimator.

Lots of the directional reflection measurements of a surface are called a bidirectional reflectance distribution function (BRDF), more convenient description of most of them is BRF. Depending on the field of view (FOV) of the data acquisition device and illumination, those measurements should be carefully classified. Such kind of physically based separation proposed by (Nicodemus et al., 1977) and their leaves standard reflectance terms are defined. (Martonchik et al., 2000) atmospherically corrected terms of reflectance to the remote sensing case. (Schaepman-Strub et al., 2006) redefined reflectance terminology based on (Nicodemus et al., 1977) and according to his work, the configuration of this setup is the biconical-biconical reflectance factor (CCRF), but our solid angles are small. Fig. 11 shows definitions of illumination and observation geometry. The FOV of one pixel of LCTF camera is horizontally and vertically both around  $0.1^\circ$  and middle of camera view is always pointing to the center of the target leaf, the corresponding ground FOV of one pixel is square about 1.6 by 1.6 mm for nadir view. Parallel wavefronts reflector of halogen lamp was selected by 5.7 cm diameter of the mirror for the light source. Although this measurement is similar with CCRF, it can be called BRF that based on a calculation made by (Schaepman-Strub et al., 2006) who calculated a relative difference between HDRF and BRF in single view angle products. A relative difference is lower than 14%.

### 2.2.2 Materials and apparatus

The goniometer system is a mechanical instrument for changing the position of the light source and observation view, and operation of the system is synchronized with software of LCTF imager on the computer. This system consists of four rotating axes. The view zenith has 92 cm radius of half arch, 115 cm long and 88 cm height of parallelepiped arch with a camera stand mount. It can fix the position of the camera from  $0^\circ$  to  $90^\circ$ ; the relative azimuth is the camera referenced from the light source on a horizontal plane, in a clockwise direction. Specifications of the relative azimuth, observation zenith and linear polarizer are shown in Table 2. Light source axis has an aluminum 75cm long arm which is also the distance between measurement target and illumination.

Table 2

Specifications of motorized axes of the goniometer

Axis	Minimum	Maximum	Accuracy
Azimuth	0°	359.99°	0.01°
Zenith	-90°	90°	0.01°
Polarizer	0°	180°	2.4°

The light source, relative azimuth, and rotating polarizer axes have motorized rotating stage which is the choice for many precision motion control applications and made in by JY Instrument Co., Ltd. Light zenith angle's stepper motor one step precision is 2 degrees. A stepper motor connected to worm gear with a ratio of 1:200 inside the rotating stages with the 2 degrees accuracy of stepper motors. It means the goniometers minimum movement step is

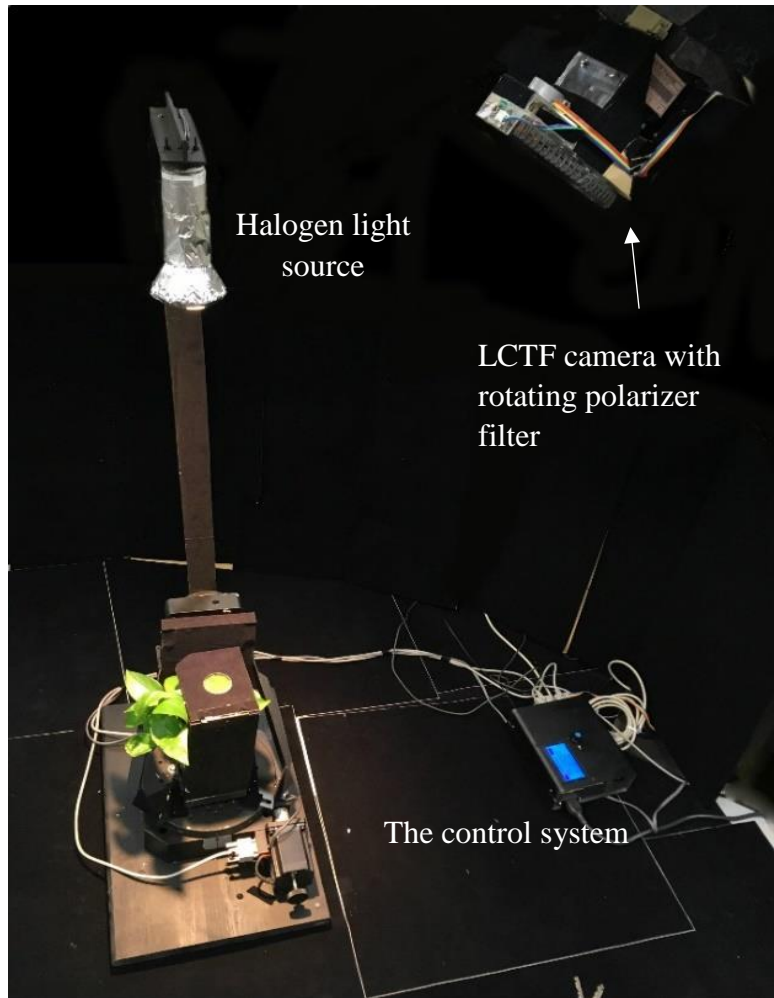


Fig. 25. The automatic goniometer system with a plant storage box, a leaf holder and the control system of goniometer.

0.01 degree for illumination zenith and relative azimuth axes. For polarizer axis, we used 1:3 ratio of two circle gears with a 7.2-degree accuracy of the stepper motor.

When the automatic goniometer was developing, following lists of materials are required;

Table 3

A list of used items for electronics of the goniometer system.






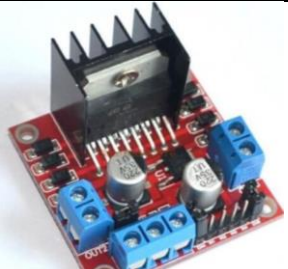




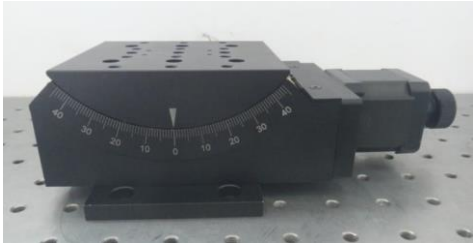
	Name	Quantity	Specification or website	Picture
1	Enclosure box	1	Size is bigger than W x L x H – 130x180x50mm Material: Aluminum or Plastic	
2	Serial cable 9pin	4	1.5m long, extension	
3	Serial connector	4	Female	
4	Serial connector	2	Male	
5	Power supply adapter	1	AC110V to DC12V, current>4A	
6	Stepper motor driver	4	Voltage: DC12V Current: >2A	
7	Relay	1	Coil voltage DC12V Maximum current for load: >3A	
8	Electric cable with a plug	1	3m long AC110V, maximum current 3A	

Table 4

A list of used items for mechanics of the goniometer system.

	Name	Quantity	Specification or website	Picture
1	Motorized Rotation Stage: J02DX100	1	Mini Motorized Rotation Stage (diameter 100mm with 30mm through hole)	
2	Motorized Rotation Stage: J03DX200	1	/Heavy Loading Motorized Rotation Stage (diameter 200mm with 90mm through hole)	
3	Motorized Goniometer Stages, Angle Range +/- 45° J03DJ45	1	Worm gear structure ensure the stage with high loading and accuracy  (not using now)	

These mechanical parts are bought from <http://jyinstrument.com/>.

### 2.2.3 Electronics control system

Electronics hardware of the goniometer is RAMPS 1.4 control board of open hardware 3D printer, which can be re-programmed in C++ programming language using the Arduino development environment. Author of this dissertation developed software of the system at the winter of 2016. This electronics board consist of power regulators, graphic LCD connection, four stepper motor driver, AVR Atmega 256 series microcontroller, USB controller, and many other things.

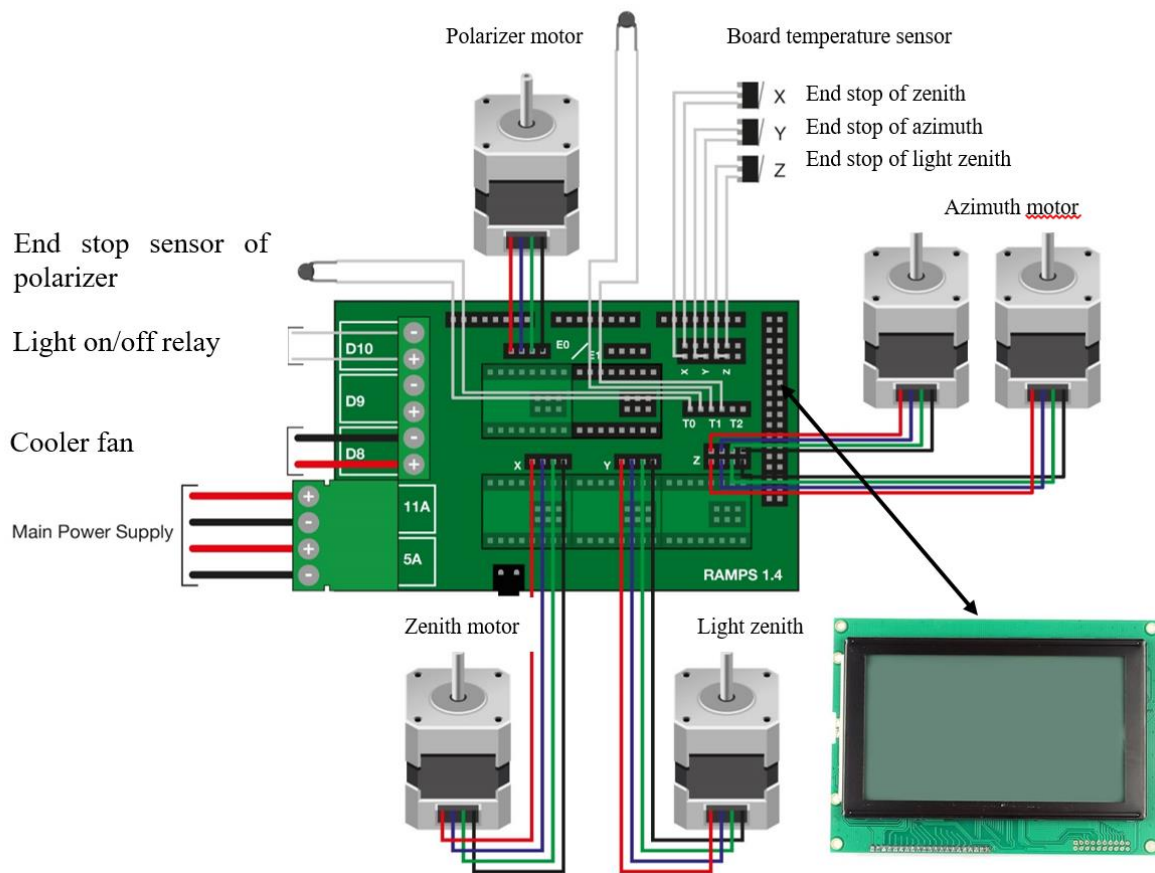


Fig. 25. Wiring diagram of electronics control system of the goniometer.



#### 2.2.4 Controlling algorithms and software

The purpose of this section is to show a detailed description of the Real-time Camera Spectroscopy software, it is written for the handy spectrometer. It will explain purposes and features of the system, the interfaces of the software, what the system will do, the constraints over which it must operate and how the system will react to external stimuli. This document is intended for both the stakeholder and the developers of the system and will be proposed to the Spectrometer Developers for its approval.

This software system will be a spectroscopy's image analysis system for a spectrum researcher, who works in the visible and near field infrared electromagnetic wave. This software is designed to facilitate the user's productivity by providing tools to assist in automating the process of plot graph and save data, which would otherwise have to be performed manually. By maximizing the user's work efficiency and production, the system will meet the present-day's requirements while remaining easy to understand and use.

More specifically, this software is designed to allow the user to automatically plot the graph of wavelength versus intensity and save text data and image from the camera. The software will facilitate communication between spectrometer, camera, and data via Graphic User Interface (GUI). The automated saving section can adjust the time period of storage in every single second to every 100 seconds via the application's numeric up down text box. The software also contains relational calibration functions between camera pixel number and wavelength of the light spectrum. The software with functions expands the scope and give the opportunity to able to use on any spectroscope with prism and CCD camera.

The Real-time camera spectrometer software's main window has four active sections and six menu button on the top. Text file, a graph of wavelength versus intensity, and camera images are output by the accompanying software, so a quantitative analysis is done easily. Using the dedicated software Real-time camera Spectrometer software you can operate the camera system, view the results and analyze them within a few button click commands. The user can easily select an area of spectrum line using the calibration section. The selected area is white rectangular into the top of the picture box.

The wavelength selection box can be chosen in the wavelength (or frequency) range between 200 nm and 1300 nm with a step by 1nm, where about 80 percent of the energy of the

sun is present. Picture box's pixel size is 480x640 (VGA). Numeric up-down box of pixel selection is possible to select pixel number between 10 and 630 with a step of 1.

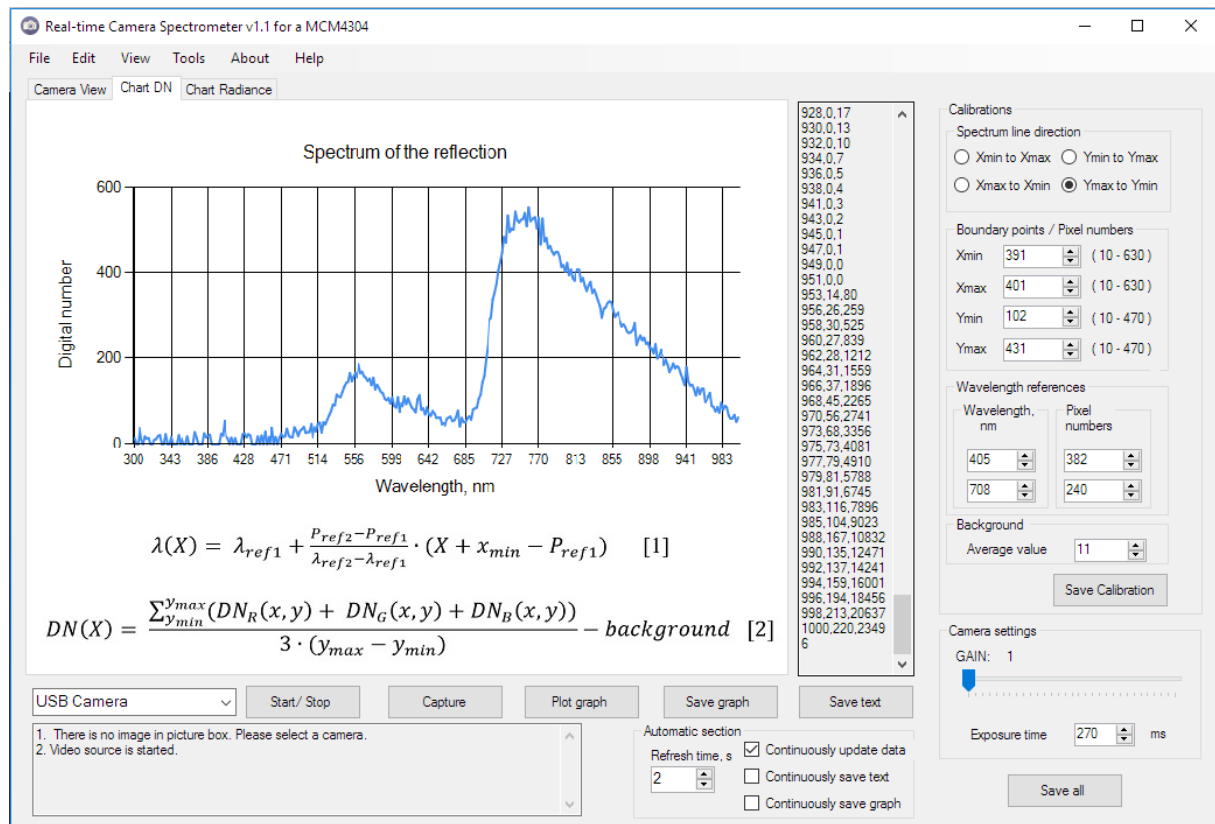


Fig. 26. Real-time Camera Spectrophotometer software's main window.

This section contains graph of intensity vs. wavelength, one text box, three command buttons, and automatic three checkboxes. If you click the plot graph button, it will automatically analyze data from picture box of the camera then data will be plotted on graph section and textbox will have 2 line text. The first column is a wavelength in nanometer and second is relative intensity with a decimal number.

For save graph button, this commands will save a current plot to an image file format including Portable Document Format (pdf), an Image file (png) in selected path folder by the user. The format is derived from the filename extension. If you click save text, the command will wave a current text on the textbox to a \*.txt format text file in your selected path. There are three checkboxes in the automatic section. If you check this three, commands will be performed frequently with a time step between 1 second to 100 seconds. Numeric up down textbox is named "Refresh time," which box adjusts time step.

The picture box's horizontal x, vertical y maximum numbers are 640 pixels, and 480 pixels, respectively. When the mouse cursor is moving on the picture box, the label shows coordinates on the north right corner of the box using the label, and also mouse cursor will have a cross shape. Using this function, you will easy to find any point's pixel number from the camera. Note: Camera's VGA (480x640) video quality is very suitable for this software.

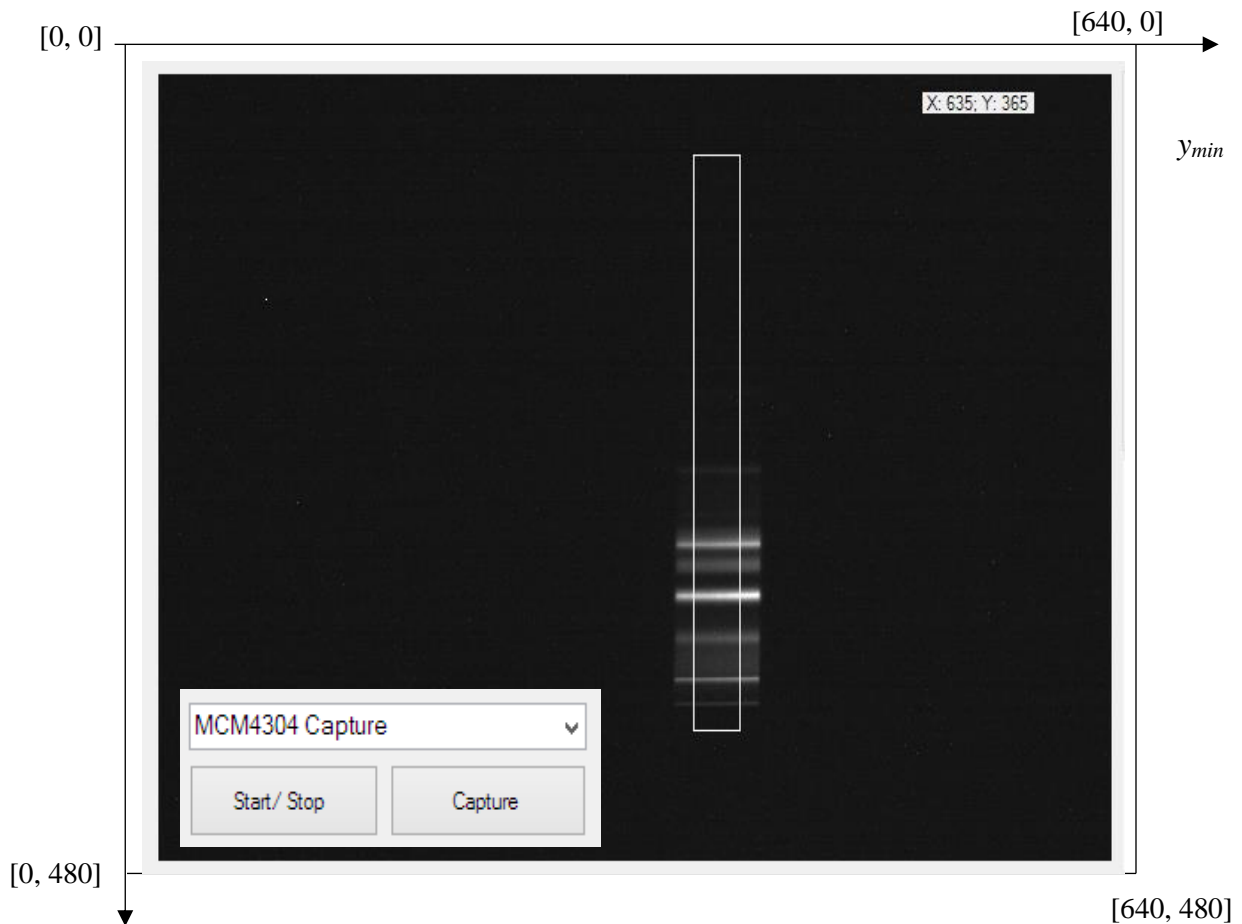


Fig. 27. Camera screen display with an explanation.

There are two options open a picture from a computer or real-time view camera from any selectable video source. If you want to open the image, click File menu – Open command. Otherwise select video source with a combo box that located on the south left corner of the Real-time Camera Spectrometer software. When you have selected camera source, it is possible to capture a picture using the “Capture” button or keyboard CTRL + L.

Hardware Requirements that the minimum hardware requirements are 512 MB of RAM and a 1-GHz processor. However, due to the large sizes of the image files that the camera cell analysis system creates, a several of RAM will prevent paging and thus increase performance.

Software Requirement is that you must have Windows XP, Windows 2000, or a later version of the operating system (Windows) installed on your computer. The latest service pack and any other critical updates for the operating system must be included. You need to install the Microsoft .NET Framework 2.0, or a later version. If you have a Windows 7, 8, and 10 operation system you do not worry about .NET frameworks, which already installed in installed default on your computer. Real-time camera spectrometer software can work on 32 bit and 64-bit operating system both.

Real-time camera spectrometer software has been written on the Visual Studio 2015 using a C# programming language, and the setup file also built on the visual studio.

### 2.3 MEASUREMENT CONFIGURATION

The goniometer operation is automatically changed position for illumination zenith from  $0^\circ$  to  $72^\circ$  with a step of  $12^\circ$ , relative azimuth from  $10^\circ$  to  $180^\circ$  degree with a step of  $10^\circ$ , and rotating linear polarizer  $0^\circ$ ,  $45^\circ$ ,  $90^\circ$ ,  $135^\circ$ , respectively. Observation zenith angles are fixed manually at  $0^\circ$ ,  $12^\circ$ ,  $24^\circ$ ,  $36^\circ$ ,  $42^\circ$ ,  $48^\circ$ ,  $54^\circ$ ,  $60^\circ$ ,  $66^\circ$ , and  $72^\circ$ . LCTF camera can select every single wavelength band between 460 to 780 nm and take pictures on any arbitrary steps. We chose may influence and important 36 bands {460, 466, 472, 478:  $\beta$ - carotene tallest absorption peak, 485, 492, 500, 510, 518:  $\beta$ - carotene last absorption peak, 525, 535, 550, 560, 570, 585, 600, 615, 628, 636, 642: Second peak of chlorophyll b, 646, 650, 656, 662, 668, 674, 680, 687, 695, 703, 710, 725, 740, 750, 765, 780 nm}. The camera took total 188,440 images for one leaf, and adaxial side of 9 coffee, 9 pothos, and 10 strawberry leaves was successfully measured with chlorophyll content and thickness of the leaf for BRDF measurement.

Total reflectance of leaves is a sum of reflectance of the waxy cuticle and diffuse. Although a structure of most leaves has several layers, light reflectance strongly depends on the optical property of top skin at shallow view angles and mirror reflection indicates refractive index of the surface. Mirror reflections of all leaves were additionally measured from  $3.6^\circ$  to  $68.4^\circ$  with an accuracy of  $1.8^\circ$  for estimating surface roughness. In this measurement condition, the

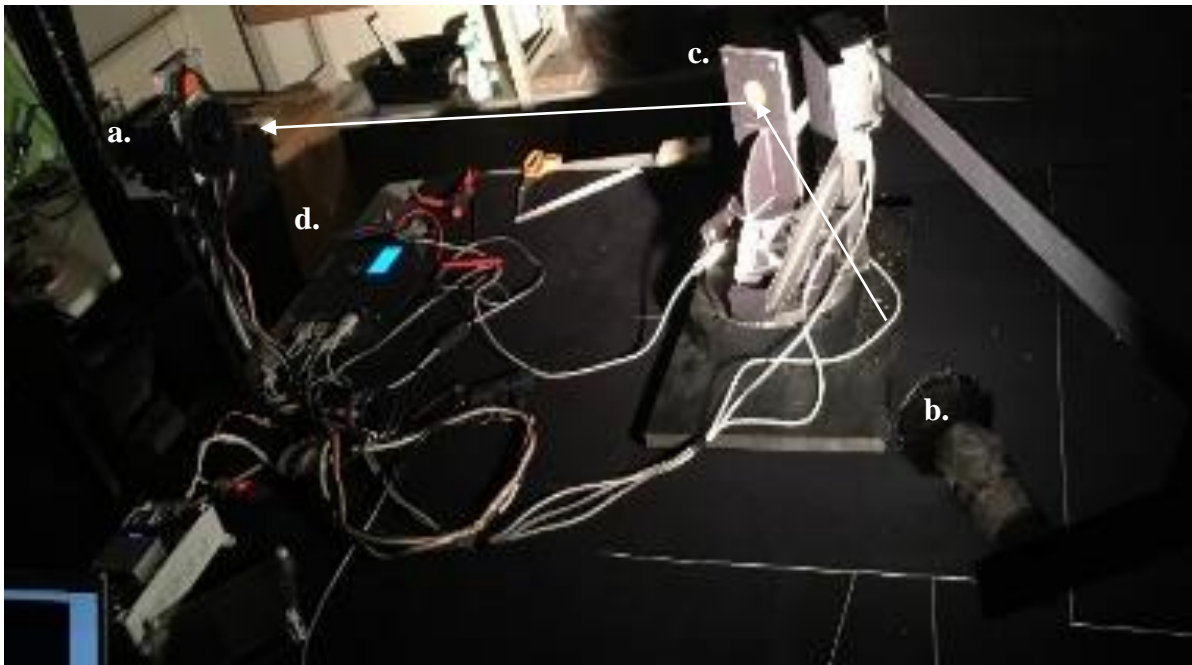


Fig. 28. Mirror reflection measurement mode of the goniometer. Here a. LCTF camera with rotating polarizer, b. halogen light source, c. base rotating plane with target leaf, d. control system, and arrows are incident and reflected light.

goniometer changed an operation mode, and one more base rotation axis was added to the

system. The position of LCTF camera is fixed, and the angular moving speed of light source is two times higher than base rotating axis that means both illumination zenith and observation zenith angles are always relatively same with the normal vector of the target plane (Fig. 28).

Transmitted light gets more information about the inside structure, pigment contents, and morphology when the light passing through the leaf. Transmitted radiances were also measured using an almost same setup with mirror reflection measurement at 180° of relative azimuth angle.

#### **2.4 TRANSMISSION ELECTRON MICROSCOPE MEASUREMENT PREPARATION**

For defining a refractive index of the leaf by Brewster's angle, we have repeatedly made mirror reflection measurement on the surface of the leaf. We have seen different phenomena from surface reflectance of the leaf, rather than the surface polarization (perpendicular and parallel reflectance). Small amplitudes were observed for the angle of reflection during the measurement. Our expectation on that phenomena was thin-film interference, which is a characteristic phenomenon in light waves reflected by the top and lower boundaries of a thin film interfere with each other, either constructive or destructive the reflected light. Then the thickness of wax cuticle is calculated on these reflections in terms of optics. So we would like to check this calculation on Transmission Electron Microscope (TEM) at Agriculture school, Hokkaido University.

Coffee and pothos leaves have the strong effect of amplitude wave on mirror reflection graph, due to four leaves selected to measure on TEM. Fresh leaves around the 1×3 mm<sup>2</sup> area were processed for sections, as reported previously (Kim et al., 2012). Briefly, We were immersed in a modified fixative overnight and washed with buffer (pH 7.2). They were then postfixed with 1% osmium tetroxide. After dehydration in a graded ethanol series, the specimens were embedded in resin. Semithin 1 μm thick sections were made with an ultramicrotome and stained with toluidine blue, and examined using a microscope. Ultrathin sections were stained with 2% uranyl acetate and Reynolds' lead citrate. The sections were examined with a Transmission Electron Microscope (TEM) at an accelerating voltage 80 kV.

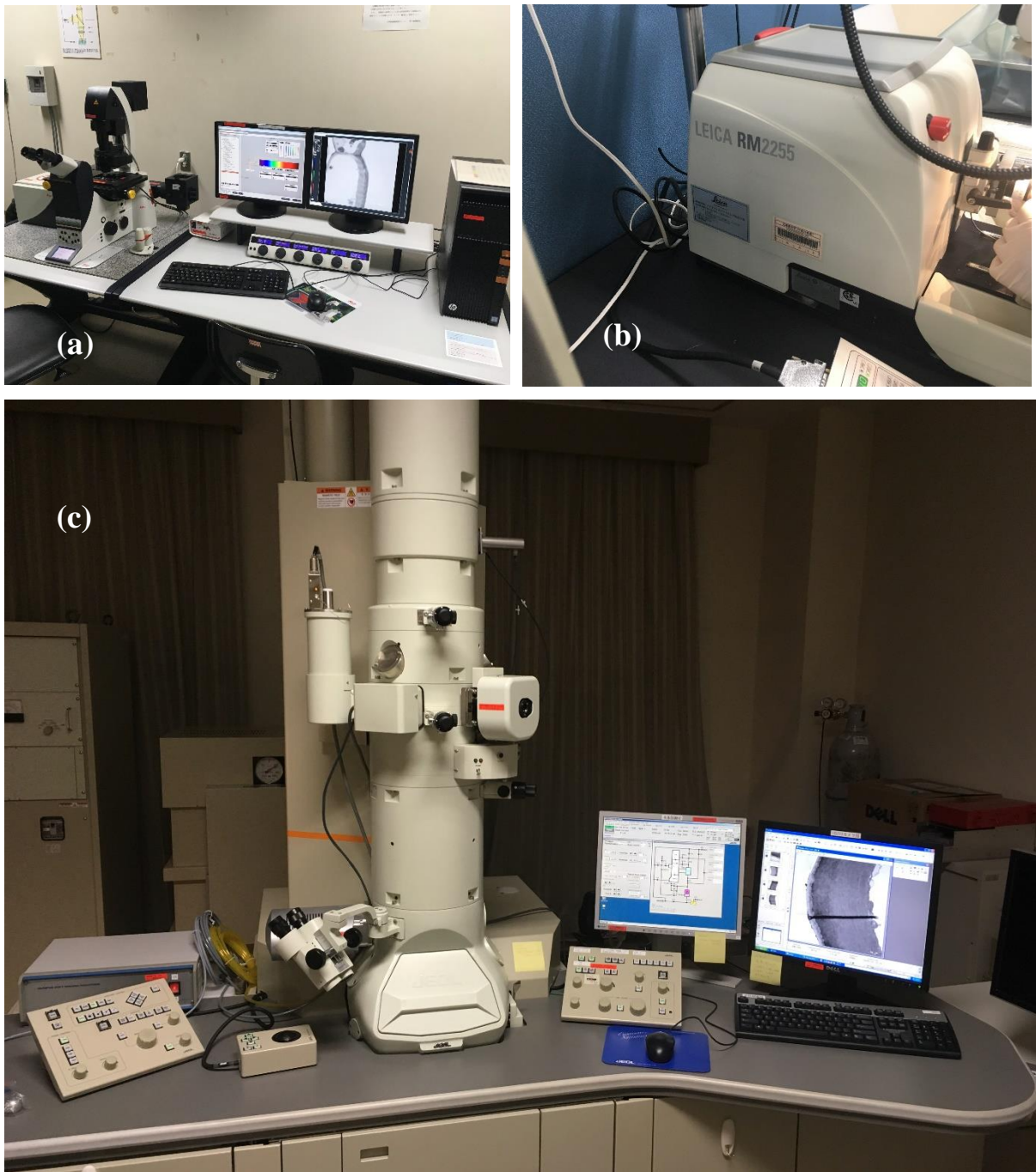


Fig. 29. Transmission Electron Microscope sample preparation. a. Laser microscope, b. fully automated Leica RM2255 rotary microtome, c. Transmission Electron microscope.

## 2.5 SAMPLE LEAVES OF PLANT SPECIES

Spectro-polarimetric measurements were made on leaves of *Coffea canephora* Pierre (Coffee), *Epipremnum aureum* (Pothos), and *Fragaria × ananassa* (Strawberry) during spring of 2017. The camera took total 188,440 images for one leaf, and adaxial side of 9 coffee, 9 pothos, and 10 strawberry leaves was successfully measured with chlorophyll content and thickness of the leaf for BRDF measurement.



Fig. 30. Selected leaves species for the measurements.

The LCTF camera field-of-view (FOV depends on how many pixels are selected), angular sampling resolution, and the measurement distance were carefully chosen following the scale of the target structure. Generally, the leaves need to have a big surface ( $2 \times 2 \text{ cm}^2$ ) in the far field and exhibit small solid angles. At the same time, the averaging area of the LCTF camera's pixels must be small to filter reflectance singularities and to keep the number of samples required to cover the hemisphere manageably small. Ideally, BRDF data sets cover the entire hemisphere with maximum data dynamics and are consistent for different areas of the target surface.

Coffee leaves rust is for the coffee business potentially one of the reasons for a manageability emergency. Almost all coffee species are woody evergreens, yet the plants go in size from little bushes to trees more than 10 meters tall. Leaves shift in color from yellowish to dark green, with touches of bronze or purple. The size and shape of leaves also vary, yet most coffee leaves are oval or curved. The young leaves of coffee plants are shiny, so that is why they are chosen for measurement. The pothos care is simple and enjoys a broad scope of conditions even in the home. The pothos grows well in bright indirect light as well as low light and can be grown in dry soil or vases of water. The surface of pothos leaves are excellent plant due to it was easy to measure. Strawberry leaves are hairy (trichome).



### CHAPTER 3: SPECTRO-POLARIMETRIC BRF MEASUREMENT RESULTS

Polarization techniques separated the polarized and unpolarized reflectance of the leaf, and the sum of those two parts is equal to the total reflectance which is reflectance measurement result without a linear polarizer. Using that separated part and estimation of the refractive index of surfaces can be made accurate calculations of diffuse and specular reflectance.

#### 3.1 THE TOTAL BRF PATTERNS OF LEAVES

The leaves were measured at an observation angle of up to  $72^\circ$  degree, and measurement configuration is more detailly explained in section 1.6. The (9a) and (9b) equations describe the method of estimating polarized and unpolarized light reflectance factor from measurements. The sum of these two dimensions of the reflectance factor must be equal to the total reflectance factor of the light, which is also the same as a measurement result when the polarization filter is not used. Fig. 32.a, b, and c show three dimensional the total reflectance factors for coffee, pothos, and strawberry leaves respectively. It is similar plots with (Walter-Shea et al., 1989) and one of the differences in these graphs is that the points of use of boundary observation zenith angles are up to  $\theta_r \in [-72^\circ +72^\circ]$  degrees. Fig. 31 shows how to read the graph and the next graphs are similar to those shown here. Reflectance factors are calculated on camera pixels, which is able to crop surface area of a leaf that means it can select an arbitrary size of the field of view and to identify lethe af area. However, measuring using cameras is a precise to

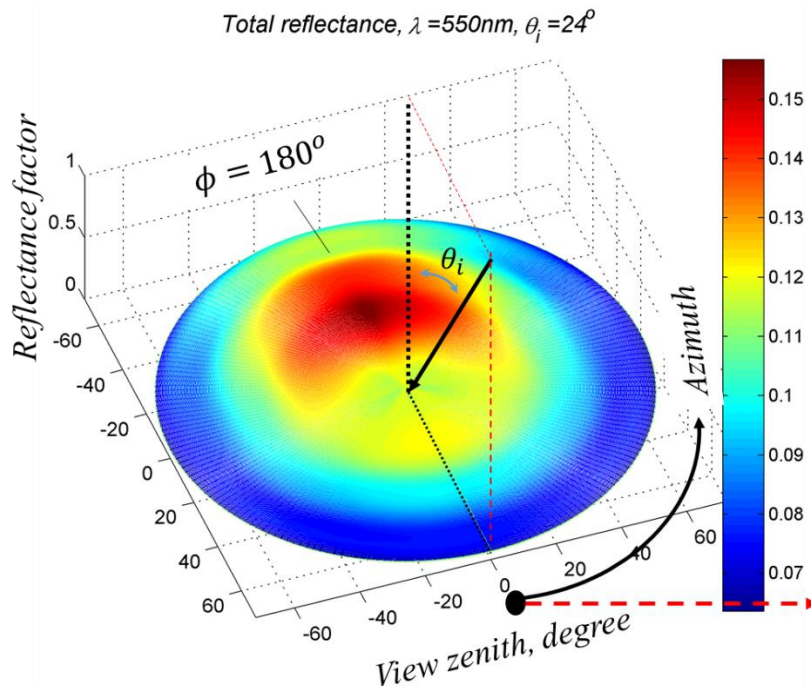


Fig. 31. The total reflectance factor of coffee leaf at wavelength band 550 nm illuminated from  $24^\circ$  with axis notations. The boundary observation zenith angles are up to  $\theta_r \in [-72^\circ +72^\circ]$  degrees.

determine where you are measuring on leaf, pixels view area increases when viewed from the

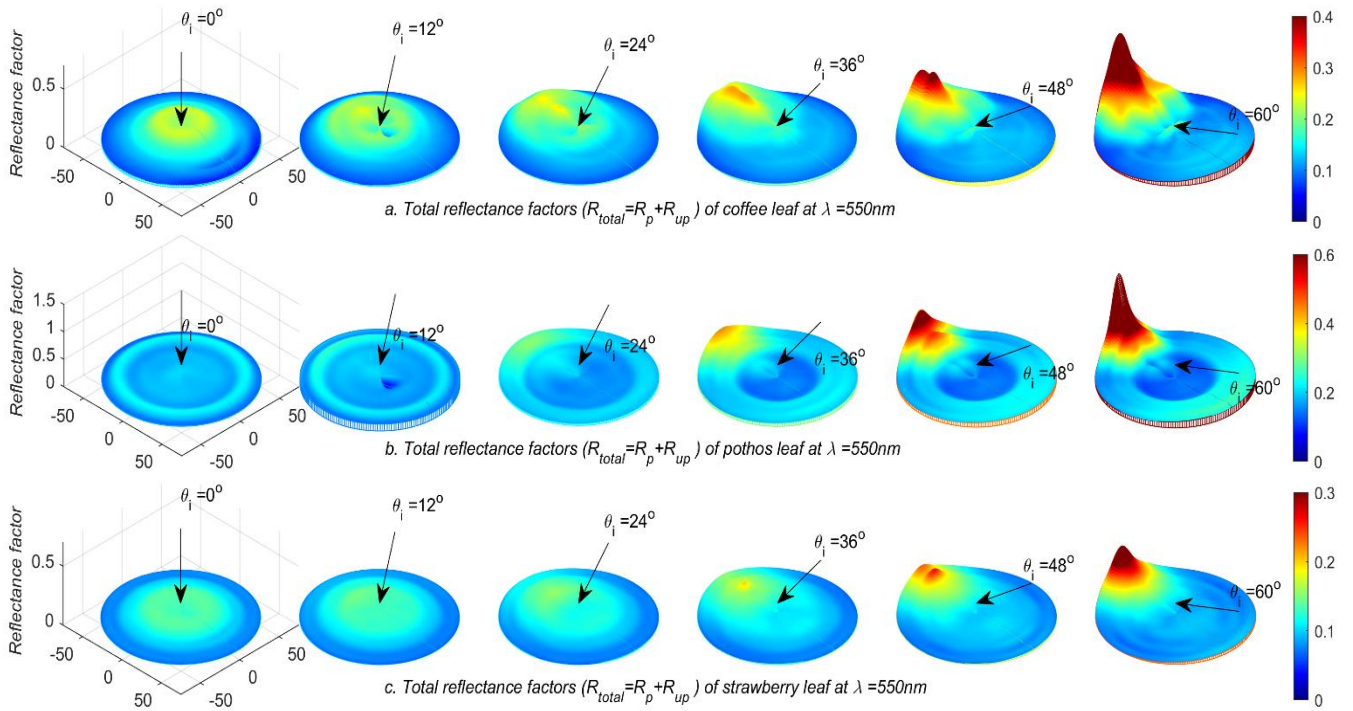


Fig. 32. Polar plots of measured the total (the sum of polarized and unpolarized reflectance factors) BRF values of (top) a. the leaf of the coffee plant, (middle) b. pothos, and (bottom) c. strawberry leaf observed for illumination angle  $\theta_i = \{0^\circ, 12^\circ, 24^\circ, 36^\circ, 48^\circ, \text{ and } 60^\circ\}$  at wavelength 550 nm; illumination angle  $72^\circ$  was also measured. The bar scales of the graphs in the same row are same and located on the right. Note all plots are viewed at zenith  $45^\circ$  and azimuth  $50^\circ$ ; A zenith axis is showed until  $72^\circ$ .

side of the sharp angle. This has reduced our measurement observation zenith limits.

Spectropolarimetric measurements were made at all the wavelengths mentioned above, but only one band's (550 nm) reflectance factor is shown in Fig. 10. The general shape of the leaf BRF result was independent of the wavelength if a common constant part is removed. Because a review of previous studies, the total BRF is the sum of the specular and diffuse components and the internal diffuse component is a perfect Lambertian scatterer. The results of this measurement can be made the same conclusion as (Bousquet et al., 2005) on the total reflectance factor plots. Leaf BRF is less dependence on the low observation angles, due to measurement is less accurate than sharp slope angles. Measurement points were made more significant in size with a step of  $6^\circ$  from  $12^\circ$  by interpolation for zenith view.

Data acquisition area is picked from the flat plate section of the leaf that is about 9x9 pixels (an area is around 1.4x1.4 cm) at nadir direction for pothos and strawberry. The number of pixels is adjusted by a selected section area as constant as possible. For instance, when the angle of observation was  $\theta_r = 48^\circ$ , the FOV were chosen to be 9x6 pixels. If the surface of

the leaf is flat at all, it does not need to make this pixel change. As for coffee leaves, we chose a smaller area (5x5 pixels) because the surface was curved convex in macro level. Some surface of the leaves are crinkly, veined, convex, or hairy in nature (strawberry leaf is hairy), therefore the isotropic and the anisotropic properties of the leaf must be considered. The natural properties of the anisotropy were already marked by (Comar et al., 2012; Combes et al., 2007). Nevertheless, depending on small part of the leaf section is selected or the characteristics of selected leaves are may isotropic, the properties of the anisotropy were not observed perceivably in our measurement result.

In spite of the fact that the coffee leaves look shinier than other measured leaves with eye observation, the pothos leaves generally had most reflection when measuring the slope angle. One of the conclusions of (Bousquet et al., 2005) was that the BRF shape is mainly affected by the surface roughness of leaves. According to this conclusion, it is possible to reach the inference that the canopy of pothos is mostly smooth than other measured leaves or perhaps refractive indices of the waxy cuticle layers are different values. Also, when pothos is illuminated the light to straight down ( $\theta_i = 0^\circ$ ), a small circle of peathe k is formed at about  $\theta_r = 50^\circ$  of observation (see Fig. 32.b the first graph). The diameter of a circle becomes bigger when the wavelength of the the light increases. our point of view that a circle is due to the thickness of waxy cuticle.

### 3.2 POLARIZED AND UNPOLARIZED REFLECTANCE FACTORS

At about one point of observation, the four images were taken at  $\alpha = 0^\circ, 45^\circ, 90^\circ,$  and  $135^\circ$  by LCTF camera for estimating polarized and unpolarized reflectance factor and section 1.6 explains the method for calculating these factors. Fig. 33 shows separation polarized  $R_p$  and unpolarized reflectance factor  $R_{up}$  of coffee, pothos and

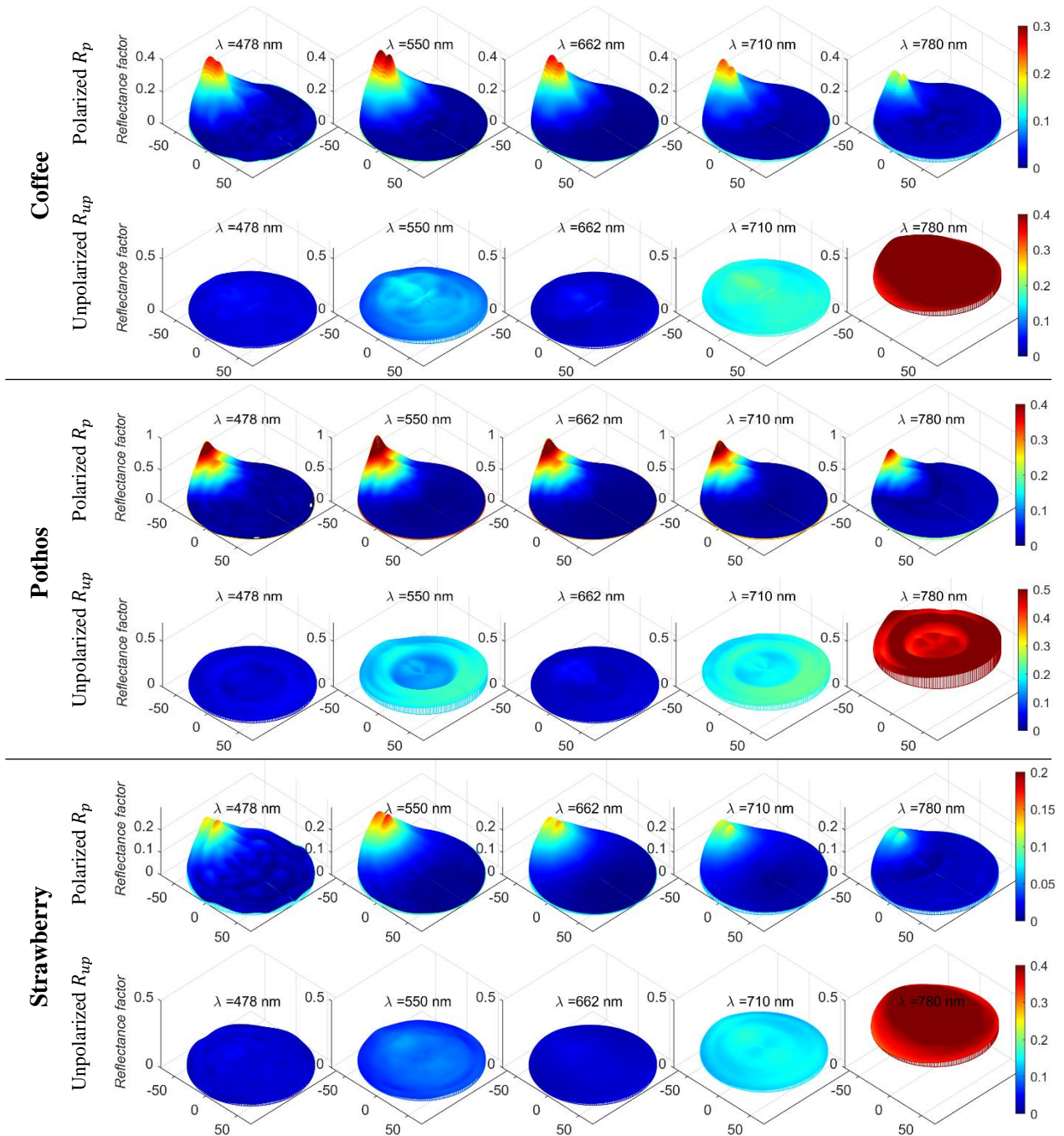


Fig. 33. The spectro-polarimetric BRF measurement results of the adaxial sides of coffee, pothos and strawberry leaves at  $\theta_i = 48^\circ$  illumination angle in three dimensional polar plots. Note all plots are viewed at zenith  $45^\circ$  and azimuth  $50^\circ$ ; A zenith axis is showed until  $72^\circ$ .

strawberry leaves in three dimensional polar plots. Even though these plots were drawn at all of the mentioned wavelengths and also on all angles of illumination, graphs of  $R_p$  and  $R_{up}$  factors at  $\theta_i = 48^\circ$  illumination angle are selected in this article. The reason for showing is that polarized reflectance strongly depends on relative azimuth  $\phi$  and zenith view  $\theta_r$  angles and the unpolarized part looks almost independent at that illumination angle relatively. The polarization is less perceptible in the lower angles of light incidence but is mightily perceptible in higher angles.  $\theta_i = 48^\circ$  is close to Brewster's angle and the average of these boundaries for our measurement.

In Fig 33, plotted results indicated that polarized part is caused by waxy cuticle which is a transparent (no absorption,  $n = n + ik : k = 0$ ) canopy layer, and  $R_{up}$  has weak relationship with pigment compounds including chlorophyll and carotenoids inside a leaf (almost independent of the wavelength). The polarized light reflection appears to decrease slightly in the NIR region, we need to check it out. The unpolarized part  $R_{up}$  evolves significantly with the wavelength as a result of the absorption features of leaf pigments.

According to the calculation of  $R_p$  and  $R_{up}$ , we assumed root-mean-square deviation (*RMSD*) and coefficient of variation (*CV*) of between the unpolarized reflectance factors and their average value  $\bar{R}_{up}$  at  $\theta_i = 48^\circ$  illumination angle. On the other hand, these deviations show the degree of stability of the unpolarized reflectance factors. *RMSD* and *CV* were numerically calculated as

$$\bar{R}_{up}(\lambda) = \frac{\sum_{\phi=0}^{360^\circ} \sum_{\theta_r=0}^{72^\circ} R_{up}(\phi, \theta_r, \lambda)}{N_\phi N_{\theta_r}}, \quad (28.a)$$

$$RMSD(\lambda) = \sqrt{\frac{\sum_{\phi=0}^{360^\circ} \sum_{\theta_r=0}^{72^\circ} (R_{up}(\phi, \theta_r, \lambda) - \bar{R}_{up}(\lambda))^2}{N_\phi N_{\theta_r}}}, \quad (28.b)$$

$$CV(\lambda) = \frac{RMSD(\lambda)}{\bar{R}_{up}(\lambda)}, \quad (28.c)$$

where  $N_\phi$  and  $N_{\theta_r}$  are a number of measurement points at relative azimuth and observation zenith axis respectively. The results using equations are shown in Table 5. The most stable unpolarized reflectance factor is the strawberry leaf and the most volatile is the coffee leaf. The deviations of  $R_p$  in some, the wavelength bands (for instance 662 nm) are conspicuous high, but it depends on a range of the angle of observation ( $0^\circ$  to  $72^\circ$ ) and the light absorption. If this

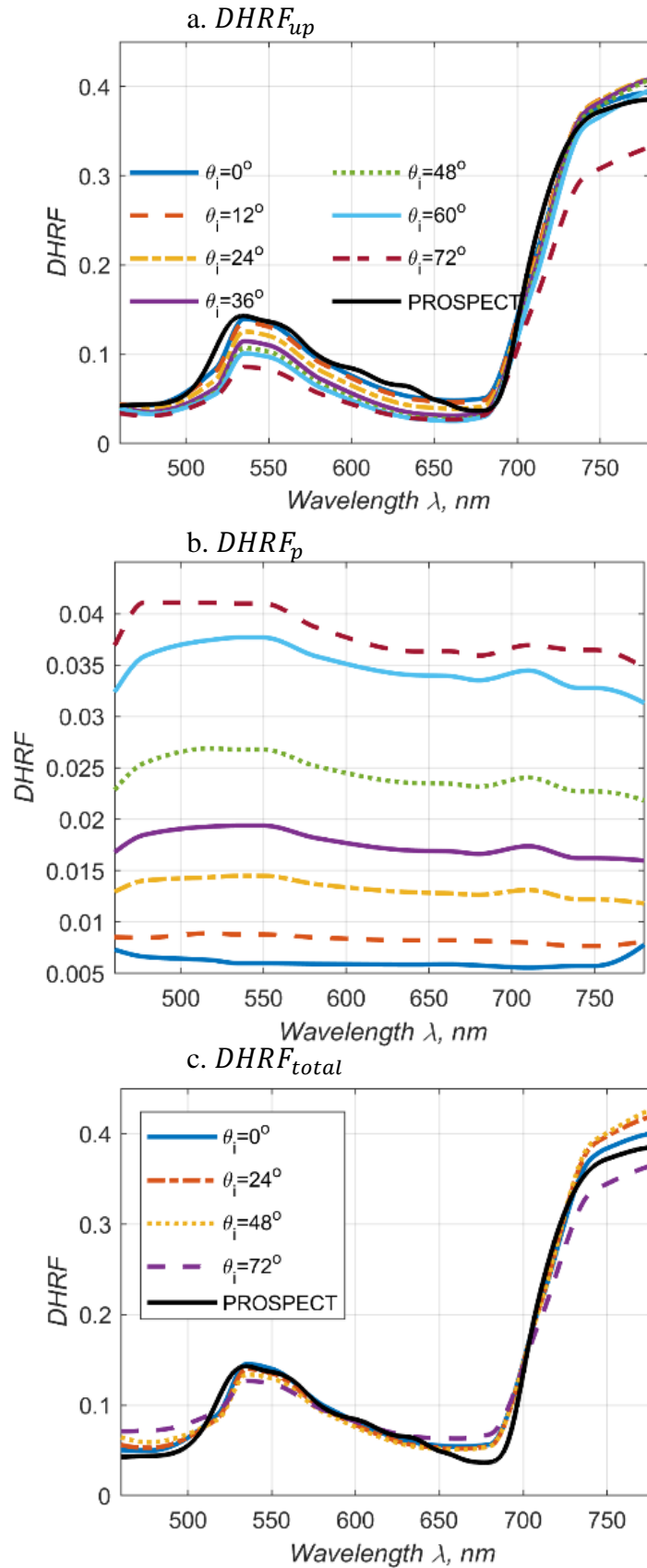


Fig. 34. The directional hemispherical reflectance factors a. unpolarized b. polarized and c. the total for an adaxial face of coffee leaf. The a and b plots have same legend, which is located in the first plot.

range is reduced from a wide angle to zero, the deviation will decrease significantly. As

considered at the 780 nm wavelength band, the variation coefficients were not exceeded 17% under  $\theta_i = 60^\circ$  illumination angle.

If the coefficient of variation is low or unpolarized reflectance factors are stable, DHRF should be less dependent on the light illumination angle. Thus, we assumed this factor for changing illumination angle. Traditional DHRF measurements are generally based on total light reflection, while the calculations for this work were estimated on both polarized and unpolarized BRDF.  $DHRF_p(\theta_i, \lambda)$  and  $DHRF_{up}(\theta_i, \lambda)$  were numerically calculated on  $R_p(\theta_i, \lambda)$  and  $R_{up}(\theta_i, \lambda)$  respectively by Eq. 6. Of course, the sum of  $DHRF_p(\theta_i, \lambda)$  and  $DHRF_{up}(\theta_i, \lambda)$  is equal to  $DHRF_{total}(\theta_i, \lambda)$ . Fig. 34 shows results of DHRF calculation for an adaxial face of coffee leaf because of the most variation, that is why the plots of the coffee leaf was chosen to display.

The results obtained in Fig. 34 are different from the original definition Eq. 6, indicating that the top and bottom limits of the integral were chosen until observation boundary of measurement, which is  $0^\circ$  and  $72^\circ$ . As a result of the absence measurements for  $\theta_r > 72^\circ$ , the integration over the entire range of  $\theta_r$  was computed assuming a linear relationship with  $\theta_r$  of the term  $BRDF(\theta_i, \phi, \theta_r, \lambda) \cos\theta_r \sin\theta_r d\theta_r d\phi$  for  $72^\circ < \theta_r < 90^\circ$ , taking advantage of the property:  $\cos(90^\circ) = 0$ . On the other hand, the low angles of light illumination do not significantly affect the reflectance factor at the observation range of  $72^\circ < \theta_r < 90^\circ$ .

Leaf DHRF are typically made using the integrating sphere, and the measurement at the angle of the illumination angle of  $0^\circ$  should match the results of the PROSPECT model. The measurement results of unpolarized and total DHRF were plotted with spectral signature of model simulation results in Fig. 12.a and c respectively. Surprisingly, the result of spectral reflectance model (PROSPECT) and unpolarized DHRF results was well suited without calibration coefficients at the illumination angle of  $0^\circ$  for every selected species leaves, and a small amount of difference was sighted at different illumination angles. Polarized DHRF results in Fig. 34.b shows polarized DHRF results at  $\theta_i = 0^\circ$  illumination is relatively very low. As the angle of light illumination is increasing, the polarized DHRF result increases, its interaction is described and the surface roughness must be included in order to find a complete dependence. The distribution of correlation coefficients between unpolarized DHRF at the  $0^\circ$  illumination angle and the PROSPECT model result was always higher than 95% in this measurement analysis.

If BRF measurements are a stable (constant) or small deviation on observation zenith and azimuth axis, then BRF measurements and DHRF calculation results should be mathematically equal ( $DHRF(\theta_i, \lambda) = BRF(\theta_i, \lambda)$ ,  $\theta_r \in [0, 90^\circ]$ ). Probably in a field, leaf DHRF is difficult to determine in real life, the integrating sphere is needed or hundreds of leaf BRF measurement is required at the outside. Veritably BRF measurement results strongly depend on the angle of illumination and the angle of observation both. If a method of stabilizing is exist, it is possible to quickly determine the biochemical contents of the leaves using the PROSPECT model in a field. Thus, the results show that spectro-polarimetric measurement is able to do that. Despite the high deviations in Table 5, it is predictable and able to be improved by examining it further in the future by doing more research in this issue.

Table 5  
Root-mean-square deviation (*RMSD*) and coefficient of variation (*CV*) of between the unpolarized reflectance factors and their average value  $\bar{R}_{up}$  at different illumination angles.

Wavelength →		478 nm	550 nm	662 nm
Coffee	$\bar{R}_{up}$	0.038	0.116	0.032
	<i>CV at at <math>\theta_i = 0^\circ</math></i>	39.8 %	33.3 %	54.0 %
	<i>CV at at <math>\theta_i = 12^\circ</math></i>	33.5 %	29.7 %	47.4 %
	<i>CV at at <math>\theta_i = 24^\circ</math></i>	27.8 %	25.7 %	45.1 %
	<i>CV at at <math>\theta_i = 36^\circ</math></i>	23.1 %	22.0 %	39.2 %
	<i>CV at at <math>\theta_i = 48^\circ</math></i>	17.9 %	16.8 %	31.0 %
	<i>CV at at <math>\theta_i = 60^\circ</math></i>	20.3 %	14.8 %	36.0 %
	<i>CV at at <math>\theta_i = 72^\circ</math></i>	53.5 %	38.1 %	104.8 %
Pothos	$\bar{R}_{up}$	0.041	0.16	0.036
	<i>CV at at <math>\theta_i = 0^\circ</math></i>	17.9 %	10.8 %	29.7 %
	<i>CV at at <math>\theta_i = 12^\circ</math></i>	17.4 %	12.9 %	30.4 %
	<i>CV at at <math>\theta_i = 24^\circ</math></i>	11.2 %	8.6 %	30.7 %
	<i>CV at at <math>\theta_i = 36^\circ</math></i>	13.0 %	13.3 %	32.1 %
	<i>CV at at <math>\theta_i = 48^\circ</math></i>	14.9 %	16.9 %	25.2 %
	<i>CV at at <math>\theta_i = 60^\circ</math></i>	26.4 %	23.8 %	44.6 %
	<i>CV at at <math>\theta_i = 72^\circ</math></i>	64.2 %	45.0 %	145.9 %
Strawberry	$\bar{R}_{up}$	0.031	0.086	0.030
	<i>CV at at <math>\theta_i = 0^\circ</math></i>	24.1 %	25.8 %	34.8 %
	<i>CV at at <math>\theta_i = 12^\circ</math></i>	22.7 %	24.4 %	33.4 %
	<i>CV at at <math>\theta_i = 24^\circ</math></i>	18.1 %	21.2 %	29.6 %
	<i>CV at at <math>\theta_i = 36^\circ</math></i>	18.1 %	18.6 %	23.6 %
	<i>CV at at <math>\theta_i = 48^\circ</math></i>	15.5 %	14.5 %	15.2 %
	<i>CV at at <math>\theta_i = 60^\circ</math></i>	19.2 %	11.9 %	25.1 %
	<i>CV at at <math>\theta_i = 72^\circ</math></i>	52.1 %	31.0 %	76.0 %



### 3.3 OPTICAL ESTIMATION OF SURFACE RMS ROUGHNESS

Refractive indices of materials are determined based on two parts ( $n = n + ik$ ): the real part  $n$  indicates the phase velocity, and it has no power loss; the imaginary part  $k$  is indicative of how much energy is attenuated, and called the extinction coefficient. Leaves contain a variety of pigment molecules which use light as their source of energy that pigment absorption and scattering pneumonia are connected to extinction coefficient for the leaf. Although absorbed and scattered power is essential, this paper focuses on bidirectional reflectance distribution of

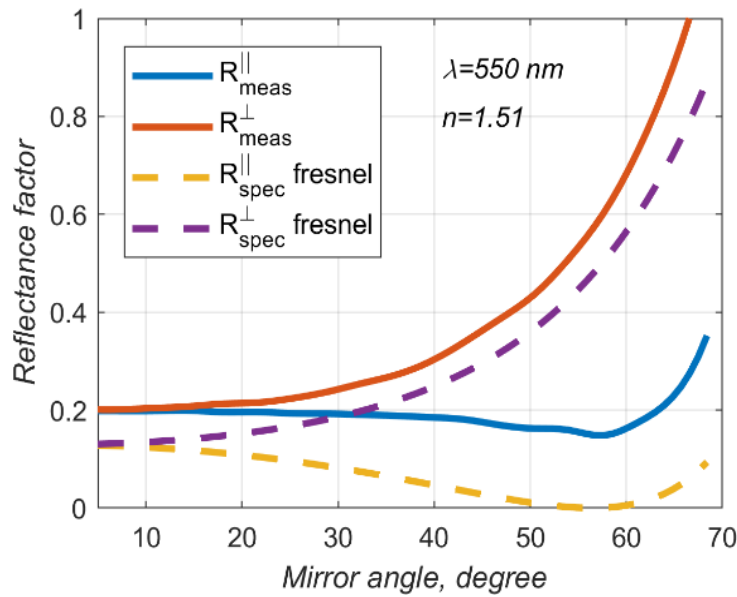


Fig. 36. Sample measurement result of reflectance factors of pothos leaf at 550 nm and Fresnel's factors are plotted for the refractive index of  $n=1.51$ .

leaves and most canopy reflectance models consider that diffuse reflectances are perfect Lambertian scatterers in VIS. On the top of the upper epidermis, leaves have the transparent waxy cuticle layer which protects them from diseases and loss of water. Also, the waxy cuticle of many leaves can cause high specular reflectance and occupies most of the specular part (Vanderbilt and Grant, 1985). Shiny leaf surfaces are not optically smooth, but they are sufficiently smooth to partially polarize the incident light over a broad range of incident angles. Depending on our selection of plant species and our narrow field of view, we can use the Fresnel's equations in this case.

In light mirror reflection condition, the maximum value of the reflectance is along to vertical axis of polarization that called perpendicular reflectance. Also, the minimum amount of the reflectance is along to the horizontal axis, which is parallel reflectance. Fresnel equations can describe specular reflectance, and transmittance of the light occur at the boundary between

air and transparent layers of the leaf. The incident light is separated two fractions which depend on the indices of refraction and incident light direction. Specular parallel and perpendicular reflectance factors can be defined for the smooth surface as:

$$R_{spec}^{\perp} = \pi \cdot \left| \frac{n_w^2 \cdot \cos\theta_i - \sqrt{n_w^2 - \sin^2\theta_i}}{n_w^2 \cdot \cos\theta_i + \sqrt{n_w^2 - \sin^2\theta_i}} \right|^2, \quad (29.a)$$

$$R_{spec}^{\parallel} = \pi \cdot \left| \frac{\cos\theta_i - \sqrt{n_w^2 - \sin^2\theta_i}}{\cos\theta_i + \sqrt{n_w^2 - \sin^2\theta_i}} \right|^2. \quad (29.b)$$

where  $n_w$  is surface refractive index of the leaf or waxy cuticle's,  $R_{spec}^{\perp}$  is specular perpendicular reflectance, and  $R_{spec}^{\parallel}$  is specular parallel reflectance. Total specular  $R_{spec}$  is equal to the arithmetic mean of  $R_{spec}^{\perp}$  and  $R_{spec}^{\parallel}$  when the surface roughness is not calculated or for a smooth surface. The waxy cuticle layer of the leaves strongly affects the fracture of the light and refractive index difference of inside transparent layers (such as epidermis) are relatively small. Amounts of perpendicular and parallel polarized lights passing through the transparent layer of the leaves (transmittance factors) are defined as  $T_{spec}^{\perp} = \pi - R_{spec}^{\perp}$  and  $T_{spec}^{\parallel} = \pi - R_{spec}^{\parallel}$  respectively.

When the light encounters a boundary between two transparent media with different refractive indices and the angle between reflection and transmission is equal to  $90^\circ$ , reflected light is 100% linearly polarized. This condition is called Brewster's angle, and it can be used to determine the refractive index (Eq. 30).

$$n_w = \tan(\theta_b). \quad (30)$$

Most reflectance models of the single leaf consider that diffuse reflection is perfect scatterers (like a Lambertian) and perpendicular and parallel reflectance are equal to each other inside the leaf. when parallel reflectance factor is minimum, the related reflection angle seems Brewster's angle. but our measurement observed that the refractive index could not be found from minimum of mirror reflection due to the internal scattering and surface roughness. Minimum of parallel reflectance factor may have shifted to a higher from Brewster's angle. In Fig. 36, the sample measurement result of reflectance factors of pothos leaf at 550 nm and Fresnel's factor which is calculated by Eq. 29 a and b, are plotted. The difference between

measured total parallel and Fresnel parallel reflectance factor is equal to diffuse parallel reflectance factor which should be constant according to Lambertian reflection.

The quantity of leaf surface roughness is generally measured by Scanning Electron Microscope (SEM), the roughness of the hairy leaves many times higher than hairless leaves (Kearns and Bärlocher, 2008; Kim et al., 2011; Walker et al., 2015) and the range of rms surface roughness,  $\sigma_s$ .

Main impacts of surface roughness scatter light on the surface of any optical measurement samples. The ratio between the total reflected radiant power and diffusely reflected power is called Total Integrated Scatter (TIS) which was first found a functional relationship by (Bennett and Porteus, 1961) and that relationship has an exponential correlation with an intrinsic RMS roughness. After many research results, the scattering form is not defined solely by RMS roughness,  $\sigma_s$ , that is calculated on the surface height distribution and we also need to consider about relevant statistical surface characteristics that are the relevant band-limited rms roughness  $\sigma_{rel}$ , and the autocovariance width,  $l_c$ . The Generalized Harvey-Shack (GHS) method has been developed a very well description of these concepts (Harvey et al., 2010). TIS can be defined with relevant surface roughness,  $\sigma_{rel}$  by Eq. 31 (Harvey, 2012).

$$TIS = 1 - e^{-\left(\frac{4\pi\cos\theta_i\sigma_{rel}}{\lambda}\right)^2} . \quad (31)$$

According to the basic definition of total integrated scatter, the total integrated scattering factor  $R_{scat}^{total}$  on the surface should be equal to the product of the total reflection and TIS in the measurements of leaves. The second part of Eq. 31 indicates the ratio between a specular reflection and the total reflection on the surface of the leaf. From here specular reflectance factor  $R_{spec}$  of the surface can be re-expressed as:

$$R_{scat} = \left(\frac{R_{spec}^\perp + R_{spec}^\parallel}{2}\right) \cdot TIS \quad , \quad (32)$$

$$R_{spec} = \left(\frac{R_{spec}^\perp + R_{spec}^\parallel}{2}\right) \cdot e^{-\left(\frac{4\pi\cos\theta_i\sigma_{rel}}{\lambda}\right)^2} . \quad (33)$$

One of the features of our work is polarization measurements of the leaf mirror reflection, which allows for estimating the relative roughness of leaves surface using Eq. 33, and a polarization dependent function  $Q$ . The results of a mirror reflection measurements should

be the sum of the scattered inner light from pigments and the reflection of the surface. It can be expressed by the following equations:

$$R_{meas}^{\parallel} = R_{spec}^{\parallel} + R_{diff}^{\parallel} \quad (34.a)$$

$$R_{meas}^{\perp} = R_{spec}^{\perp} + R_{diff}^{\perp} \quad (34.b)$$

All rough surface Spectro-polarimetric BRDF measurements were made before mirror reflection measurements on same leaves. Although some types of leaves have azimuthal anisotropy (Comar et al., 2014), all of our selected leaves were the isotropic surface properties. The GHS formulation is used a Gaussian surface height distribution function and the surface autocovariance (ACV) function and that two functions are independent with azimuthal orientation (symmetric) of the measured surface profile for isotropic cases. ACV function is written in Eq. 24 for such kind of surface case.

Leaf unpolarized light reflection part cannot be regarded as equal to diffuse reflection component, possible it contains the major part of the diffuse component and unpolarized part of a specular component. To differentiate these parts sufficient clear, the surface refractive indexes and roughnesses need to be carefully considered. Using Brewster's angle, the refractive index of the surface can be found for smooth and transparent surfaces, but this method cannot be work for the leaf surface. The internal scattering of a leaf and surface roughness must be examined with the measurement result for finding the refractive index.

Sample measurement result was showed in the previous section, and Fresnel's factors (perpendicular and parallel) also were plotted in Fig. 36. According to the design we described in the next chapter, recorded reflectance factors by the measurements equal to the sum of specular reflectance factor and internal light scattering by pigments and is given by Eq. 34. The total reflected light on the leaf surface is assumed the same as Fresnel's equations in this research. Fig. 13 shows the ratio between a specular and the total reflectance factors by Eq. 33 and the relevant ( $\sigma_{rel}$ ) is not equal to rms surface roughness  $\sigma_s$ , but a band-limited quantity that depends upon the wavelength and illumination angle (Church and Takacs, 1995; Harvey, 2012). Equation is calculated for 10 different value of surface roughness from  $0.25 \mu\text{m}$  to  $2.5 \mu\text{m}$ , a step with  $0.25 \mu\text{m}$ . Curves present the influence of root mean square surface roughness ( $\sigma_s$ ), to specular reflectance and how much different from a smooth surface reflectance. As the incidence angle increases, results of Fresnel's equations are close to specular components of rough leaves surface.

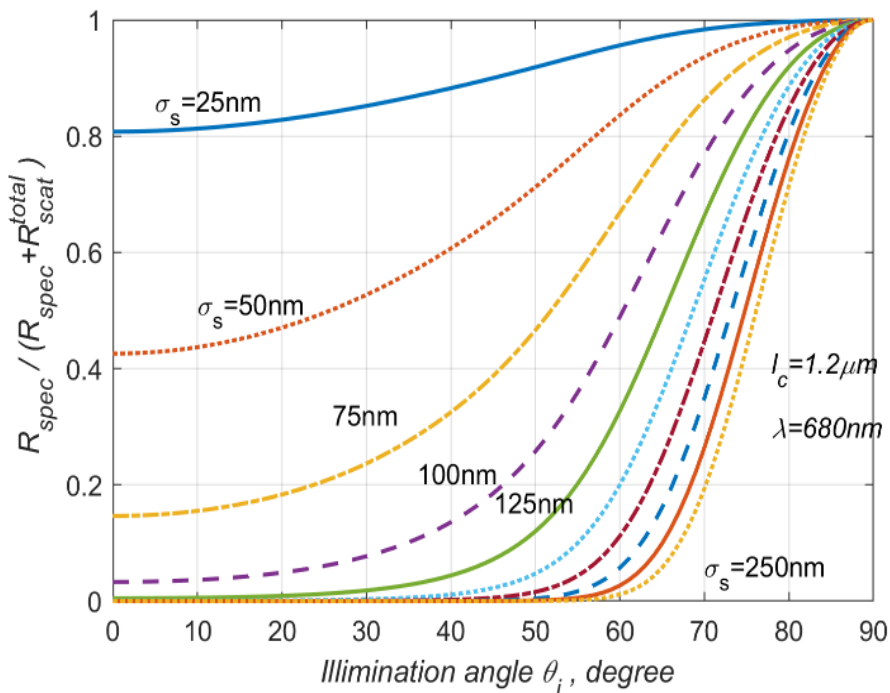


Fig. 13. Parametric curves illustrating the ratio between a specular and the total reflectance factors with illumination angle and different surface roughnesses.

The BRDF model (Bousquet et al., 2005) has three input parameters ( $k_L$ ,  $n$ , and  $\sigma$ ), and if the surface roughness theory is replaced by GHS, the correlation width ( $l_c$ ) is added to the model. Also, their work is a scalar for calculating the total reflectance factor, the model needs

to be added to the polarization dependence function for separating polarized and unpolarized components.

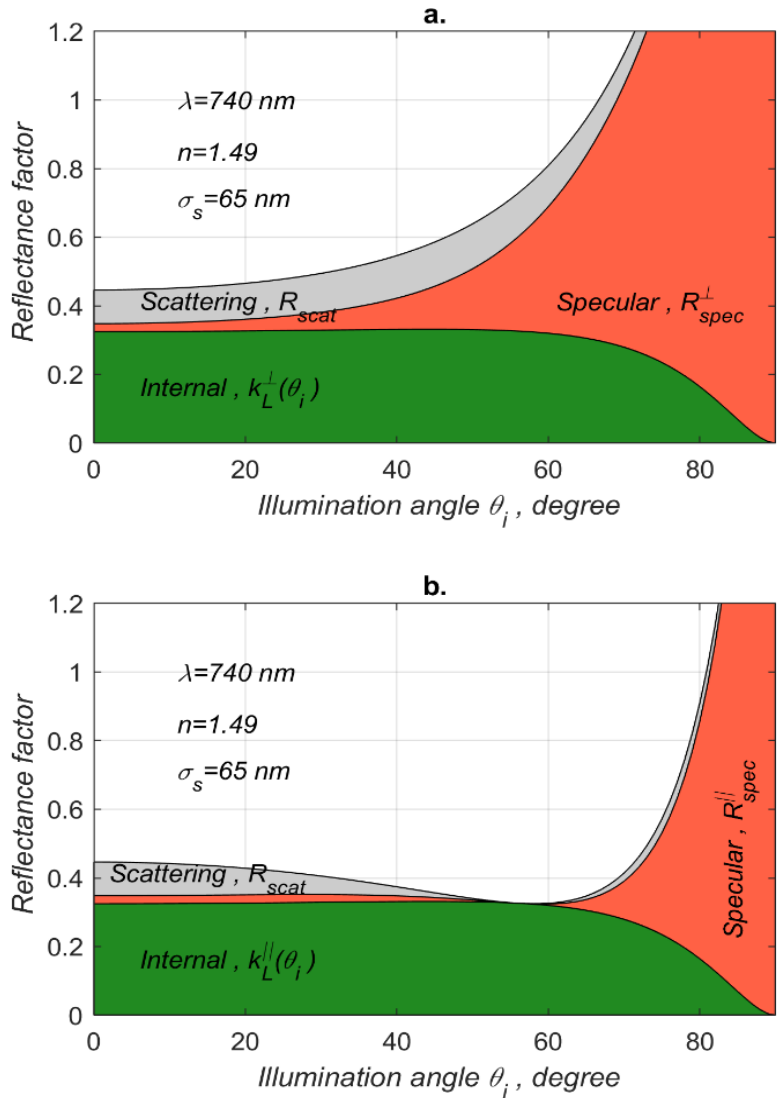


Fig. 37. (a) Perpendicular reflectance factor; (b) Parallel reflectance factor by the mirror reflection model.

In order to evaluate the surface roughness first, we found the Lambert parameter ( $k_L$ ) based on normal reflectance factor value and the real part of refractive index of the epicuticular wax is considered from 1.52 to 1.48 in 460-780 nm band by (Kuusk, 1994; Vanderbilt and Grant, 1985). In the case of the model we are concerned, the coefficient of proportionality ( $c$ ) is equal to the value of normal reflectance factor measurements. Perhaps the refractive index of the wax layer may be different. However, the surface is a homogeneous oily chemical compound and is unlikely to have a different refractive index for other leaves.

The effect of the ratio between a specular and the total reflectance factors as changing correlation width is significantly low when correlation width is higher than the wavelength ( $l_c > \lambda$ ). Therefore, the surface roughness is fitted with mirror reflection measurement when the correlation width is about  $1.2 \mu m$  ( $l_c = 1.2 \mu m$ ). Fig. 37 illustrates how light reflect on the leaves as our expected model. We can fit  $\sigma_s$  at each leaves separately by minimizing the merit function  $\chi^2$  defined as:

$$\chi^2 = \sum_{\sigma_s=10nm}^{\sigma_s=250nm} \left( \frac{R_{meas} - R_{model}}{R_{model}} \right)^2, \quad (35)$$

where lower and upper parameter bounds are 10 nm and 250 nm, respectively. The optimization algorithm is used for finding best fitting value of  $\sigma_s$ .

Table 6

The values of surface roughness of three species of leaves compared to the results of the measurements.

	The mean of $\sigma_s$ , nm	The standard deviation, nm	Max, nm	Min, nm
Coffee	71.67	$\pm 12.24$	87.22	57.25
Pothos	46.11	$\pm 6.83$	55.37	38.7
Strawberry	92.41	$\pm 9.48$	115.0	79.17

Nine or ten leaves of each of the per three species were measured, and the adaxial side's surface roughness of the leaves are estimated in this analysis. Table 6 shows the mean surface roughness ( $\sigma_s$ ) which is averaged the best fitting values of each leaves, and also shows the standart deviation, maximum, and mimumum of surface roughnesses. The leaves of one kind species have close values of RMS surface roughness in the estimation method.

The result is that an optimal surface roughness of about 46.1 nm is obtained for pothos leaves, which is almost two higher compared to strawberry leaves. The rms surface roughness reached is 71.67 nm for pothos leaves, 92.41 nm for strawberry leaves. The smoothest surfaces of leaves are pothos, and the roughest are strawberry leaves in the plants we measured. Note that although the surface roughness of strawberry is considerably higher than for pothos, The light penetration into the leaves is equal for all plants at same wavelength band. First, the light transmittance from air to leaf inside majorly depends on the refractive index of the epicuticular wax. Second, the bidirectional reflectance factor for mirror reflection is sensitive to varying illumination angle between 30° and 90°, and it looks like Brewster’s angle always shifts to a considerably higher angle. The angle at the minimum of parallel reflectance factor is actually not equal to Brewster’s angle. The minimum shifts to higher angle due to internal pigment scattering and the light passes through one medium to another (refraction).

Fig. 38 shows a comparison between mirror reflection measurement (dashed line) and mirror reflection model result (solid line) with the best fitting  $\sigma_s$  values at some considerable

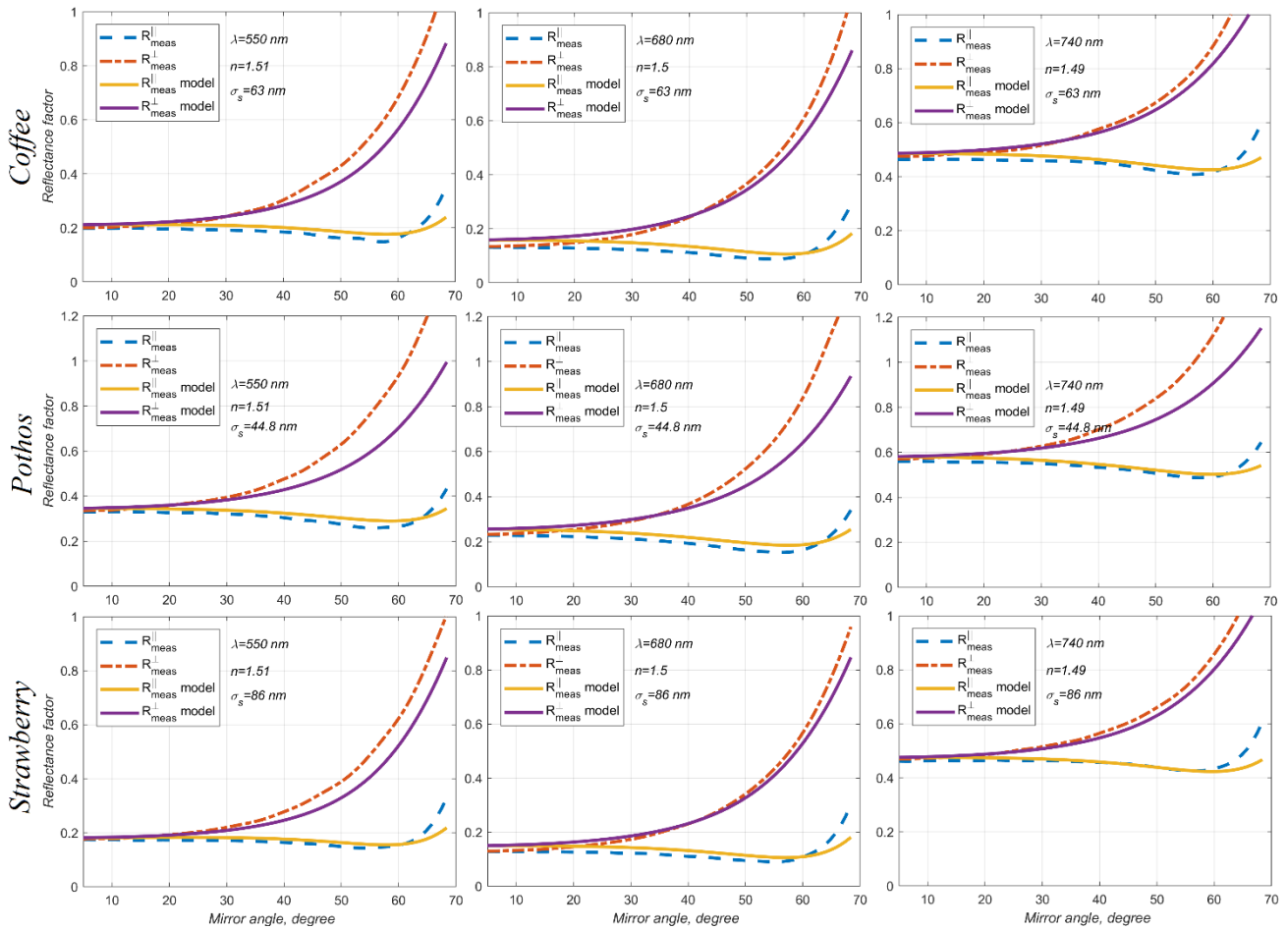


Fig. 38. Comparisons between mirror reflection measurement results and model reflectance factors for coffee, pothos, and strawberry.



wavelengths for plants. One leaf of each plant was arbitrarily chosen by from leaves for showing perpendicular and parallel reflectance factors.

### 3.4 ESTIMATIONS OF THE THICKNESS OF WAXY CUTICLE

For defining a refractive index of the leaf by Brewster's angle, we have repeatedly made mirror reflection measurement on the surface of the leaf. We have seen different phenomena from surface reflectance of the leaf, rather than the surface polarization (perpendicular and parallel reflectance). Small amplitudes were observed for the angle of reflection during the measurement. Our expectation on that phenomena was thin-film interference, which is a characteristic phenomenon in light waves reflected by the top and lower boundaries of a thin film interfere with each other, either constructive or destructive the reflected light. Then the thickness of wax cuticle is calculated on these reflections in terms of optics. So we would like to check this calculation on Transmission Electron Microscope (TEM) at Agriculture school, Hokkaido University.

#### 3.4.1 Optical estimation

If there are two different medium with different refractive indexes, also the outer shell is thin, the interference is likely to occur. This happens between light reflected from different mediums of a thin film; consequently, obstruction impacts are known as thin film interference. As saw previously, interference impacts are most unmistakable when light interacts with something having a size similar to its wavelength. A thin film is having a thickness  $t$  close to the wavelength of light. Since color is related in an indirectly with wavelength and since all

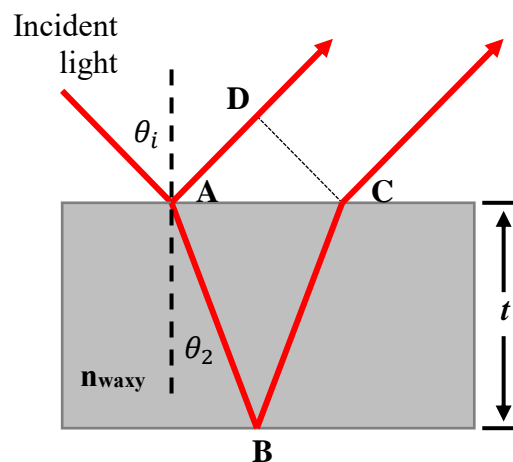


Fig. 39. Thin film interference condition.

interference depends in some way on the ratio of wavelength to the size of the object involved, we should expect to see a different color for the different thickness of a film.

Using Fig. 39, we can find the optical pathlength difference ( $\Gamma = n(AB + BC) - AD$ ). Using geometric expressions and trigonometric functions, thin film interference conditions can be found as;

$$\text{Destructive interference: } 2tn_{waxy} \cdot \cos\theta_2 = m\lambda, \text{ if a phase change is equal to } 180^\circ; \quad (36a)$$

$$\text{Constructive interference: } 2tn_{waxy} \cdot \cos\theta_2 = (m - \frac{1}{2})\lambda, \text{ if a phase change is equal to } 180^\circ; \quad (36b)$$

where  $t$  is the thickness of waxy cuticle layer,  $n_{waxy}$  is a refractive index,  $m$  is real numbers. The main parameter of these equations is a refractive index. (Kuusk, 1994; Vanderbilt and Grant, 1985) calculated refractive index (real part) of the wax cuticle layer. Refractive index of wet mesophyll cell wall computed utilizing the Dale and Gladstone law (Baranoski, 2006), and considering the refractive index of wet mesophyll cell walls measured by (Woolley, 1975) at 800nm equal to 1.415 (Woolley, 1975). These studies suggest that the refractive index of the waxy cuticle layer is higher than a refractive index of the wet mesophyll cell wall (see Fig. 9), which means phase change is equal to  $180^\circ$ . If it is lower than a refractive index of wet mesophyll, a phase change will be zero degrees.

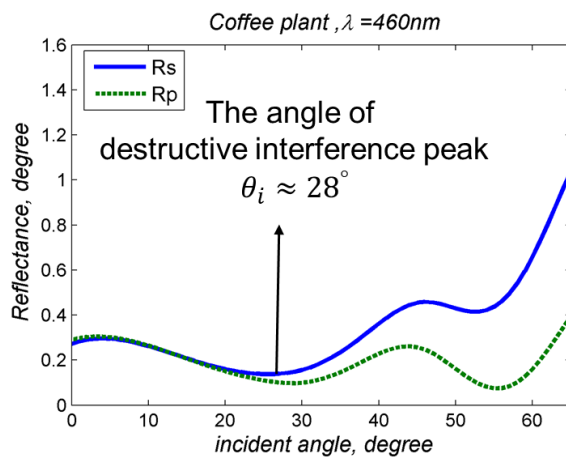


Fig. 39. Mirror reflection measurement result of coffee leaf at 460 nm.

In another hand, we measured mirror reflection of coffee leaf, one of measurement result at wavelength 460 nm is shown in Fig. 39. The destructive interference peak occurred at

incident angle  $28^\circ$ . With the Snell's law ( $n_{air} \cdot \sin \theta_i = n_{waxy} \cdot \sin \theta_2$ ), the thickness of the waxy cuticle layer can be found by

$$t = \frac{\left(m - \frac{1}{2}\right)\lambda}{2n_{waxy} \cos(\theta_2)}, \quad (40)$$

where  $n_{waxy} \approx 1.5$ ,  $\lambda = 460 \text{ nm}$ ,  $\theta_2 = 18.2^\circ$ .

So when  $m=1$ , the thickness of waxy cuticle is equal to  $t \approx 80 \text{ nm}$ ,

when  $m=2$ , the thickness of waxy cuticle is equal to  $t \approx 242 \text{ nm}$ ,

when  $m=3$ , the thickness of waxy cuticle is equal to  $t \approx 403 \text{ nm}$ .

This is a simple estimation, but in our measurements, the peak number of pothos plants leaves in the range is more than the number of coffee leaves. In the same estimation, the waxy cuticle of pothos leaf is about  $4.2 \mu\text{m}$  thick.

The thickness can be determined depending on the number of occurrences. Fig. 40 shows mirror reflection measurement result of pothos leaf at  $460 \text{ nm}$  and a relationship between a constructive interference peak numbers and the thickness of the waxy cuticle layer. The right-hand image in Fig. 40 depicts how often a constructive interference will occur within our measurement limits.

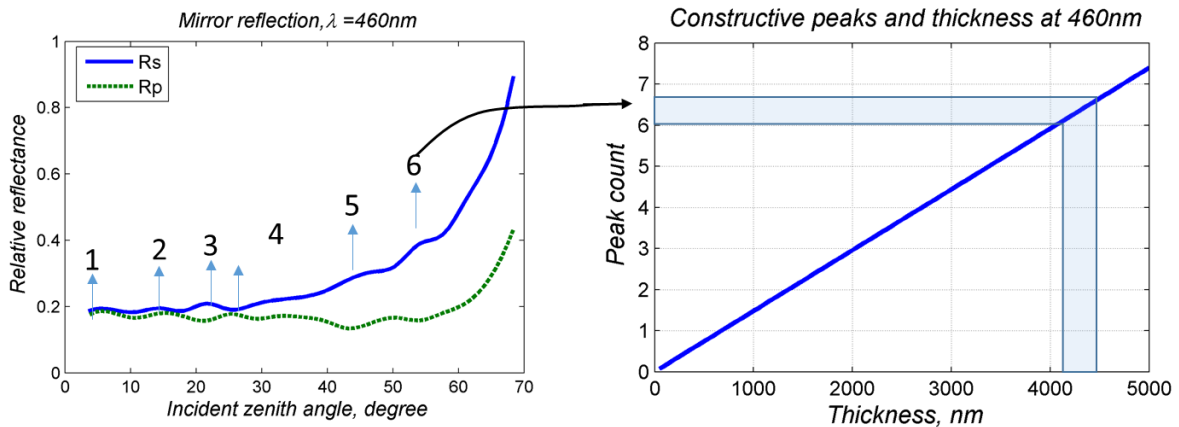


Fig. 40. Mirror reflection measurement result of pothos leaf at  $460 \text{ nm}$  and a relationship between a constructive interference peak numbers and the thickness of the waxy cuticle layer. Vertical axis is Bidirectional Reflectance Factor (BRF) for left hand graph.

This kind of effect is not seen only on the reflection of the mirror, but also in the BRF measurements of coffee plant leaf. The constructive or destructive peak strongly observed at a

wavelength of 550 nm from 460 nm therefore is much larger than the refractive index of the waxy cuticle layer in the light wavelength of misophyll layer in this light wavelength. From the leaves of strawberries, we did not see the interference waves.

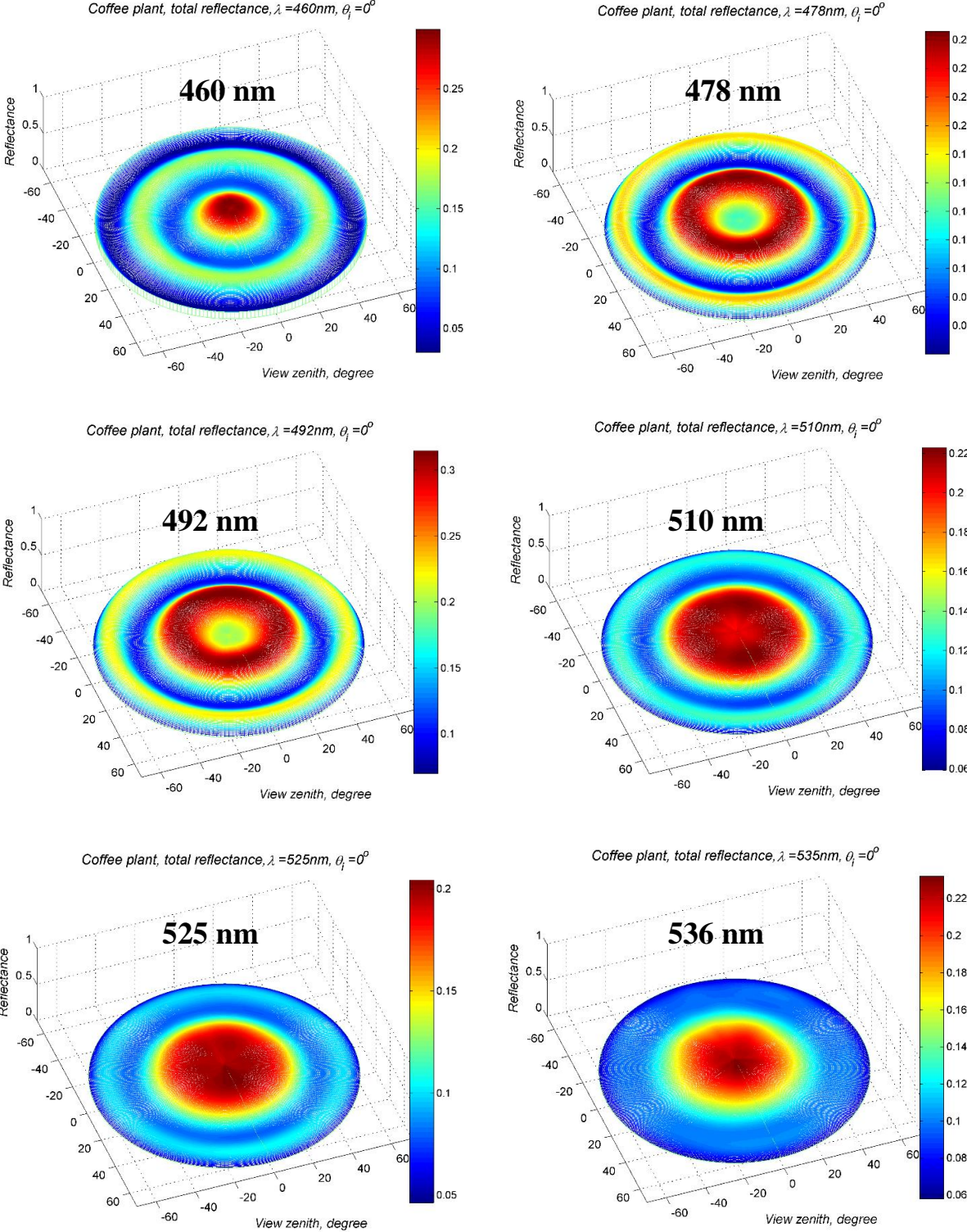


Fig. 41. Total BRDF of coffee leaf at different wavelengths. The destructive interference peak is moving to high observation zenith angle, its due to thin film interference.

### 3.4.2 Electron microscope measurement

From the optical measurements and calculations, the thickness of the waxy cuticle layer of coffee leaves about 403 nm and 4.2  $\mu\text{m}$  for the pothos. Then it was possible to check on the electron microscope. The two thicknesses determined by each other are matched.

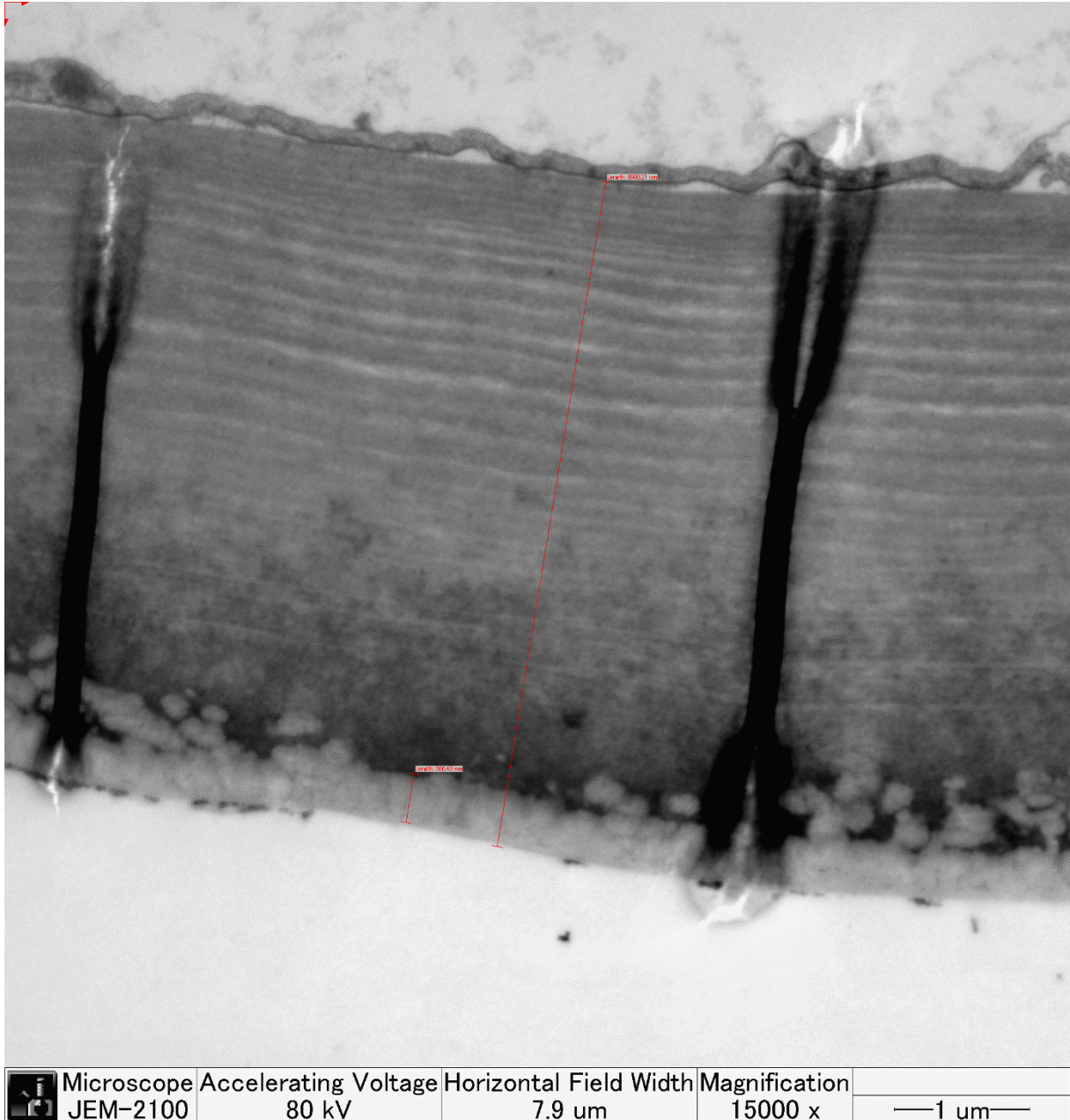


Fig. 42. The image of Transmission Electron Microscope (TEM). Image shows cross section of waxy cuticle layer of coffee leaf (adaxial side), which consist of several sections. The most top section layer is around 400 nm thick.

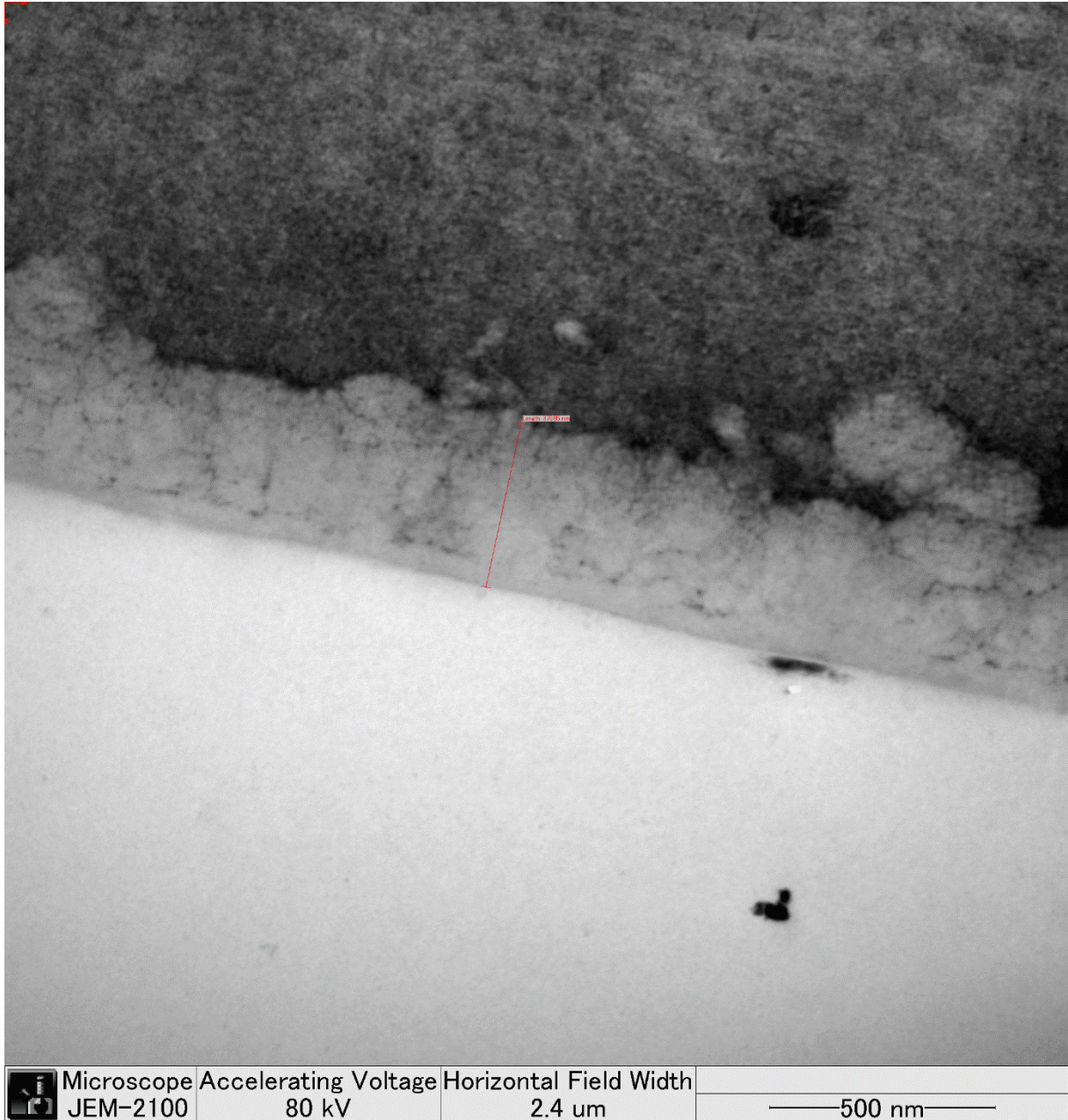


Fig. 43. Previous image is zoomed. It shows the most top section layer of waxy layer (coffee), which is about 400 nm thick.

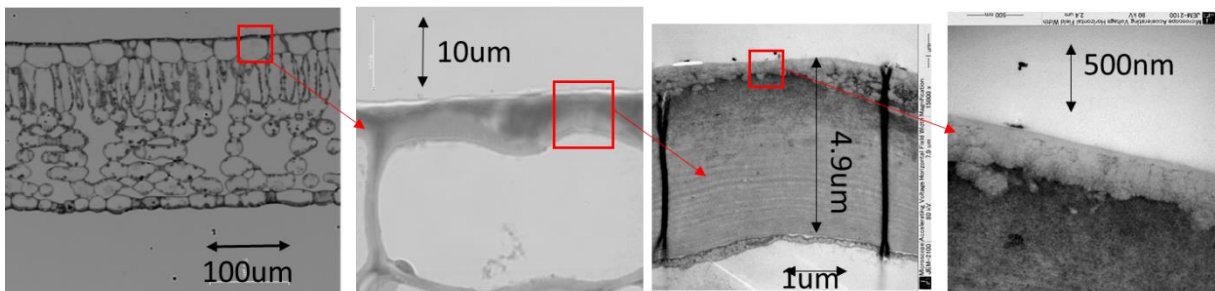


Fig. 44. Cross section of coffee leaf is zoomed on step by step.

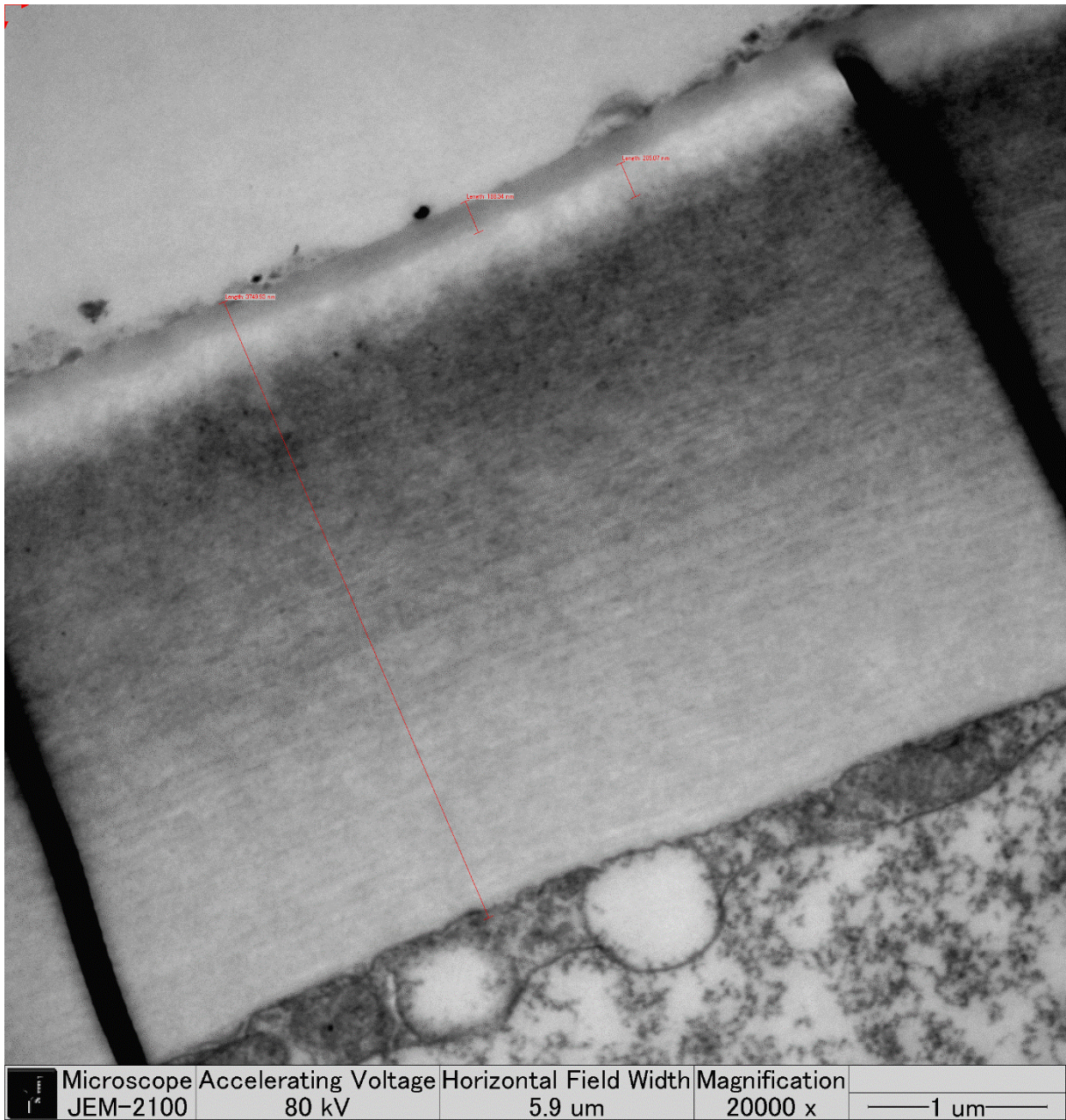


Fig. 45. The waxy cuticle layer of pothos leaf.

## CHAPTER 4: LEAF SPECTRO-POLARIMETRIC BRF PREDICTION

### 4.1 SPECTRO-POLARIMETRIC MODEL EXPECTATION

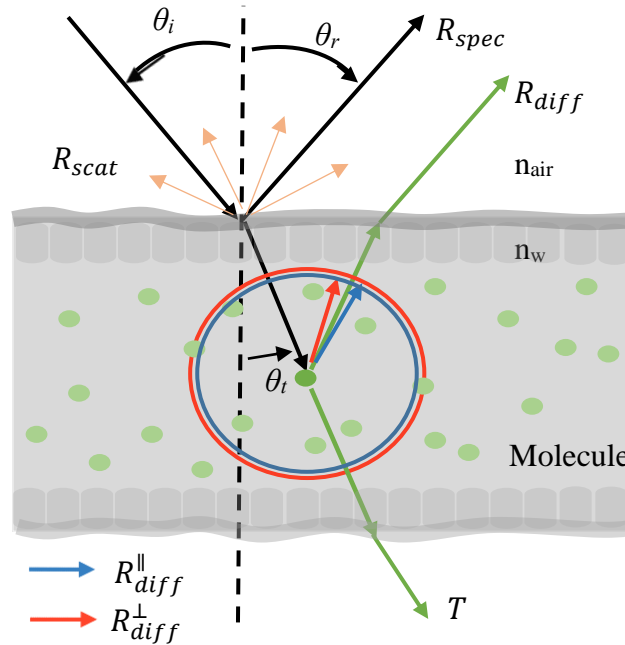


Fig. 46. Mirror reflection on the leaf and expected model ( $\theta_i = \theta_r$ ).

Although the main focus of this work was spectro-polarimetric BRF measurement of leaves using hyperspectral imaging camera, our work also considered the leaf optical reflection model, polarization property, and a method to determine surface roughness of leaves which usually measured using the scanning electron microscope (SEM) by a digital processing technique. The roughness of the surface is the key parameter for a pattern of leaf BRF that can be described by Generalized Harvey-Shack (GHS) scattering theory after determination of surface roughness analysis. This section contains the results of leaf BRF simulation and the comparison between the spectro-polarimetric model and the actual measurement.

Light scattering, always occurs when electromagnetic waves encounter molecules, and is classified by relative size of a scattering particle  $x$  (Eq. 42: where  $r$  is diameter of a molecule). Leaves have several pigments molecules such as chlorophylls, lutein,  $\beta$ -Carotenoids, and Anthocyanins. Pores diameter of those particles are all smaller than 3 nm, for example, the chlorophyll molecule is formed of a porphyrin ring of 1.5 nm by 1.5 nm head and a phytol tail of 2 nm length (Gaonkar et al., 2014, p. 300). Rayleigh scattering covers regime of particles much smaller than the wavelength of the light which means this approximation theory may able



to explain the light scattering in the leaves only for angle distribution of bidirectional reflectance and transmittance.

$$x = \frac{2\pi r}{\lambda} . \quad (41)$$

When unpolarized incident wave encounters pigment molecules in the leaves, some part energy is absorbed and their electrons are moved to perpendicular direction relative with the original wave direction and then re-radiated by oscillating electric dipoles at the molecule. Therefore maximum intensity of the scattered light is along to perpendicular direction and there is no parallel scattering relative with the original direction of propagation.

However the light scattering process of the leaf is not explained by single particle scattering, describes a radiative transfer model. It is similar to the SLOP (Stochastic model for Leaf Optical Properties) model which is originally proposed by (Tucker and Garratt, 1977) and improved by (Maier et al., 1999). The first transition of pigment molecules have a higher probability to perfectly polarized, but after second transitions, parallel diffuse reflectance cannot be polarized 100%. The characteristic polarization continues to decline meanwhile, the scattered light from internal leaf will be independent of the polarization angle (Lambertian). According to this model, we have modeled and described this process in Fig. 46. by the pigment molecules in a homogeneous transparent liquid and a rough leaf surface.

In a mirror reflection, diffuse parallel and perpendicular reflectance factors can be defined as:

$$R_{diff}^{\perp} = k_L \cdot t_{21}^{\perp} , \quad (41.a)$$

$$R_{diff}^{\parallel} = k_L \cdot t_{21}^{\parallel} . \quad (41.b)$$

where  $t_{21}^{\perp}$ , and  $t_{21}^{\parallel}$  are perpendicular and parallel transmittance respectively from the diffuse scattering to view direction, and  $k_L$  is the Lambert coefficient, which would be linear proportional to transmittance of air to leaf. According to this,  $k_L$  is written as:

$$k_L(\theta_i, \lambda) = c(\lambda) \cdot (1 - R_{spec}(\theta_i) - R_{scat}^{total}(\theta_i)) , \quad (42)$$

where  $R_{scat}^{total}$  is the total integrated scattering factor,  $c(\lambda)$  is the coefficient of proportionality, which linearly depends on an absorption of internal pigment molecules. The second part of the

Eq. 42 is Fresnel's transmittance and its members are related to the roughness and a refractive index of the surface. We will explain about the surface roughness of the leaf in the previous chapter's subsection.

In Eq. 41, transmittances are possible to easily described with the refractive index value by Fresnel's equations and Snell law:

$$\sin\theta_t = \sin\theta_r/n_w \quad (43)$$

Using Fresnel's equation, where  $t_{21}^\perp$ , and  $t_{21}^\parallel$  can be expressed with observation angle and refractive index of outer layer as

$$t_{21}^\perp = \left| \frac{n_w \sqrt{1 - \sin^2 \theta_r / n_w^2 - \cos \theta_r}}{n_w \sqrt{1 - \sin^2 \theta_r / n_w^2 + \cos \theta_r}} \right|^2, \quad (44.a)$$

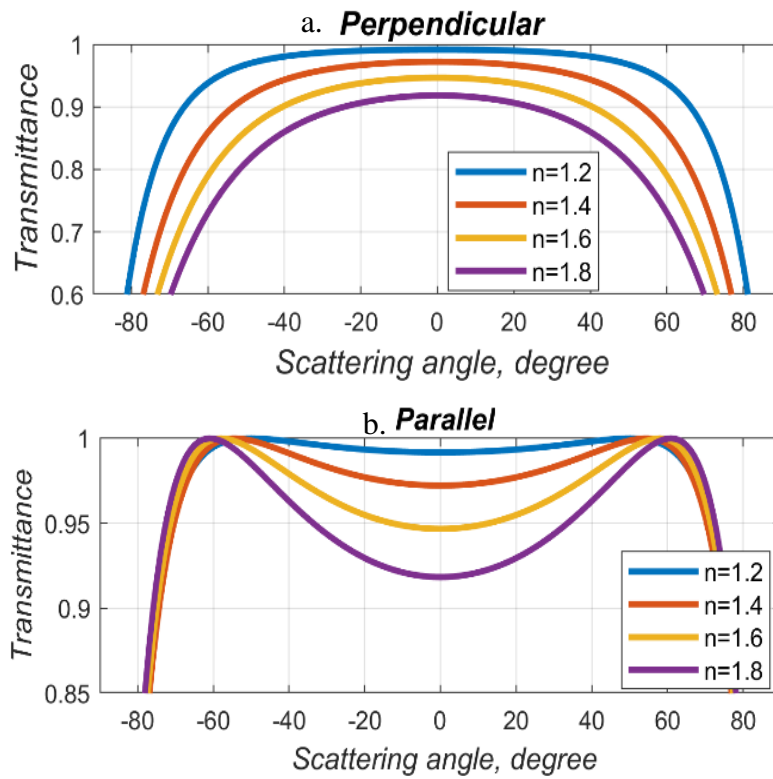


Fig. 47. a. Perpendicular  $t_{21}^\perp$ , and b. Parallel  $t_{21}^\parallel$ , transmittances of internal medium to air at different refractive indices after internal scattering light is passing through waxy cuticle layer.

$$t_{21}^{\parallel} = \left| \frac{n_w \cos \theta_r - \sqrt{1 - \sin^2 \theta_r / n_w^2}}{n_w \cos \theta_r + \sqrt{1 - \sin^2 \theta_r / n_w^2}} \right|^2. \quad (44.b)$$

Expressions have written in Eq. 44 for different refractive indices, it is shown in Fig. 47. If the polarizing filter is placed at the parallel direction ( $\alpha = 90^\circ$ ) and the leaves are measured, most higher internal scattering is located at the middle of Brewster's region.

## 4.2 MODEL PERFORMANCE

We aim to differentiate the diffuse internal scattering from the specular reflectance using the physical optics reflection model in this study. As a result the previous measurement analysis, the surface roughness of the leaves shows the values that are relatively acceptability to each other. Based on these values, the GHS theory was used to estimate the specular reflectance factors which are plotted in the two-dimensional graph (Fig. 48. a) at four different illumination angles. The angle spread function's ( $ASF(\theta_i, \phi, \theta_r)$ ) relative intensity values are not sharp when the angle of light illumination is low (for instance  $\theta_i = 0^\circ$ ), but it is quite widespread, other hands the incidence angle increases the function's intensity values are higher and sharp, and the graphic shown in Fig. 16.a is after the multiplication of Fresnel's reflection according to original. Fig. 44.a was thought to be surface roughness about  $\sigma_s = 71 \text{ nm}$  and the correlation lengths

were  $l_c = 1.2 \mu\text{m}$ , which is equal to an estimated average of the coffee leaves from the previous section.

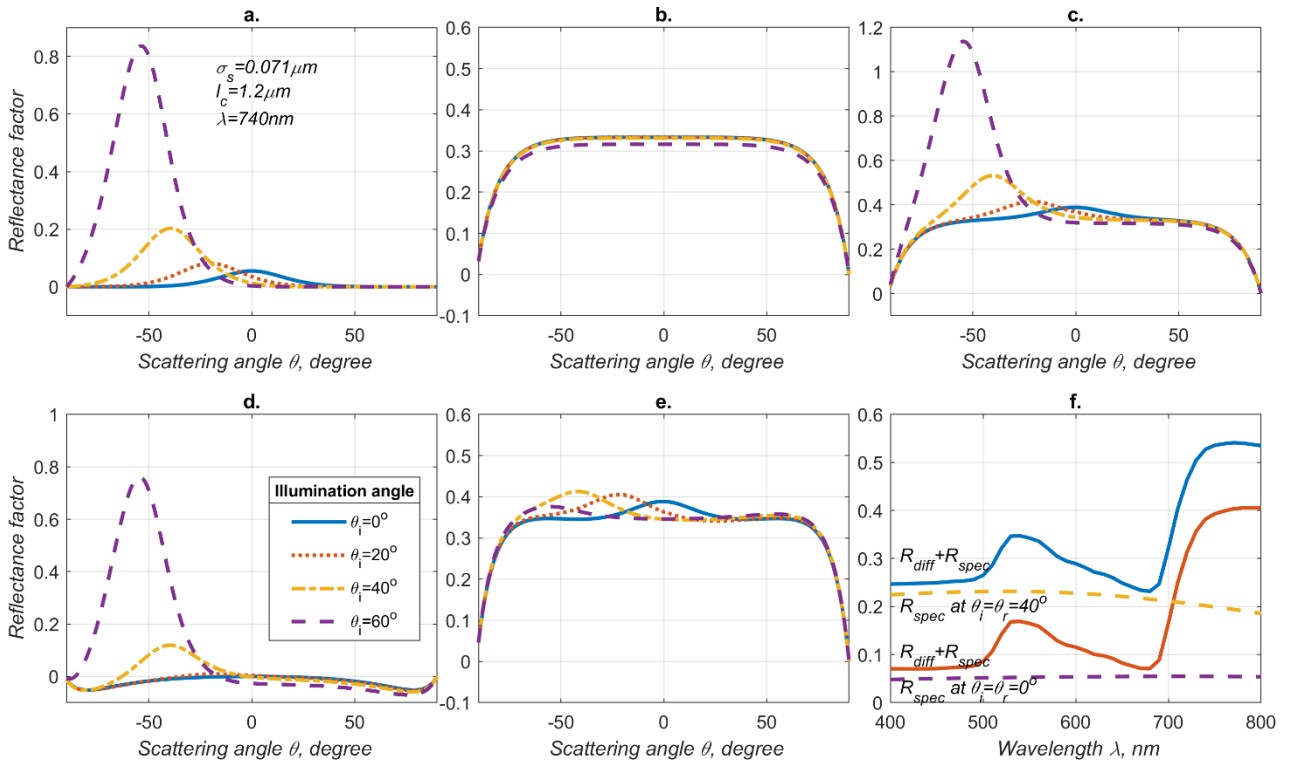


Fig. 48. Simulated a. specular, b. diffuse, c. the total, d. polarized, e. unpolarized reflectance factors all illuminated at  $0^\circ$ ,  $20^\circ$ ,  $40^\circ$ , and  $60^\circ$ , and f. the total reflectance and specular reflectance factors are observed and illuminated both at  $0^\circ$  and  $40^\circ$  for coffee leaf. The description legends of the lines in a plot (e) are illustrated, and the descriptions are identical to those in (a), (b), (c) and (e) graphs.

Fig. 48.b shows the diffuse reflectance component which was approximated as the minimum of the BRF measurement values ( $k_L = \min(BRF(\phi_i, \theta_r))$ ) at each wavelength and each illumination angle by (Comar et al., 2012), and also it is the difference between the PROSPECT model and DHRF when illumination angle is  $\theta_i = 0^\circ$  by (Bousquet et al., 2005). Our model considers that thus the coefficient of proportionality is equal to output value of PROSPECT model. Although the diffuse component is Lambertian inside of the leaves, the distribution of the internal scattering is affected by waxy cuticle layer of leaves (Eq. 42). The refractive index of the epicuticular wax is approximately 1.5 (Brewster's angle  $56.3^\circ$ ), so the total transmittance (separates to perpendicular and parallel direction) passing through the wax layer to inside the leaf is weakly correlated until illumination  $60^\circ$ . The internal diffuse light scattering of leaves

is independent on the relative azimuth angle. The sum of specular (a) and diffuse (b) components are the total reflectance factor which is shown in Fig. 48.c.

The model here specifies that polarization does not depend solely on the surface reflection of the leaf, and the inner scattering light of the leaf is refracted to make polarization when passing through the waxy cuticle layer of the leaf. On the other hand, the total polarized light (Fig. 48.d) is the sum of the surface polarized and internal polarization components. The original polarized light definition is that polarized intensity equal to the difference between the most bright and the dimmest light intensity during the turning of the polarizer. Thus the polarized reflectance can be written as

$$BRF_{pol} = Q_{spec} \cdot BRF_{spec} + Q_{diff} \cdot BRF_{diff}, \quad (45.a)$$

$$BRF_{up} = BRF_{total} - BRF_{pol}, \quad (45.b)$$

$$Q_{spec} = \frac{R_{spec}^{\perp} - R_{spec}^{\parallel}}{R_{spec}^{\perp} + R_{spec}^{\parallel}}, \quad (45.c)$$

$$Q_{diff} = \frac{R_{diff}^{\perp} - R_{diff}^{\parallel}}{R_{diff}^{\perp} + R_{diff}^{\parallel}}. \quad (45.d)$$

For a polarization dependent function of the diffuse component ( $Q_{diff}$ ), the minimum and the maximum values of reflectance factors correspond to parallel and perpendicular directions, respectively.  $Q_{diff}$  does not depend on the relative azimuth angles, and is isotropic. A specular polarization dependent function ( $Q_{spec}$ ) exactly matches the above equation at the azimuth angle  $0^{\circ}$  and  $180^{\circ}$ . Although the most bright and the dimmest is discordant with parallel and perpendicular directions for other angles, the difference on the result is significant small. In some cases the polarized reflectance factor has a negative values that means the diffuse reflectance factor coming from the parallel direction is greater than the perpendicular direction ( $R_{diff}^{\perp} < R_{diff}^{\parallel}$ ).

Fig. 48.f shows the relationship between the reflectance factors of the leaves and the wavelength at the illumination angle  $0^{\circ}$  and  $40^{\circ}$ . The diffuse light reflection has a small change when the illumination angle increases, but the specular reflectance factor decreases on the red and NIR comparing with the blue color. A shorter wavelength of the light on the rough surface is more dispersive that the specular component of shorter light is lower than a longer one.

However, the surface refractive index of leaves is high at 400 nm and refraction decreases to a longer wavelength (Kuusk, 1994; Vanderbilt and Grant, 1985).

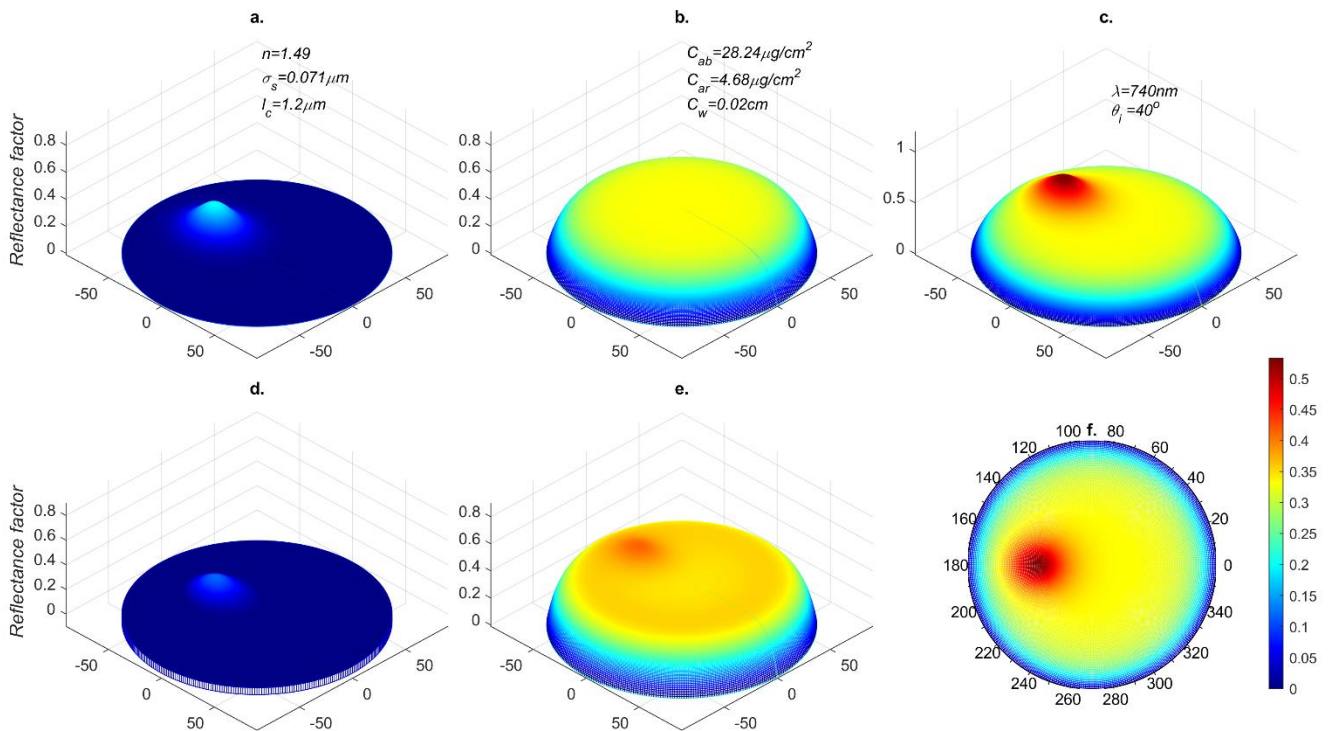


Fig. 49. Three dimensional simulated a. specular, b. diffuse, c. the total, d. polarized, e. unpolarized reflectance factors, and f. a representation of total reflectance factor which is same as plot (e), these are all illuminated at  $40^\circ$  for coffee leaf. Note: first 5 plots are viewed at zenith  $45^\circ$  and azimuth  $50^\circ$ , and the last one is viewed at zenith  $0^\circ$  and azimuth  $90^\circ$ ; A zenith axis is showed until  $90^\circ$ .

All reflectance factors are plotted on the three-dimensional polar coordinate system in the same way as previous plot in Fig. 49.

## CHAPTER 5: DISCUSSIONS

### 5.1 About spectro-polarimetric measurement results

Specular reflectance of the leaf strongly depends on a combination of the angle of incidence of the light source and the angle of observation view. The leaves look shiny at the shallow angle, where the most of this reflection is polarized from the surface of leaves. Although the leaf spectral reflectance which is a point of convergence for many types of research, the study of spectral measurement with polarization in a single leaf is largely unexplored. Knowledge of how to reflect the light on one leaf becomes more important, and better study is needed when observation distance come closer. The first goal of this dissertation was to introduce a spectro-polarimetric BRF measurement of leaves using Liquid Crystal Tunable Filter (LCTF) camera in a laboratory and to verify directional optical properties how consistent with previous works. However, the primary goal of this thesis was that it would have been possible to investigate the possibility of knowing the spectral information on green leaves more stable using light polarization property.

The first systematic precise research works on bidirectional reflectance (also transmission) property of single leaf (individual) was accomplished by (Breece III and Holmes, 1971). Measurements of fresh soybean and corn leaves procured in the principal plane in 19 narrow wavelength bands from 375 nm to 1000 nm indicated strong specular reflectance property at wavelength bands of strong absorptions, which are located at the blue and red chlorophyll absorption bands. Transmission qualities were all way direction same (Lambertian) for all wavelength bands occupied in any case. Walter-Shea (Walter-Shea et al., 1989) continued the study of Breece and Holmes one more step further by obtaining information in different view azimuth planes. In their exploration, the Bidirectional Reflectance Factor (BRF) of corn and soybean single leaves demonstrated increasingly non-Lambertian properties with increasing light source zenith angle, and these results are consistent with our measurement on all three leaves (Fig. 32). This result was concluded to specular reflectance on the adaxial side (top side of the leaf) of leaf surface that can be considered as consisting of a distribution of facets that specular reflected light on the leaf is according to Fresnel's equations (Vanderbilt et al., 1985; Woolley, 1975).

The reflectance of the leaf consists not only of its intensity but also of polarization, and the polarization techniques are generally used for separating specular reflectance from diffuse

reflectance. Brakke (Brakke et al. 1993; Brakke, 1994) utilized polarization to differentiate radiation scattered from leaves into its diffuse and specular components. The internal diffuse component of the spectral reflectance contains the details of the biochemical properties of the plant, an activity of photosynthesis, an expected amount of harvest, and water condition. While the reflectance from the adaxial side of single leaves of tree species, for example, yellow poplar, red oak, and red maple demonstrated strong non-Lambertian reflectance property with a distinct forward scattering peak particularly in the visible range, transmitted light appeared relatively isotropic.

The reflectance from the abaxial (lower) side of tree leaves was additionally fairly uniform due to its rougher surface, which enhances scattering, especially in the NIR range. The main dependence of BRF measurement shape caused on the specular reflectance by waxy cuticle which is the outer surface layer of leaves. (Bousquet et al., 2005) found a surface roughness of the leaf mainly drives the specular component's BRF shape in the wavelength range from 480 to 880 nm. Specular component not correlated with the wavelength which means the surface of the leaf is optically non-dispersive in that band. They observed a strong acceptance with the BRF measured with a goniometer over three plant leaves showing no anisotropic roughness features. Some sort of leaves is azimuthal anisotropy of monocot individual, which was first observed by (Comar et al., 2012; Combes et al., 2007). Comar picked up Bousquet's idea of leaf BRF model and developed to add as the azimuthal anisotropy of individual leaves surface (Comar et al., 2014). Our measurement results shows that the general shape of leaf BRF result was independent of the wavelength if a common constant part is removed. Because a review of previous studies, the total BRF is the sum of the specular and diffuse components and the internal diffuse component is a perfect Lambertian scatterer. The results of this measurement can be made the same conclusion as (Bousquet et al., 2005) on the total reflectance factor plots. Leaf BRF is less dependence on the low observation angles, due to measurement is less accurate than sharp slope angles. Although some types of leaves have azimuthal anisotropy (Comar et al., 2014), all of our selected leaves were the isotropic surface properties.

Previous studies are not used polarization technique for separating specular and diffuse reflectance components on individual single leaves. The contrast of this work is that the camera is being used for the first time in a single leaf BRF measurement, as well as the spectrum signature and polarization both are considered in this dissertation. However polarization method is not new for measuring canopy vegetation, with LCTF camera measurement can be made more accurately than the traditional spectrophotometric analysis, and the combination



between spectral measurement and polarimetry experiments is unique for an optical property of the individual leaf. We mentioned that the reflectance of the leaf consists not only of its intensity but also of polarization. The leaf BRDF intensity was measured (Bousquet et al., 2007, 2005, Comar et al., 2014, 2012; Combes et al., 2007; Peltoniemi et al., 2005; Weiss and Baret, 1999) or the canopy polarization measured alone for whole vegetations (Dong et al., 2018; Sokolov et al., 1999; Sun et al., 2018) in many articles and the polarization of reflected light on the leaf was well studied by (Grant et al., 1993; Vanderbilt et al., 1991; Vanderbilt and Grant, 1985; Vern C. Vanderbilt and Lois Grant, 2000). However, as well as both the spectrum signature and polarization were not considered simultaneously. So we will verify our experiment directional optical properties how consistent with previous works.

Polarimetry systems are a well-established technique in a variety of systems for improving the visibility of objects such as differentiating specular and diffuse reflection, edge identification between objects and background and discrimination between metal and dielectric surfaces. Although the leaf spectral reflectance which is a point of convergence for many types of research, we plan to introduce a spectro-polarimetric BRDF measurement of leaves using Liquid Crystal Tunable Filter camera in a laboratory. Such kind results will be totally new for an optical property of single leaves such as polarized and unpolarized reflectance factors are separated the first time for showing three individual leaves (coffee, pothos, and strawberry). Spectro-polarimetric measurement shows that unpolarized reflectance factors are stable (less dependent) on both the observation and illumination angle (See Fig. 33).

In a field, leaf Directional Hemispherical Reflectance Factor (DHRF) is difficult to determine in real life, the integrating sphere is needed or hundreds leaf BRDF measurement is required at the outside. Leaf DHRF are typically made using the integrating sphere and the mensuration at the angle of the illumination angle of  $0^\circ$  should match the results of the PROSPECT model. Traditional DHRF measurements are normally based on total light reflection, while the calculations for this work were estimated on both polarized and unpolarized BRDF. That means we first show calculation of polarized DHRF and unpolarized DHRF in Fig. 34. Surprisingly, the result of spectral reflectance model (PROSPECT) and unpolarized DHRF results were well suited without calibration (or adjustment) coefficients at the illumination angle of  $0^\circ$  for every selected species leaves, and a small amount of difference was sighted at different illumination angles. Veritably BRDF measurement results strongly depend on the angle of illumination and the angle of observation both. If a method of stabilizing is exist, it is possible to quickly determine the biochemical contents of the leaves using the

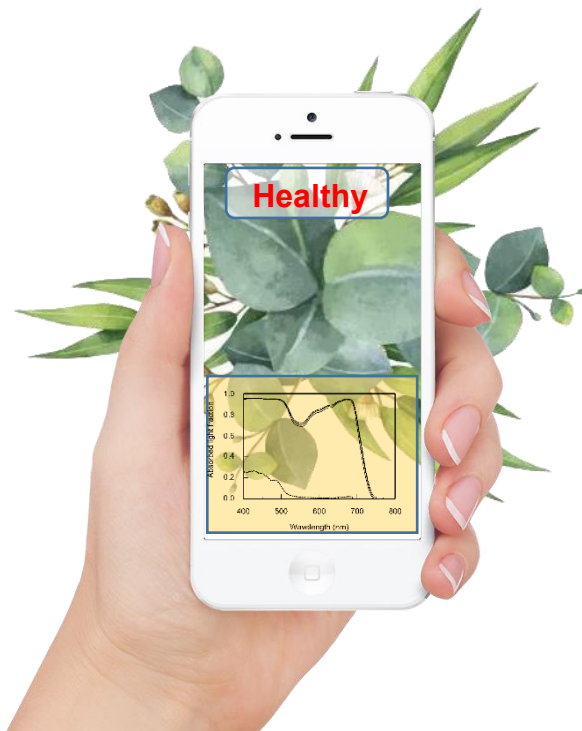


Fig. 50. Future technology of leaf health condition using spectro-polarimetric observation. Technology gives us to quickly determine the biochemical contents of the leaves more precisely in a field.

PROSPECT model in a field. Thus, the results show that spectro-polarimetric measurement is able to do that. In other words, the outer shells of the leaf will get rid of the light spectrum and the inner details of the leaves will be more delicate.

## 5.2 About optical estimations for leaf surface

Leaf surface roughness has extraordinary interest in agricultural spraying since it is utilized to characterize leaf surface wettability to foresee the behavior of droplets on a leaf surface. Surface roughness of leaves surfaces is majorly caused by surface contour, hairiness, trichomes and waxes, and may be further altered by environmental factors such as dust and moisture deficit (Journaux et al., 2011). We are more interested in the optical side, and the individual leaves reflectance models usually use the Cook-Torrance model (Bousquet et al., 2005; Comar et al., 2014a; Combes et al., 2007) that is may not suitable for leaf reflectance in our observations because the surface roughness cannot be determined by the actual measurement.

There are two way to estimate leaf surface roughness; one is proposed using image processing based on Generalized Fourier Descriptors for instance (Bediaf et al., 2015); another way is that the quantity of leaf surface roughness is generally measured by Scanning Electron

Microscope (SEM), so comparisons between optical calculations and microscopic measurements are still required to be considered for the leaf surface roughness. Due to this reason, one of the goals of this thesis is to find a comfortable and new approach to estimate the surface roughness of leaves. We introduced a new approach to estimate leaf surface roughness based on the ratio between the total reflected radiant power and diffusely reflected power, which is called Total Integrated Scatter (TIS) which was first found a functional relationship by (Bennett and Porteus, 1961) and that relationship has an exponential correlation with an intrinsic RMS roughness.

Results of new approach to estimate the surface roughness of leaves were relatively reasonable about 46.1 nm for pothos, 71.67 nm for coffee, and 92.41 nm for strawberry leaves (chapter 3.3). However, related people of this thesis did not make a comparison measurement or calculation between a new approach and existed method

Plant epicuticular waxy cuticle layer are found on many vegetation surfaces such as leaves, fruits, grass and shoots. Waxy cuticles have been studied first by light microscopy and later by Transmission electron microscopy (TEM) (MARTIN and JUNIPER, 1970). Including the content of Scanning Electron Microscopy (SEM), various scientific works published about epicuticular wax layer and reviewed many times (Baker, 1982; Barthlott, 1981; Barton et al., 1992; Johnson and Jeffree, 1970). Cuticular waxes consist of several type of mixture of lipids that have been studied strongly after being washed the leaf surface by organic solutions (Baker, 1982; Tulloch, 1976). Because of such investigations it wound up obvious that the occurrence of certain wax crystals frequently connected with the presence of explicit parts inside within the wax, prompting several papers managing the interrelation between chemical composition and micromorphology of crystal types.

For defining a refractive index of the leaf, repeatedly made mirror reflection measurements were made repeatedly on the surface of the leaf. We have seen different phenomena from surface reflectance of the leaf, rather than the surface polarization connecting Fresnel's law(perpendicular and parallel reflectance). Several amplitudes were observed for the angle of reflection during the measurement. Our expectation on that phenomena was thin-film interference, which is a characteristic phenomenon in light waves reflected by the top and lower boundaries of a thin film interfere with each other, either constructive or destructive the reflected light. Then the thickness of wax cuticle is calculated on these reflections in terms of optics. So we would like to check this calculation on Transmission Electron Microscope (TEM).

Our question was that is it possible to estimate the thickness of the waxy cuticle by optically instead of an electron microscope. Although several methods have measured the thickness epicuticular waxes, their approaches are using the direct access to isolated individual wax crystals by electron microscopes (Ensikat et al., 2000). The optical estimation to find the thickness of the waxy cuticle layer could give much cheaper and spends less time in a laboratory. Also, it gives new and helpful information to answer such questions. We would like to introduce a new approach that finds the thickness of the epicuticular wax layer from leaf surfaces. Then the thickness of wax cuticle is calculated on these reflections concerning optics. From the optical measurements and calculations, the thickness of the waxy cuticle layer of coffee leaves about 403 nm and 4.2  $\mu\text{m}$  for the pothos. Then it was possible to check on the electron microscope. The two founded thicknesses (optical and TEM) are matched each other.

### 5.3 About experimental setup

Many types of research facility goniometers of radiometric measurement have been constructed for studying the BRDF of materials, earth surface even other planet or moon. Cosmologists have utilized goniometers for reflectance estimations of terrestrial surfaces, for example: rock samples, soils, powders, and snow so as to clarify the reflectance properties of lunar surface (Coulson et al., 1965; Di Girolamo, 2003; Hapke and van Hoen, 1963; Kamei et al., 1997; Yin et al., 2018). Remote sensing researchers previously investigated the scattering and polarization properties of vegetation leaves with small-target goniometers (Bousquet et al., 2005; Brakke, 1994; Brakke et al., 1989; Breece III and Holmes, 1971; Vanderbilt and Grant, 1985), and since the beginning of the 1990s to until now, substantial goniometers have been deployed to explore the BRDF properties of vegetation canopies for instance (Sun et al., 2017b).

The optical property of the individual leaves are usually studied using short distance or small target goniometers for instance: (Brakke, 1994; Breece III and Holmes, 1971; Vanderbilt et al., 1985) and measured in a laboratory. Darkroom measurements supply much better control of the light source incidence angle than outside field measurements, and also it can be more precisely defined the diffuse compounds (Dangel et al., 2003). We built the automatic goniometer with LCTF camera starting from summer of 2016 in Hokkaido University.

In any case, since it is basically difficult to record reflectance at all angles, the BRDF is rather evaluated as a function of multiple reflectance data acquired at discrete points. In the field, and also in laboratory experiments, the direct measurement of bidirectional reflectance

factor is recorded with the guidance of a goniometer, which is an instrument that positions a sensor to obtain spectral measurements over a full scope of viewing angles. The subsequent BRDF of an objective yields important information about the physical structure of the object that can't be created from single-point spectral measurements (Barnsley et al., 1994; Combal et al., 2003). For this reason, our first goal is to create a new measuring goniometer system, which is suitable for Liquid Crystal Tunable Filter (LCTF) camera with polarization filters. Such kind of experimental setup is being used for the first time in a single spectro-polarimetric leaf BRF measurement. This imaging technique has a great advantage in measuring a selected leaf area with an arbitrary size of the field of view. One of the purposes of this work was to develop a methodology for measuring leaf BRDF using LCTF cameras.

#### 5.4 About new Spectro-Polarimetric BRF model of leaves

Modeling the optical property of the leaf was first established by (Allen et al., 1969) when he estimated the effective index of refraction and an absorption coefficient of a corn leaf by inverting the plate model on the geometric optic. Most of the papers have focused on spectral reflectance and transmittance of the leaf in connection with their chlorophyll content, water, dry matter, cellulose, nitrogen content and their structure of layers. Based on these research works, a radiative transfer model PROSPECT has been designed by (Jacquemoud and Baret, 1990), which has widespread usage in the remote sensing community and based on Allen's generalized "plate model" considers in optical visible and infra-red band from 400 nm to 2500 nm. This optical region is divided into three parts by absorption property of contents (Jacquemoud and Ustin, 2001). 400-800 nm visible light (VIS) and near infra-red (NIR) has a strong absorption by photosynthetic chlorophyll and other pigments in the leaf. 800-1100 nm near infra-red where absorption is limited to dry matter but where be multiple scattering within the leaf. 1100-2500 nm middle infrared also has strong absorption by water in a fresh leaf and dry matter. From such separation, pigment contents occupy the most important role on the leaf spectral reflectance that has a weak correlation with water and dry matter content in the VIS and NIR.

Based on previous works, many models have been published during the last two decades, but the most popular is the SAIL canopy bidirectional reflectance model (Jacquemoud et al., 2009) which is combined with PROSPECT model. These two models give a chance to determine spectral and directional reflectance by Earth observation sensors regarding leaf biochemical contents and canopy structure. Many researchers confuse distinguishing the BRF

models of single leaf (individual) from plant canopy models, so sail model is canopy. But individual leaf models are more physical, and plant canopy models are the more statistically significant. Connecting with plant bidirectional reflectance, polarized reflectance models exist for natural Earth surfaces such as Nadal-Breon (NB) Polarized Reflectance Model (Nadal and Breon, 1999), One-Parameter Polarized Reflectance Model (Maignan et al., 2009), and Diner Polarized Reflectance Model (Diner et al., 2002). But in case of a individual leaf, the polarization model is not yet studied. After our experiment of light polarization, it is possible to formulate of bidirectional polarized reflectance pneumonia on the leaves with spectral information.

The individual leaves bidirectional reflectance models usually use the Cook-Torrance model (Bousquet et al., 2005; Comar et al., 2014a; Combes et al., 2007) that is may not suitable for leaf reflectance in our observations because the actual measurement cannot determine the surface roughness. The Generalized Harvey-Shack (GHS) scattering theory is well studied from rebound models determined by height distribution (Krywonos, 2006) and the GHS theory is not limited to any special wavelength range and RMS roughness value. Our biggest goal is to replace a method of the specular component descriptions by physical surface roughness theory by GHS scattering theory. We have developed a new model of individual leaf bidirectional reflectance combined with PROSPECT D spectral model, and such new model covers the spectral property, polarimetric characteristics, three-dimensional BRDF pattern, and surface roughness of leaves. Thin film interference effect has not consisted of this numerical model.

## CHAPTER 6: SUMMARY AND CONCLUSIONS

### 6.1 THESIS CONCLUSIONS

This paper presents spectro-polarimetric BRF measurement results of three sort of plant leaves in a laboratory using LCTF camera on the type of self-made automatic goniometer envelopes observation zenith angles up to  $\theta_r \in [-72^\circ +72^\circ]$  and relative azimuth angle,  $\phi \in [0^\circ 180]$  degrees. The one of contrast is that the multispectral camera is being used for the first time in a such kind of experiment. Reflectance factors were calculated on pixels, which is able to crop surface area of a leaf that means it can select an arbitrary size of the field of view and to identify leaf area helps us to determine precisely where measurement is made on leaf. The total reflectance components of quantification approved the previous work, videlicet the general shape of leaf BRF result was independent of the wavelength if a diffuse component is removed (Bousquet et al., 2005), and the light reflectance increases at the sharp slope angle of view (Bousquet et al., 2005; Brakke, 1994; Comar et al., 2014; Combes et al., 2007; Walter-Shea et al., 1989). The canopy of pothos is mostly smooth than other measured leaves or perhaps surface roughness of the waxy cuticle layers are small, because measured the total reflectance factors of pothos were highest that could reach about 0.8 at Brewster's angle ( $\approx 57^\circ$ ).

Motorized linear polarizer was put in front of LCTF camera lens, normally doing the measurement at  $\alpha = 0^\circ, 45^\circ, 90^\circ, \text{ and } 135^\circ$  by LCTF camera for separating polarized and unpolarized reflectance factors by Stock's parameters. Using that separated parts and an estimation of the surface roughness can be made accurate calculations of diffuse and specular reflectance. One interesting interpretation can be made to understand why a polarimetric results show polarization does not only depend on light reflection of outermost waxy cuticle layer, but it also depends on the internal diffuse scattering. For instance, the polarized light reflection appears to decrease slightly in the NIR region. Thus we focused on the Lambertian scattered light coming from inside refracts on outer epidermis layer and modeled our expectation. The distribution of correlation coefficients between unpolarized DHRF from the  $0^\circ$  to  $60^\circ$  illumination angle and the PROSPECT model results were normally higher than 95% in polarimetric analysis. Veritably the total BRF measurement results strongly depend on the angle of illumination and the angle of observation both. But unpolarized BRF measurements were a stable (constant) or small deviation on observation zenith and azimuth axis measurements. Coefficients of variation (CV) between the unpolarized reflectance factors and their average

value  $\bar{R}_{up}$  reach an impressive 8.6 % for coffee, 3.7 % for pothos, and 8.1% for strawberry in NIR band that gives us to quickly determine the biochemical contents of the leaves more precisely using the PROSPECT model in a field. Although leaf DHRF is difficult to determine in real life and the integrating sphere is needed or hundreds leaf BRF measurement is required at the outside, polarization techniques allows to make a few measurements for estimating biochemical contents in a leaf.

Our analysis considered the waxy cuticle is a homogeneous, oily chemical compound and cannot be a different refractive index for all leaves. The real part of refractive index of the epicuticular wax is 1.52 to 1.48 in 460-780 nm band by (Kuusk, 1994; Vanderbilt and Grant, 1985). The surface roughness of most outer layer is calculable by the optimization if reflective indices are fixed. Mirror reflections of all leaves were additionally measured from  $3.6^\circ$  to  $68.4^\circ$  with an accuracy of  $1.8^\circ$  for estimating surface roughness. The result is that an optimal surface roughness of about 46.1 nm is obtained for pothos leaves, which is almost two higher compared to strawberry leaves. The rms surface roughness reached is 71.67 nm for coffee leaves, 92.41 nm for strawberry leaves. The quantity of leaf surface roughness is generally measured by Scanning Electron Microscope (SEM), so comparisons between optical calculations and microscopic measurements are still required to be considered for the leaf surface roughness.

Amplitudes were observed for the angle of reflection during the mirror reflection measurement even from leaf BRF (weaker than mirror). Our expectation on that phenomena was thin-film interference, which is a characteristic phenomenon in light waves reflected by the top and lower boundaries of a thin film interfere with each other, either constructive or destructive the reflected light. Then the thickness of wax cuticle is calculated on these reflections in terms of optics. From the optical measurements and calculations, the thickness of the waxy cuticle layer of coffee leaves about 403 nm and 4.2  $\mu\text{m}$  for the pothos. Then it was possible to check on the electron microscope. The two founded thicknesses (optical and TEM) are matched each other.

The individual leaves reflectance models usually use the Cook-Torrance model (Bousquet et al., 2005; Comar et al., 2014; Combes et al., 2007) that is may not suitable for leaf reflectance in our observations because the surface roughness cannot be determined by the actual measurement. The Generalized Harvey-Shack (GHS) scattering theory is well studied from rebound models determined by height distribution (Krywonos, 2006) and the GHS theory is not limited to any special wavelength range and RMS roughness value. The authors of this article



received the main ideas of prior knowledge and only tried to replace a method of the specular reflection pattern by physical theory. The parameter being added to the previous models is the autocovariance width,  $l_c$  of the surface and this parameter has more control over the spread of specular compounds. The study of GHS theory on the leaf has led us to an infinite number of questions. For instance, the autocovariance width is always equal to  $1.2\mu m$  in this paper, but it may increase the value with surface roughness. because relevant statistical surface characteristics are the relevant band-limited rms roughness  $\sigma_{rel}$ . It became a new model covering both spectral and polarization property of the leaves.

## 6.2 FUTURE WORK

Various measurements, calculations, and experiments have been left on spectro-polarimetric measurement and model for the future due to lack of time (for instance: the experiments on BRDF measurements of leaves are usually very time consuming, requiring even days to finish a single run). Future work concerns the more in-depth analysis of polarization property of leaves, new proposals to try different approaches, or just curiosity. Although, as we have mentioned, we consider that the goal of the thesis has been completed, there are plenty of new improvements that could be finished in order to achieve better results.

For experimental physics or experimental science, cutting edge technologies and accurate measurement technologies have always been new scientific discoveries and the beginning of new things. We used the spaceborne hyperspectral camera with Liquid Crystal Tunable Filter (LCTF) to measure the bidirectional reflectance factors of an individual leaf in a laboratory using automatic goniometer system. Although, using LCTF camera was great advantage of this work, the automatic goniometer system we are using needs more development. Furthermore, it is necessary to measure the spectro-polarimetric property of other surfaces such as soil, rock, sand, snow, ice, and so on. That is why we are planning to design a more precise system. Fig. 51 shows new sketch design of BRDF goniometer.

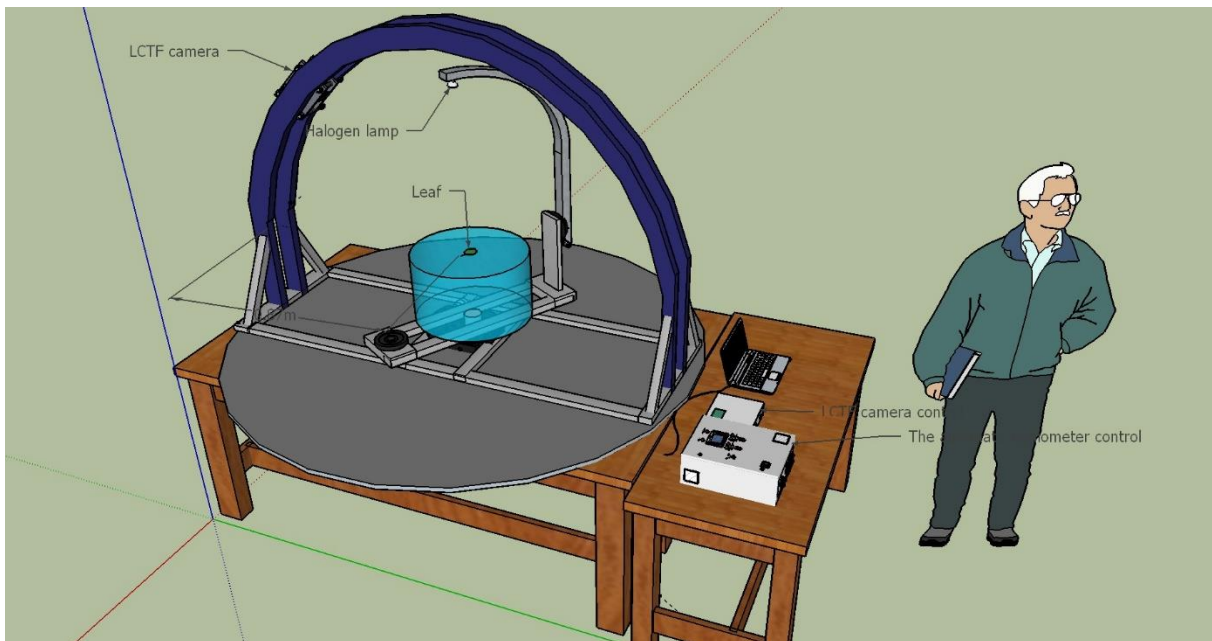


Fig. 51. New design of spectro-polarimetric BRDF Goniometer.

## REFERENCES

- Allen, W.A., Gausman, H.W., Richardson, A.J., Thomas, J.R., 1969. Interaction of Isotropic Light with a Compact Plant Leaf\*. *J. Opt. Soc. Am.* 59, 1376.  
<https://doi.org/10.1364/JOSA.59.001376>
- Baker, E.A., 1982. Chemistry and morphology of plant epicuticular waxes. *Linn. Soc. Symp. Ser.*
- Barnsley, M.J., Strahler, A.H., Morris, K.P., Muller, J., 1994. Sampling the surface bidirectional reflectance distribution function (BRDF): 1. Evaluation of current and future satellite sensors. *Remote Sens. Rev.* 8, 271–311.  
<https://doi.org/10.1080/02757259409532205>
- Barthlott, W., 1981. Epidermal and seed surface characters of plants: systematic applicability and some evolutionary aspects. *Nord. J. Bot.* 1, 345–355. <https://doi.org/10.1111/j.1756-1051.1981.tb00704.x>
- Barton, F.E., Himmelsbach, D.S., Duckworth, J.H., Smith, M.J., 1992. Two-Dimensional Vibration Spectroscopy: Correlation of Mid- and Near-Infrared Regions. *Appl. Spectrosc.* 46, 420–429. <https://doi.org/10.1366/0003702924125375>
- Bennett, H.E., Porteus, J.O., 1961. Relation Between Surface Roughness and Specular Reflectance at Normal Incidence. *J. Opt. Soc. Am.* 51, 123.  
<https://doi.org/10.1364/JOSA.51.000123>
- Bousquet, L., Lachéradé, S., Jacquemoud, S., Moya, I., 2007. Corrigendum to “Leaf BRDF measurements and model for specular and diffuse components differentiation.” *Remote Sens. Environ.* <https://doi.org/10.1016/j.rse.2007.03.006>
- Bousquet, L., Lachéradé, S., Jacquemoud, S., Moya, I., 2005. Leaf BRDF measurements and model for specular and diffuse components differentiation. *Remote Sens. Environ.* 98, 201–211. <https://doi.org/10.1016/J.RSE.2005.07.005>
- Brakke, T.W., 1994. Specular and diffuse components of radiation scattered by leaves. *Agric. For. Meteorol.* 71, 283–295. [https://doi.org/10.1016/0168-1923\(94\)90016-7](https://doi.org/10.1016/0168-1923(94)90016-7)
- Brakke, T.W., Smith, J.A., Harnden, J.M., 1989. Bidirectional scattering of light from tree leaves. *Remote Sens. Environ.* 29, 175–183. [https://doi.org/10.1016/0034-4257\(89\)90025-4](https://doi.org/10.1016/0034-4257(89)90025-4)
- Breece III, H.T., Holmes, R.A., 1971. Bidirectional Scattering Characteristics of Healthy Green Soybean and Corn Leaves in Vivo. *Appl. Opt.* 10, 119.  
<https://doi.org/10.1364/AO.10.000119>
- Church, E.L., 1979. Relationship between Surface Scattering and Microtopographic Features. *Opt. Eng.* <https://doi.org/10.1117/12.7972337>
- Church, E.L., Takacs, P.Z., 1995. Light scattering from non-Gaussian surfaces, in: Stover, J.C. (Ed.), . *International Society for Optics and Photonics*, pp. 91–107.  
<https://doi.org/10.1117/12.218325>
- Cole, T.A., Molthan, A.L., Schultz, L.A., Roman, M.O., Wanik, D.W., 2016. Improvements to Lunar BRDF-Corrected Nighttime Satellite Imagery: Uses and Applications.
- Comar, A., Baret, F., Obein, G., Simonot, L., Meneveaux, D., Viénot, F., de Solan, B., 2014.

- ACT: A leaf BRDF model taking into account the azimuthal anisotropy of monocotyledonous leaf surface. *Remote Sens. Environ.* 143, 112–121.  
<https://doi.org/10.1016/j.rse.2013.12.006>
- Comar, A., Baret, F., Viénot, F., Yan, L., de Solan, B., 2012. Wheat leaf bidirectional reflectance measurements: Description and quantification of the volume, specular and hot-spot scattering features. *Remote Sens. Environ.* 121, 26–35.  
<https://doi.org/10.1016/j.rse.2011.01.028>
- Combal, B., Baret, F., Weiss, M., Trubuil, A., Macé, D., Pragnère, A., Myneni, R., Knyazikhin, Y., Wang, L., 2003. Retrieval of canopy biophysical variables from bidirectional reflectance: Using prior information to solve the ill-posed inverse problem. *Remote Sens. Environ.* 84, 1–15. [https://doi.org/10.1016/S0034-4257\(02\)00035-4](https://doi.org/10.1016/S0034-4257(02)00035-4)
- Combes, D., Bousquet, L., Jacquemoud, S., Sinoquet, H., Varlet-Grancher, C., Moya, I., 2007. A new spectrogoniophotometer to measure leaf spectral and directional optical properties. *Remote Sens. Environ.* 109, 107–117.  
<https://doi.org/10.1016/j.rse.2006.12.007>
- Cook, R.L., Torrance, K.E., 1981. A reflectance model for computer graphics, in: *Proceedings of the 8th Annual Conference on Computer Graphics and Interactive Techniques - SIGGRAPH '81*. ACM Press, New York, New York, USA, pp. 307–316.  
<https://doi.org/10.1145/800224.806819>
- Coulson, K.L., Bouricius, G.M., Gray, E.L., 1965. Optical reflection properties of natural surfaces. *J. Geophys. Res.* 70, 4601–4611. <https://doi.org/10.1029/JZ070i018p04601>
- Dangel, S., Kneubuhler, M., Schaepman, M., Schopfer, J., Schaepman-Strub, G., Itten, K., Ieee, 2003. Combined field and laboratory goniometer system - FIGOS and LAGOS. *Igarss 2003 Ieee Int. Geosci. Remote Sens. Symp. Vols I - Vii, Proc. Learn. from Earth's Shapes Sizes 00*, 4428–4430. <https://doi.org/10.1109/IGARSS.2003.1295536>
- Di Girolamo, L., 2003. Generalizing the definition of the bi-directional reflectance distribution function, *Remote Sensing of Environment*.  
<https://doi.org/10.1016/j.rse.2003.07.004>
- Diner, D.J., Beckert, J.C., Bothwell, G.W., Rodriguez, J.I., 2002. Performance of the MISR instrument during its first 20 months in Earth orbit. *IEEE Trans. Geosci. Remote Sens.* 40, 1449–1466. <https://doi.org/10.1109/TGRS.2002.801584>
- Dong, Y., Jiao, Z., Ding, A., Zhang, H., Zhang, X., Li, Y., He, D., Yin, S., Cui, L., 2018. A modified version of the kernel-driven model for correcting the diffuse light of ground multi-angular measurements. *Remote Sens. Environ.* 210, 325–344.  
<https://doi.org/10.1016/j.rse.2018.03.030>
- Ensikat, Neinhuis, Barthlott, 2000. Direct Access to Plant Epicuticular Wax Crystals by a New Mechanical Isolation Method. *Int. J. Plant Sci.* 161, 143–148.
- Gaonkar, A.G., Vasisht, N., Khare, A.R., Sobel, R., 2014. *Microencapsulation in the food industry : a practical implementation guide*. Elsevier Science.
- Grant, L., Daughtry, C.S.T., Vanderbilt, V.C., 1993. Polarized and specular reflectance variation with leaf surface features. *Physiol. Plant.* 88, 1–9.  
<https://doi.org/10.1034/j.1399-3054.1993.880101.x>
- Grant, L., Daughtry, C.S.T., Vanderbilt, V.C., 1987. Variations in the polarized leaf

- reflectance of *Sorghum bicolor*. *Remote Sens. Environ.* 21, 333–339.  
[https://doi.org/10.1016/0034-4257\(87\)90016-2](https://doi.org/10.1016/0034-4257(87)90016-2)
- Grum, F., Luckey, G.W., 1968. Optical Sphere Paint and a Working Standard of Reflectance. *Appl. Opt.* 7, 2289. <https://doi.org/10.1364/AO.7.002289>
- Hapke, B., van Hoen, H., 1963. Photometric studies of complex surfaces, with applications to the Moon. *J. Geophys. Res.* 68, 4545–4570. <https://doi.org/10.1029/JZ068i015p04545>
- Harvey, J.E., 2012. Total integrated scatter from surfaces with arbitrary roughness, correlation widths, and incident angles. *Opt. Eng.* 51, 013402.  
<https://doi.org/10.1117/1.OE.51.1.013402>
- Harvey, J.E., 1977. Light-Scattering Characteristics Of Optical Surfaces. *Proc. SPIE 0107, Stray Light Probl. Opt. Syst.* 41–47. <https://doi.org/10.1117/12.964594>
- Harvey, J.E., Choi, N., Krywonos, A., 2010. Scattering from moderately rough interfaces between two arbitrary media 77940V. <https://doi.org/10.1117/12.863995>
- Harvey, J.E., Choi, N., Schroeder, S., Duparré, A., 2012. Total integrated scatter from surfaces with arbitrary roughness, correlation widths, and incident angles. *Opt. Eng.* 51, 013402. <https://doi.org/10.1117/1.OE.51.1.013402>
- Huang, Z., Yang, S., Zhang, H., Zhang, M., Cao, W., 2015. Replication of Leaf Surface Structures for Light Harvesting. *Sci. Rep.* 5, 14281. <https://doi.org/10.1038/srep14281>
- Ishida, T., Kurihara, J., Viray, F.A., Namuco, S.B., Paringit, E.C., Perez, G.J., Takahashi, Y., Marciano, J.J., 2018. A novel approach for vegetation classification using UAV-based hyperspectral imaging. *Comput. Electron. Agric.* 144, 80–85.  
<https://doi.org/10.1016/J.COMPAG.2017.11.027>
- Jacquemoud, S., Ustin, S.L., 2001. Leaf optical properties: a state of the art. *Proc. 8th Int. Symp. Phys. Meas. Signatures Remote Sens.* 223–232.  
<https://doi.org/10.1017/CBO9781107415324.004>
- Jacquemoud, S., Ustin, S.L., Verdebout, J., Schmuck, G., Andreoli, G., Hosgood, B., 1996. Estimating leaf biochemistry using the PROSPECT leaf optical properties model. *Remote Sens. Environ.* 56, 194–202. [https://doi.org/10.1016/0034-4257\(95\)00238-3](https://doi.org/10.1016/0034-4257(95)00238-3)
- Johansen, V.E., 2015. Preparing the generalized Harvey – Shack rough surface scattering method for use with the discrete ordinates method. *J. Opt. Soc. Am. A* 32, 186–194.
- Johnson, R.P.C., Jeffree, C.E., 1970. Negative stain in wax tubes from the surface of Sitka spruce leaves. *Planta* 95, 179–182. <https://doi.org/10.1007/BF00387249>
- Journaux, L., Simon, J.-C., Destain, M.F., Cointault, F., Miteran, J., Piron, A., 2011. Plant leaf roughness analysis by texture classification with generalized Fourier descriptors in a dimensionality reduction context. *Precis. Agric.* 12, 345–360.  
<https://doi.org/10.1007/s11119-010-9208-z>
- Jurik, T.W., Chabot, J.F., Chabot, B.F., 1982. Effects of Light and Nutrients on Leaf Size, CO<sub>2</sub> Exchange, and Anatomy in Wild Strawberry (*Fragaria virginiana*). *Plant Physiol.* 70, 1044–1048. <https://doi.org/10.1104/pp.70.4.1044>
- Kamei, T., Kumano, H., Masumura, S., 1997. Changes of Immunoregulatory Cells Associated with Psychological Stress and Humor. *Percept. Mot. Skills* 84, 1296–1298.  
<https://doi.org/10.2466/pms.1997.84.3c.1296>

- Kearns, S.G., Bärlocher, F., 2008. Leaf surface roughness influences colonization success of aquatic hyphomycete conidia. *Fungal Ecol.* 1, 13–18.  
<https://doi.org/10.1016/j.funeco.2007.07.001>
- Kim, K.W., Cho, D.-H., Kim, P.-G., 2011. Morphology of Foliar Trichomes of the Chinese Cork Oak *Quercus variabilis* by Electron Microscopy and Three-Dimensional Surface Profiling. *Microsc. Microanal.* 17, 461–468.  
<https://doi.org/10.1017/S1431927611000407>
- Knyazikhin, Y., Schull, M., ... P.S.-P. of the, 2013, undefined, n.d. Hyperspectral remote sensing of foliar nitrogen content. *Natl. Acad Sci.*
- Krywonos, A., 2006. Predicting Surface Scatter Using a Linear Systems Formulation of Non-Paraxial Scalar Diffraction.
- Krywonos, A., Harvey, J.E., Choi, N., 2011. Linear systems formulation of scattering theory for rough surfaces with arbitrary incident and scattering angles. *J. Opt. Soc. Am. A.*  
<https://doi.org/10.1364/JOSAA.28.001121>
- Kuusk, A., 1994. A multispectral canopy reflectance model. *Remote Sens. Environ.* 50, 75–82. [https://doi.org/10.1016/0034-4257\(94\)90035-3](https://doi.org/10.1016/0034-4257(94)90035-3)
- Li-Beisson, Y., Verdier, G., Xu, L., Beisson, F., 2016. Cutin and Suberin Polyesters, in: *ELS*. John Wiley & Sons, Ltd, Chichester, UK, pp. 1–12.  
<https://doi.org/10.1002/9780470015902.a0001920.pub3>
- Liang, S., Zhang, X., Xiao, Z., Cheng, J., Liu, Q., Zhao, X., 2014. Global LAnd Surface Satellite (GLASS) Products. <https://doi.org/10.1007/978-3-319-02588-9>
- Lloyd, J., Bloomfield, K., Domingues, T.F., Farquhar, G.D., 2013. Photosynthetically relevant foliar traits correlating better on a mass vs an area basis: of ecophysiological relevance or just a case of mathematical imperatives and statistical quicksand? *New Phytol.* 199, 311–321. <https://doi.org/10.1111/nph.12281>
- López-Álvarez, M.A., Hernández-Andrés, J., Romero, J., Campos, J., Pons, A., 2009. Calibrating the Elements of a Multispectral Imaging System. *J. Imaging Sci. Technol.*  
<https://doi.org/10.2352/J.ImagingSci.Technol.2009.53.3.031102>
- Maier, S.W., Lüdeker, W., Günther, K.P., 1999. SLOP: A Revised Version of the Stochastic Model for Leaf Optical Properties. *Remote Sens. Environ.* 68, 273–280.  
[https://doi.org/10.1016/S0034-4257\(98\)00118-7](https://doi.org/10.1016/S0034-4257(98)00118-7)
- Maignan, F., Bréon, F.-M., Fédèle, E., Bouvier, M., 2009. Polarized reflectances of natural surfaces: Spaceborne measurements and analytical modeling. *Remote Sens. Environ.* 113, 2642–2650. <https://doi.org/10.1016/j.rse.2009.07.022>
- MARTIN, J.T., JUNIPER, B.E., 1970. *The Cuticles of Plants.* The Cuticles of Plants.
- Martonchik, J. V., Bruegge, C.J., Strahler, A.H., 2000. A review of reflectance nomenclature used in remote sensing. *Remote Sens. Rev.* 19, 9–20.  
<https://doi.org/10.1080/02757250009532407>
- Nadal, F., Breon, F.-M., 1999. Parameterization of surface polarized reflectance derived from POLDER spaceborne measurements. *IEEE Trans. Geosci. Remote Sens.* 37, 1709–1718.  
<https://doi.org/10.1109/36.763292>
- Netto, A.T., Campostrini, E., Gonçalves De Oliveira, J., Bressan-Smith, R.E., 2005.

- Photosynthetic pigments, nitrogen, chlorophyll a fluorescence and SPAD-502 readings in coffee leaves. *Sci. Hortic. (Amsterdam)*. <https://doi.org/10.1016/j.scienta.2004.08.013>
- Nicodemus, F., Richmond, J., Hsia, J., Ginsberg, I., Limperis, T., 1977. Geometrical Considerations and Nomenclature for Reflectance.
- Ougham, H.J., Morris, P., Thomas, H., 2005. The Colors of Autumn Leaves as Symptoms of Cellular Recycling and Defenses Against Environmental Stresses, in: *Current Topics in Developmental Biology*. pp. 135–160. [https://doi.org/10.1016/S0070-2153\(05\)66004-8](https://doi.org/10.1016/S0070-2153(05)66004-8)
- Painter, T.H., Dozier, J., 2004. Measurements of the hemispherical-directional reflectance of snow at fine spectral and angular resolution. *J. Geophys. Res.* 109, D18115. <https://doi.org/10.1029/2003JD004458>
- Peltoniemi, J.I., Kaasalainen, S., Näränen, J., Rautiainen, M., Stenberg, P., Smolander, H., Smolander, S., Voipio, P., 2005. BRDF measurement of understory vegetation in pine forests: dwarf shrubs, lichen, and moss. *Remote Sens. Environ.* 94, 343–354. <https://doi.org/10.1016/j.rse.2004.10.009>
- Pickering, J.W., Moes, C.J.M., Sterenborg, H.J.C.M., Prahl, S.A., van Gemert, M.J.C., 1992. Two integrating spheres with an intervening scattering sample. *J. Opt. Soc. Am. A* 9, 621. <https://doi.org/10.1364/JOSAA.9.000621>
- Rouse, J.W., Hass, R.H., Schell, J.A., Deering, D.W., 1972. Monitoring Vegetation Systems in the Great Plains with ERTS, Third Earth Resources Technology Satellite-1 Symposium.
- Sandmeier, S.R., Itten, K.I., 1999. A field goniometer system (FIGOS) for acquisition of hyperspectral BRDF data. *IEEE Trans. Geosci. Remote Sens.* 37, 978–986. <https://doi.org/10.1109/36.752216>
- Schaepman-Strub, G., Schaepman, M.E., Painter, T.H., Dangel, S., Martonchik, J. V., 2006. Reflectance quantities in optical remote sensing-definitions and case studies. *Remote Sens. Environ.* 103, 27–42. <https://doi.org/10.1016/j.rse.2006.03.002>
- Skamoto, Y., Sugimura, N., Fukuda, K., Kuwahara, T., Yoshida, K., Kurihara, J., Fukuhara, T., Takahashi, Y., 2015. Development and Flight Results of Microsatellite Bus System for RISING-2 14, 89–96.
- Sokolov, K., Drezek, R., Gossage, K., Richards-Kortum, R., 1999. Reflectance spectroscopy with polarized light: is it sensitive to cellular and nuclear morphology. *Opt. Express* 5, 302. <https://doi.org/10.1364/OE.5.000302>
- Sun, Z., Peng, Z., Wu, D., Lv, Y., 2018. Photopolarimetric properties of leaf and vegetation covers over a wide range of measurement directions. *J. Quant. Spectrosc. Radiat. Transf.* 206, 273–285. <https://doi.org/10.1016/j.jqsrt.2017.11.017>
- Sun, Z., Wu, D., Lv, Y., Zhao, Y., 2017a. Polarized reflectance factors of vegetation covers from laboratory and field: A comparison with modeled results. *J. Geophys. Res.* 122, 1042–1065. <https://doi.org/10.1002/2016JD025892>
- Sun, Z., Wu, D., Lv, Y., Zhao, Y., 2017b. Polarized reflectance factors of vegetation covers from laboratory and field: A comparison with modeled results. *J. Geophys. Res. Atmos.* 122, 1042–1065. <https://doi.org/10.1002/2016JD025892>
- Tucker, C.J., Garratt, M.W., 1977. Leaf optical system modeled as a stochastic process. *Appl.*

Opt. 16, 635. <https://doi.org/10.1364/AO.16.000635>

- Tulloch, A.P., 1976. Chemistry of waxes of higher plants. *Chem. Biochem. Nat. Waxes*.
- Vanderbilt, V.C., Grant, L., 1985. Plant Canopy Specular Reflectance Model. *IEEE Trans. Geosci. Remote Sens. GE-23*, 722–730. <https://doi.org/10.1109/TGRS.1985.289390>
- Vanderbilt, V.C., Grant, L., Biehl, L.L., Robinson, B.F., 1985. Specular, diffuse, and polarized light scattered by two wheat canopies. *Appl. Opt.* 24, 2408–18. <https://doi.org/10.1364/AO.24.002408>
- Vanderbilt, V.C., Grant, L., Ustin, S.L., 1991. Polarization of Light by Vegetation, in: *Photon-Vegetation Interactions*. Springer Berlin Heidelberg, Berlin, Heidelberg, pp. 191–228. [https://doi.org/10.1007/978-3-642-75389-3\\_7](https://doi.org/10.1007/978-3-642-75389-3_7)
- Vern C. Vanderbilt and Lois Grant, 2000. POLARIZATION OF LIGHT BY VEGETATION.
- Walker, S.C., Allen, S., Bell, G., Roberts, C.J., 2015. Analysis of leaf surfaces using scanning ion conductance microscopy. *J. Microsc.* 258, 119–126. <https://doi.org/10.1111/jmi.12225>
- Walter-Shea, E.A., Norman, J.M., Blad, B.L., 1989. Leaf bidirectional reflectance and transmittance in corn and soybean. *Remote Sens. Environ.* 29, 161–174. [https://doi.org/10.1016/0034-4257\(89\)90024-2](https://doi.org/10.1016/0034-4257(89)90024-2)
- Wang, H., Shi, H., Li, Y., Wang, Y., 2014. The Effects of Leaf Roughness, Surface Free Energy and Work of Adhesion on Leaf Water Drop Adhesion. *PLoS One* 9, e107062. <https://doi.org/10.1371/journal.pone.0107062>
- Wang, Q., Chen, J., Stamps, R.H., Li, Y., 2005. Correlation of Visual Quality Grading and SPAD Reading of Green-Leaved Foliage Plants. *J. Plant Nutr.* 28, 1215–1225. <https://doi.org/10.1081/PLN-200063255>
- Weiss, M., Baret, F., 1999. Evaluation of Canopy Biophysical Variable Retrieval Performances from the Accumulation of Large Swath Satellite Data. *Remote Sens. Environ.* 70, 293–306. [https://doi.org/10.1016/S0034-4257\(99\)00045-0](https://doi.org/10.1016/S0034-4257(99)00045-0)
- Woolley, J.T., 1975. Refractive Index of Soybean Leaf Cell Walls. *PLANT Physiol.* 55, 172–174. <https://doi.org/10.1104/pp.55.2.172>
- Xue, J., Su, B., 2017. Significant Remote Sensing Vegetation Indices: A Review of Developments and Applications. *J. Sensors* 2017, 1–17. <https://doi.org/10.1155/2017/1353691>
- Yin, G., Li, A., Wu, S., Fan, W., Zeng, Y., Yan, K., Xu, B., Li, J., Liu, Q., 2018. PLC: A simple and semi-physical topographic correction method for vegetation canopies based on path length correction. *Remote Sens. Environ.* 215, 184–198. <https://doi.org/10.1016/j.rse.2018.06.009>